INVESTIGATION OF DEFORMATION PROCESS AND MECHANICAL PROPERTIES OF SINGLE CRYSTALS BY FINITE ELEMENT ANALYSIS

By

CHULHO YANG

A DISSERTATION PRESENTED TO THE GRADUATE SCHOOL
OF THE UNIVERSITY OF FLORIDA IN PARTIAL FULFILLMENT
OF THE REQUIREMENTS FOR THE DEGREE OF
DOCTOR OF PHILOSOPHY

UNIVERSITY OF FLORIDA

1997

ACKNOWLEDGMENTS

I would like to express my sincere thanks to my advisor Dr. Ashok V. Kumar. Without his encouragement and careful guidance, I could not have completed this work. I would like to thank Dr. Ali A. Seireg for serving on my committee. I would like to thank Dr. Michael J. Kaufman for giving me the opportunity to work on this project. I would like to thank Dr. Fereshteh Ebrahimi for serving on my committee and for her contributions through discussions with me. I would like to thank Dr. John C. Ziegert for serving on my committee.

Next, I want to express my appreciation to Kyungyai and Peter for their tremendous contributions through their love and endless support. I would like to express my appreciation to my parents for their love and support throughout my life. They have always stood by me.

Funding for this project from the Air Force under Grant No. F49620-93-1-0309 has been greatly helpful to my research.

I would like to thank to Dr. V. I. Levit for his helpful discussion during this project.

TABLE OF CONTENTS

LIST OF TABLES

LIST OF FIGURES

Abstract of Dissertation Presented to the Graduate School
Of the University of Florida in Partial Fulfillment of the
Requirements for the Degree of Doctor of Philosophy

INVESTIGATION OF DEFORMATION PROCESS AND MECHANICAL PROPERTIES OF SINGLE CRYSTALS BY FINITE ELEMENT ANALYSIS

By

Chulho Yang

December 1997

Chairman : Dr. Ashok V. Kumar
Major Department : Mechanical Engineering

Deformation of NiAl single crystals was studied using finite element analysis to investigate the modes of localized deformation. Constitutive parameters and hardening characteristics of the active slip systems were estimated by comparing numerical simulation results with experimental results. Deformation of tensile specimens of NiAl single crystal was simulated when loaded along different crystal orientations to understand the deformation mechanism that results in various localized modes of deformation. In particular, the formation of shear bands and kink bands was studied and the material and geometric characteristics that influence the formation of such localization were investigated.

Hardening characteristics of NiAl single crystals were studied using the finite element method. NiAl single crystals show significant hardening at large strain

when deformed along the [$\bar{5}$57] and [110] orientations. Two-dimensional simulation of deformation along the [$\bar{5}$57] orientation matched well with experimental results. A three-dimensional finite element model is required for simulating deformation along the [110] orientation since secondary slip systems are also activated. Four possible deformation cases were simulated to observe the effect of the secondary slip system's activation during deformation along the [110] orientation. The simulated load vs. elongation curves were compared with experimental results. The simulations proved the importance of secondary system's activation in predicting the hardening behavior of NiAl single crystals.

In addition, various hardening laws that have been proposed for single crystals were compared by simulating deformation of FCC single crystals using 3D FEM models. These hardening laws were used in FEM simulations to compare their ability to predict the three stages of deformation observed in FCC single crystals. Bassani's hardening model and a modified version of Asaro's hardening model were able to predict stages I, II, and III.

CHAPTER 1
INTRODUCTION

Objective of the Study

This research is aimed at understanding the deformation process and the mechanical properties of single crystals using the finite element analysis. Most of the studies presented here are focused on the following subjects.

(i) To understand the low ductility of NiAl single crystals, it is desirable to understand the deformation mechanism responsible for its mechanical behavior over a broad range of temperatures. Localization phenomena such as shear bands and kink bands are investigated to explore the mechanism of flow localization.

(ii) Effect of rate sensitivity and hardening parameter on the localization phenomena.

(iii) To investigate whether two-dimensional simulation along the $[\bar{5}57]$ orientation can be matched with the experimental results. To estimate hardening parameters such as saturated critical resolved shear stress and initial hardening rate by comparing the simulation results with experimental results. To determine if three-dimensional finite element model is required for simulating deformation along the [110] orientation since secondary slip systems are also activated.

(iv) To modify hardening law if necessary based on the experimental results on the NiAl single crystals and to use a three-dimensional finite element model to test the modified hardening law.

(v) To study the hardening characteristics in single crystals based on the hardening models of Asaro (1983), Weng (1987) and Bassani and Wu (1991) using three-dimensional finite element model.

Concepts of Single Crystals

The discovery of diffraction of x-rays stimulated fundamental study on the structure of metallic crystals. By examining the inside of metals, the most fundamental behavior of the metals could be revealed. Metals are composed of atoms arranged in specific geometric lattices. Most of the study on the atomic structure and the plastic deformation of metals has been performed with single crystal specimens due to the complexity caused by grain boundary and the constraints imposed by neighboring grains and second-phase particles.

The millions of atoms in a crystal are arranged in a pattern that is repeated periodically. The atoms in a crystal can be represented by points in space. The arrangement pattern of atoms in crystalline metals is called a crystal lattice structure.

The periodic nature of a crystal lattice makes it possible to use the smallest crystal unit known as the elementary cell to describe the lattice structure. The most elementary crystal structure is the simple cubic lattice. Three mutually perpendicular axes are arbitrarily placed at one of the corners of the cube. Crystallographic planes and directions with respect to the axes in the cubic crystal are designated by Miller indices. A crystallographic plane can be specified by using the length of its intercepts on the three

axes, measured from the origin of the coordinate axes. To simplify the crystallographic formulas, the reciprocals of these intercepts are used. The reciprocals are reduced into the smallest integers by dividing with the largest common factor to give the Miller indices of the plane. Crystallographic directions are indicated by the vector components of the direction resolved along each of the coordinate axes and reduced to the smallest integers.

Many of the common metals have either a body-centered cubic (BCC) or face-centered cubic (FCC) crystal structure. A BCC crystal structure has a pattern of atoms that are located at each corner and at the center of a cube. An FCC crystal structure has a pattern of atoms that are located at each corner and at the center of the face of each cube.

The third common metallic crystal structure is the hexagonal close-packed (HCP) structure. The Miller-Bravais system with four indices is used to represent crystallographic planes and directions in the HCP structure. Four axes are used to specify HCP lattice structure. Three axes are 120° apart in the basal plane, and the vertical axis is normal to the basal plane.

NiAl has a B2 type ordered crystal structure similar to body centered cubic (BCC) crystals. A cubic lattice with nickel atoms at each corner of the cell and a neighboring cubic lattice with aluminum atoms at each corner of the cell interpenetrate each other as in figure 1. Mechanical properties of NiAl single crystals vary with respect to the orientation of crystal lattice. Plastic deformation in NiAl occurs predominantly due to slip in the <001> directions along either {110} or {100} planes when loaded along non-<001> direction (or soft orientations). NiAl crystal subjected to loading along the <001> direction (hard orientation) shows high flow stress at low temperatures and enhanced

creep strength at elevated temperatures. In this orientation, deformation occurs by non-<001> dislocation.

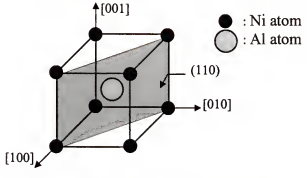

Figure 1. NiAl single crystal structure

Deformation of NiAl Single Crystals

NiAl has gained much attention as a potential structural material due to its desirable material characteristics such as high melting point, low density, good oxidation resistance and excellent mechanical properties at high temperatures including hardness, toughness, thermal stability and ductility. It has been considered a possible alternative to nickel-based super alloys for building turbine blades where due to lower weight and higher operating temperatures it is expected to provide increased engine thermodynamic efficiency. To find application as a commercial structural material, it should have desirable structural properties over a range of working temperature. However, NiAl has low ductility and poor fracture toughness at ambient temperatures. The tensile plastic strain before fracture at room temperature is typically 0.5-2.5% (Lahrman et al., 1991; Miracle, 1993). To understand its low ductility, it is desirable to understand the deformation mechanism responsible for its mechanical behavior over a broad range of

temperatures. Many modes of nonuniform deformation such as necking, localized shear, kinking etc. have been observed in NiAl single crystals. These localized deformations contribute significantly to the total plastic strain and eventual failure (Miracle, 1993). Significant tensile ductility is obtained only at and above 473 K (Wasilewski et al., 1967, Lahrman et al., 1991). Therefore, many approaches to improve the ambient temperature material properties of NiAl have been investigated (Darolia, 1991; Darolia et al., 1992; Shrivastava and Ebrahimi, 1997). A detailed survey of literature and a critical review of the physical and mechanical properties of NiAl have been presented by Miracle (1993).

Most ductile single crystals (Chang and Asaro, 1980, Peirce et al., 1982) exhibit localized deformation modes when subjected to a large plastic deformation process. Understanding the causes of localized deformation is of great importance because such nonuniform deformation creates voids or damages on the surface that eventually lead to initiation of fracture. In single crystals of NiAl, significant lattice rotation is observed especially when deformation occurs by slip in a single slip system. These lattice rotations can result in orientation or geometric softening that promotes various forms of localized deformation. Common forms of localization observed in single crystals are necking, shear localization and kink bands. Macroscopic shear bands have not been observed experimentally in NiAl; however, it is possible that microscopic shear localization may be responsible for stress concentrations and crack initiation. Kink bands have been observed in NiAl single crystals subjected to compressive loads along the orientations very close to the hard orientation (Fraser et al., 1973a, 1973b).

Asaro (1983) has reviewed the development and the theoretical basis of crystal plasticity. These theoretical formulations have since been implemented using the finite

element method to simulate deformation and to predict and study non-homogeneous deformation in single crystals. Most of the past studies have used these methods to simulate deformation in FCC (Peirce et al., 1983) and BCC single crystals (Deve et al., 1988). In this study, we have investigated various modes of localized and diffused deformation observed in NiAl and studied the role of various parameters such as lattice orientation, rate sensitivity, latent hardening ratio etc. in promoting these modes of deformation.

Hardening Characteristics of Single Crystals

Finding an appropriate hardening description for single crystals is a crucial step in the study of the deformation process of materials. It is difficult to identify the reality of behavior in terms of micro-mechanics of single crystals. Especially, in case of multi slip, description of hardening of a single crystal becomes significantly more complicated than single slip. We need to include not only hardening of slip systems itself, so called active slip hardening, but also hardening by other slip systems, so called latent hardening.

From the early 1900s several hardening laws were proposed to explain the deformation process on single crystals. Based on his experimental work on aluminum, Taylor (1934) proposed the so called isotropic hardening law that shows the same amount of constant hardening for all slip systems. Hardening of slip system is coupled with other slip system. This isotropic hardening law can not predict the higher latent hardening.

Nakada and Keh (1966) suggested a modified isotropic hardening law to explain the higher latent hardening rate based on their experiment on iron. They pointed out that iron does not slip on one distinct slip plane, so one cannot classify the dislocation interactions according to their slip systems like FCC single crystals. Higher latent hardening was

explained as follows. They used two constant parameters. For primary and coplanar slip system a lower hardening parameter was assumed and for other slip systems higher a hardening parameter was used.

Asaro (1983) adopted a hardening law that contains a latent hardening effect by using the latent hardening parameter q, which was used by Hutchinson (1970). Our previous papers (Yang et al., 1997; Yang and Kumar, 1997) used this law successfully in the case of an ideally plastic hardening case. However, higher hardening at large strain was not accomplished by using this law.

Weng (1987) proposed a hardening theory called anisotropic hardening. He used relative angles of slip systems for his latent hardening formulations. He explained that a strong latent hardening, a weak latent hardening and Bauschinger effect can be described by the measure of relative orientation of slip systems.

Bassani and co-workers (Wu et al., 1991; Bassani and Wu, 1991; Bassani, 1994) proposed a hardening law in FCC crystals based on the dislocation interactions between slip systems in the time independent frame. They tried to explain the latent hardening phenomena through their experiment using computer data acquisition on copper single crystal which is different from the back extrapolation method conventionally used by many authors (Kocks, 1964). They suggested latent hardening may be lower than self-hardening of the active slip systems. This result is quite different from the result obtained by other authors. They explained in their hardening law that the conventionally used higher latent hardening is actually strong self-hardening. So, the off-diagonal terms in the hardening matrix $[h_{\alpha\beta}]$ are less than the active-hardening terms (diagonal terms).

In this study we have proposed a hardening model to explain the extremely high hardening trends after necking at a large strain regime in NiAl single crystals. Our two-dimensional analysis is extended to the three-dimensional finite element analysis to study the multi-slip cases in the simulation. Our previously used kinematics relations in single crystals of the 2-dimensional case can be extended to this study without difficulties.

Summary of the Study

In chapter 1 of this thesis, the most basic concepts of crystals such as structures of single crystals and slip systems are explained. The deformation processes of NiAl single crystals are described also. Microscopic shear band are generally observed in [110] orientation. Localized deformations such as shear band and kink band may facilitate the initiation of micro voids and eventually lead to fracture at a low temperature. Hardening laws of single crystals are reviewed briefly. Describing the hardening properties precisely is not an easy task. Dislocation interaction and internal dislocation densities are main contributors for the hardening description from a microscopic viewpoint. Most of the available models describe hardening of single crystals by slip interactions from a macroscopic viewpoint. Latent hardening is used to represent high hardening due to the activation of other slip systems.

In chapter 2 of this thesis, the kinematic relations and elastic-plastic constitutive equations of single crystals are discussed. The slip mechanism of single crystals is explained. A rate-dependent constitutive model for single crystals is implemented into ABAQUS, a commercial finite element code that is capable of modeling large deformation and large strains. The rate dependent constitutive equation is integrated using the forward gradient method which has been found to be effective (Peirce et al.,

1983; Wenner, 1993) provided sufficiently small time-steps are used for the time integration. For the simulation of the localization (shear band and kink band), we used incompatible elements (Simo and Rifai, 1990) available in ABAQUS. These elements have been found to be particularly suitable for modeling the incompressible behavior and for modeling strain localization (Simo and Armero, 1992).

In chapter 3 of this thesis, previous studies on the localization phenomena and hardening characteristics of single crystals are reviewed. Various causes of shear localization are discussed. Latent hardening tests on the FCC crystal such as copper and aluminum or BCC such as α-iron have been performed by many authors. Latent hardening is in general greater than self-hardening.

In chapter 4 of this thesis, simulations in the rate dependent frame to understand localization phenomena in NiAl single crystals are presented. A schematic diagram of loading orientation is given.

Shear localization is observed when the loading axis was a few degrees off from the [110] orientation. Initial imperfections control the initiation points of localization. Material properties such as hardening strain rate sensitivity and geometry of specimen play an important role in the formation of the localized band. Low hardening and low strain rate sensitivity facilitate localization. Symmetric orientation without misalignment in the [110] loading direction does not show the macroscopic localization due to the no rotation of the crystal lattice. Lattice rotations cause geometrical softening and a localized band occurs.

Kink band is observed in a compression test along the hard orientation of NiAl single crystals. Loadings along the axis, 5° off and 10° off from the hard orientation, are

simulated. Both double slip system and single slip systems show the kink band. Lattice rotations also play a role in the formation of the kink band. Geometric softening occurs due to lattice rotation. The single slip case experiences more lattice rotation than the double slip case. As a result, the kink band can be seen clearly in the single slip case.

In chapter 5, hardening models for NiAl single crystals are proposed and simulations are performed to confirm our modified hardening law. Hardening laws for single crystal have been proposed by many authors based on experiment. We propose a modified hardening law based on the experimental results of NiAl single crystals. The latent hardening ratio is predicted based on our analytical prediction of four possible deformation modes. Simulation results are compared with experimental results. Loading along the [110] crystal orientation is considered for simulation. A schematic diagram of the loading orientation is presented. Hardening parameters such as saturated critical resolved shear stress, initial critical resolved shear stress and initial rate of hardening are determined by comparing the experimental results in the $[\bar{5}57]$ orientation.

In chapter 6, the hardening laws proposed by other authors are simulated to compare each law and investigate the characteristics of each formula by three-dimensional finite element analysis.

In chapter 7, some conclusions and recommendations for future work are presented.

CHAPTER 2
FINITE ELEMENT MODELING OF SINGLE CRYSTALS

Constitutive Model for Single Crystals

In this section, we present a constitutive model for the elastic-plastic behavior of single crystals. The formulation used here is based on the well-established rate dependent model for single crystals (Peirce et al., 1983; Asaro, 1983; Needleman et al., 1985). The following section clarifies the notations and details of the constitutive equation that was implemented for simulating single crystals.

Kinematics of Crystalline Deformation

The deformation of single crystal is a complicated problem and it is difficult to include all the possible deformation mechanisms into the model for simulation. For instance, plastic deformation in single crystals occurs by twinning in addition to the slipping on the crystal lattice and the shape of the crystal lattice is actually changed during plastic deformation. However, these effects on the plastic deformation of single crystals may be ignored in our model. Plastic flow of crystals is described as slipping along active slip systems macroscopically rather than by dislocation movement microscopically. Deformation in the single crystals may be described by the following fundamental assumptions. First, plastic deformation of a single crystal is produced solely by slips through the crystal lattice. So, we only consider slipping as a moving mechanism in a single crystal. As a second assumption, we assume that elastic stretching and rotation

are small. The third assumption is that the crystal lattice retains its shape and orientation during the plastic flow.

The undeformed crystal state can be regarded as a reference configuration in which a material point is described by a position vector **X** in figure 2-1. After the crystal deforms plastically and elastically, each material point can be depicted by current position vector **x**. The difference between **X** and **x** at each material point is defined as displacement vector **u** (see figure 2-1).

$$\mathbf{u} = \mathbf{x} - \mathbf{X} \tag{2.1}$$

The current position of material point vector **x** with respect to the reference configuration is expressed as follows.

$$\mathbf{x}_1 = \mathbf{X}_1 + \mathbf{u}\cos\theta, \quad \mathbf{x}_2 = \mathbf{X}_2 + \mathbf{u}\sin\theta \tag{2.2}$$

Using transformation between the lattice coordinates and the reference coordinates, the current position of material point vector **x** is expressed as follows.

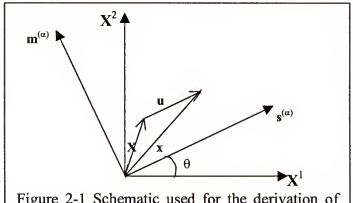

Figure 2-1 Schematic used for the derivation of the plastic deformation gradient F^p

$$\begin{aligned} \mathbf{x}_1 &= \mathbf{X}_1 + \gamma(-\mathbf{X}_1\sin\theta + \mathbf{X}_2\cos\theta)\cos\theta \\ \mathbf{x}_2 &= \mathbf{X}_2 + \gamma(-\mathbf{X}_1\sin\theta + \mathbf{X}_2\cos\theta)\sin\theta \end{aligned} \tag{2.3}$$

Plastic part of deformation gradient F^P that describes the current configuration is given by

$$\mathbf{F}^P = \partial \mathbf{x}/\partial \mathbf{X} = \mathbf{I} + \gamma(\mathbf{s}^{(\alpha)} \cdot \mathbf{m}^{(\alpha)T}) \tag{2.4}$$

where **I** is the 2nd order identity tensor.

In figure 2-2, the kinematics of single crystals is described schematically. For describing the kinematics of single crystals it is convenient to decompose the deformation gradient (**F**) of the deformed crystal into two components (Lee, 1969).

Using $\mathbf{F}^P$ to denote the plastic part of the deformation gradient.

$$d\mathbf{p} = \mathbf{F}^p \cdot d\mathbf{X} \tag{2.5}$$

where d**p** is the corresponding infinitesimal line element after deformation.

The lattice and material deform elastically together with no relative movement between the material particles and the lattice. This elastic deformation is described by

$$d\mathbf{x} = \mathbf{F}^* \cdot d\mathbf{p} \tag{2.6}$$

Inserting equation (2.5) into equation (2.6) gives total deformation gradient **F**.

$$\mathbf{F} = \mathbf{F}^* \cdot \mathbf{F}^p \tag{2.7}$$

The elastic part of deformation gradient $\mathbf{F}^*$ describes the elastic stretching and rigid body rotation of the crystal lattice and the plastic part of deformation gradient $\mathbf{F}^p$ takes part in the deformation solely by plastic shearing.

A particular slip system, α, is specified by the vectors $(\mathbf{s}^{(\alpha)}, \mathbf{m}^{(\alpha)})$, where $\mathbf{s}^{(\alpha)}$ is the slip direction vector and $\mathbf{m}^{(\alpha)}$ gives the slip plane normal vector. The vectors $\mathbf{s}^{(\alpha)}$ and $\mathbf{m}^{(\alpha)}$ are taken to be orthonormal in the undeformed lattice. According to the preceding discussion, it is obvious that this deformation and rotation are caused only by the elastic

part of deformation gradient $\mathbf{F}^*$ including rigid body rotation. As the crystal deforms, the slip direction vector $\mathbf{s}^{(\alpha)}$ convects with the lattice deformation gradient $\mathbf{F}^*$.

Deformed slip direction $\mathbf{s}^{*(\alpha)}$ and deformed slip plane normal vector $\mathbf{m}^{*(\alpha)}$ are defined as follows :

$$\mathbf{s}^{*(\alpha)} = \mathbf{F}^* \cdot \mathbf{s}^{(\alpha)} \tag{2.8}$$

$$\mathbf{m}^{*(\alpha)} = \mathbf{m}^{(\alpha)} \cdot (\mathbf{F}^*)^{-1} \tag{2.9}$$

The total velocity gradient $\mathbf{L}$ in the current configuration can be decomposed into the rate of stretching $\mathbf{D}$ and the rate of spin Ω and the rate of stretching and rate of spin can be decomposed into elastic and plastic parts.

$$\mathbf{L} = \mathbf{D} + \Omega = \mathbf{L}^* + \mathbf{L}^P \tag{2.10}$$

$$\mathbf{D} + \Omega = (\mathbf{D}^* + \Omega^*) + (\mathbf{D}^P + \Omega^P) \tag{2.11}$$

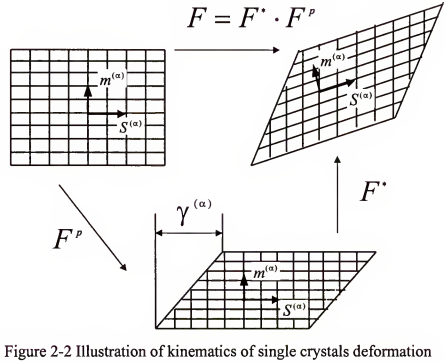

Figure 2-2 Illustration of kinematics of single crystals deformation

where $\mathbf{L}^*$ is the component of the velocity gradient associated with the elastic deformation and rotation while $\mathbf{L}^p$ is the velocity gradient due to plastic shearing. Differentiating $\mathbf{F} = \mathbf{F}^* \cdot \mathbf{F}^p$ with respect to time at a fixed material point gives the following expressions.

$$\mathbf{L} = \dot{\mathbf{F}} \cdot \mathbf{F}^{-1} = \dot{\mathbf{F}}^* \cdot \mathbf{F}^{*-1} + \mathbf{F}^* \cdot \dot{\mathbf{F}}^p \cdot \mathbf{F}^{p-1} \cdot \mathbf{F}^{*-1} \tag{2.12}$$

We can identify the elastic and plastic parts of the velocity gradient as follows.

$$\mathbf{L}^* = \mathbf{D}^* + \Omega^* = \dot{\mathbf{F}}^* \cdot \mathbf{F}^{*-1} \tag{2.13}$$

$$\mathbf{L}^p = \mathbf{D}^p + \Omega^p = \mathbf{F}^* \cdot \dot{\mathbf{F}}^p \cdot \mathbf{F}^{p-1} \cdot \mathbf{F}^{*-1} \tag{2.14}$$

Since plastic deformation occurs solely by shear along the slip planes, the plastic part of the velocity gradient can be written as

$$\mathbf{L}^p = \mathbf{D}^p + \Omega^p = \sum_{\alpha=1}^{n} \dot{\gamma}^{(\alpha)} (\mathbf{s}^{*(\alpha)} \cdot \mathbf{m}^{*(\alpha)^T}) \tag{2.15}$$

where $\dot{\gamma}^{(\alpha)}$ is the rate of shearing on the slip system α, as measured relative to the lattice. Finally the plastic part of stretching (symmetric) and the spin (skew-symmetric) are given by

$$\mathbf{D}^p = \sum_{\alpha=1}^{n} \dot{\gamma}^{(\alpha)} \cdot \mathbf{P}^{(\alpha)} \tag{2.16}$$

$$\Omega^p = \sum_{\alpha=1}^{n} \dot{\gamma}^{(\alpha)} \cdot \mathbf{W}^{(\alpha)} \tag{2.17}$$

where

$$\mathbf{P}^{(\alpha)} = \frac{1}{2} (\mathbf{s}^{(\alpha)} \cdot \mathbf{m}^{(\alpha)} + \mathbf{m}^{(\alpha)} \cdot \mathbf{s}^{(\alpha)}) \tag{2.18}$$

$$\mathbf{W}^{(\alpha)} = \frac{1}{2} (\mathbf{s}^{(\alpha)} \cdot \mathbf{m}^{(\alpha)} - \mathbf{m}^{(\alpha)} \cdot \mathbf{s}^{(\alpha)}) \tag{2.19}$$

Constitutive Law for Elastic-Plastic Single Crystals

The mathematical representation of elastic-plastic constitutive equations for single crystals using the kinematics of crystalline deformation studied in the previous part is described in this part. The rate of strain energy (per unit reference volume) is written as

$$\dot{\Phi} = \sigma : \mathbf{D} = \sigma : (\mathbf{D}^* + \mathbf{D}^p) \tag{2.20}$$

The above equation can be rewritten as follows using equation (2.13).

$$\dot{\Phi} = (\mathbf{F}^{*-1} \cdot \sigma \cdot \mathbf{F}^{*-T}) : (\mathbf{F}^{*T} \cdot \dot{\mathbf{F}}^*) + \sigma : \mathbf{D}^p \tag{2.21}$$

Then introducing the second Piola-Kirchhoff stress $\mathbf{T}$ and the Green strain $\mathbf{E}^*$

$$\mathbf{T} = \mathbf{F}^{*-1} \cdot \sigma \cdot \mathbf{F}^{*-T} \tag{2.22}$$

$$\mathbf{E}^* = \frac{1}{2}(\mathbf{F}^{*T} \cdot \mathbf{F}^* - \mathbf{I}) \tag{2.23}$$

where $\mathbf{I}$ is the identity tensor. The existence of strain energy function Φ^* for elastic response requires

$$\mathbf{T} = \frac{\partial \Phi^*}{\partial \mathbf{E}^*} \tag{2.24}$$

Neglecting any effect of plastic straining on elastic moduli, differentiating equation (2.24) gives

$$\frac{D\mathbf{T}}{Dt} = \frac{\partial}{\partial E}\left(\frac{\partial \Phi^*}{\partial E}\right)\frac{\partial E}{\partial t} = \mathbf{C} : \dot{\mathbf{E}}^* \tag{2.25}$$

$$\mathbf{C} = \mathbf{C}^T = \frac{\partial^2 \Phi^*}{\partial \mathbf{E}^{*2}} \tag{2.26}$$

where D( )/Dt is the nonobjective material derivative.

Next, from equation (2.13), equation (2.22) and equation (2.23)

$$\begin{aligned}\frac{D\sigma}{Dt} &= \dot{\mathbf{F}}^{*}\cdot\mathbf{T}\cdot\mathbf{F}^{*T}+\mathbf{F}^{*}\cdot\frac{D\mathbf{T}}{Dt}\cdot\mathbf{F}^{*T}+\mathbf{F}^{*}\cdot\mathbf{T}\cdot\dot{\mathbf{F}}^{*T}\\ &= \dot{\mathbf{F}}^{*}\cdot(\mathbf{F}^{*-1}\cdot\sigma\cdot\mathbf{F}^{*-T})\cdot\mathbf{F}^{*T}+\mathbf{F}^{*}\cdot\frac{D\mathbf{T}}{Dt}\cdot\mathbf{F}^{*T}+\mathbf{F}^{*}\cdot(\mathbf{F}^{*-1}\cdot\sigma\cdot\mathbf{F}^{*-T})\cdot\dot{\mathbf{F}}^{*T} \qquad (2.27)\\ &= (\mathbf{D}^{*}+\Omega^{*})\cdot\sigma+\mathbf{F}^{*}\cdot\frac{D\mathbf{T}}{Dt}\cdot\mathbf{F}^{*T}+\sigma\cdot(\mathbf{D}^{*}-\Omega^{*})\end{aligned}$$

Equation (2.27) can be rewritten as

$$\frac{D\sigma}{Dt}-\Omega^{*}\cdot\sigma+\sigma\cdot\Omega^{*}=\mathbf{F}^{*}\cdot\frac{D\mathbf{T}}{Dt}\cdot\mathbf{F}^{*T}+\mathbf{D}^{*}\cdot\sigma+\mathbf{D}^{*}\cdot\sigma \qquad (2.28)$$

$\mathbf{F}^{*}\cdot\frac{D\mathbf{T}}{Dt}\cdot\mathbf{F}^{*T}$ can be written as follows using equation (2.24) and $\dot{\mathbf{E}}^{*}=\mathbf{F}^{*T}\cdot\mathbf{D}\cdot\mathbf{F}^{*}$

$$\mathbf{F}^{*}\cdot\frac{D\mathbf{T}}{Dt}\cdot\mathbf{F}^{*T}=\mathbf{C}^{*}:\mathbf{D}^{*} \qquad (2.29)$$

where $\mathbf{C}^{*}=\mathbf{F}^{*}\cdot\mathbf{F}^{*}\cdot\mathbf{C}\cdot\mathbf{F}^{*T}\cdot\mathbf{F}^{*T}$, which is the instantaneous elastic moduli convected with the elastic deformation gradient, permits equation (2.27) to be rewritten as

$$\dot{\sigma}^{\nabla *}=\frac{D\sigma}{Dt}-\Omega^{*}\cdot\sigma+\sigma\cdot\Omega^{*}=\mathbf{C}^{*}:\mathbf{D}^{*}+\mathbf{D}^{*}\cdot\sigma+\sigma\cdot\mathbf{D}^{*} \qquad (2.30)$$

where $\dot{\sigma}^{\nabla *}$ is the Jaumann rate of Kirchoff stress of single crystal based on the elastic spin rate.

The equation (2.30) is satisfactory for finite as well as infinitesimal elastic deformation. The elastic strains are generally small in metal plasticity. So the stress magnitude is small compared to the magnitude of any elastic moduli and furthermore those elastic moduli can be approximated by their ground state values. Under these conditions, $\dot{\sigma}^{\nabla *}$ can be related to the elastic rate of stretching (Hill and Rice, 1972).

$$\dot{\sigma}^{\nabla *}=\mathbf{C}^{*}:\mathbf{D}^{*} \qquad (2.31)$$

The Jaumann stress rate of Kirchoff stress $\dot{\sigma}^{\nabla *}$ with respect to a coordinate that spins with the lattice is defined as

$$\dot{\sigma}^{\nabla^*} = \dot{\sigma} - \Omega^* \cdot \sigma + \sigma \cdot \Omega^* \tag{2.32}$$

where $\dot{\sigma}$ is the material time rate of the Kirchoff stress. The Jaumann stress rate of the Kirchoff stress $\dot{\sigma}^{\nabla}$ that spins with the material is given by

$$\dot{\sigma}^{\nabla} = \dot{\sigma} - \Omega \cdot \sigma + \sigma \cdot \Omega \tag{2.33}$$

The difference between these two expressions is

$$\dot{\sigma}^{\nabla^*} - \dot{\sigma}^{\nabla} = \sum_{\alpha=1}^{n} \dot{\gamma}^{(\alpha)} \cdot \mathbf{B}^{(\alpha)} \tag{2.34}$$

where $\mathbf{B}^{(\alpha)} = \mathbf{W}^{(\alpha)} \cdot \sigma - \sigma \cdot \mathbf{W}^{(\alpha)}$ (2.35)

By using equations (2.16) and (2.31), the constitutive equation can be stated as

$$\dot{\sigma}^{\nabla} = \mathbf{C}^* : \mathbf{D} - \sum_{\alpha=1}^{n} \dot{\gamma}^{(\alpha)} \mathbf{R}^{(\alpha)} \tag{2.36}$$

where $\mathbf{R}^{(\alpha)} = \mathbf{C}^* : \mathbf{P}^{(\alpha)} + \mathbf{B}^{(\alpha)}$ (2.37)

For a strain rate dependent material of the single crystal, the slip rate of the α–th slip system is assumed to be related to the resolved shear stress by the power law (Pan and Rice, 1983)

$$\dot{\gamma}^{(\alpha)} = \dot{a}^{(\alpha)} \left[\frac{\tau^{(\alpha)}}{\tau_c^{(\alpha)}} \right] \left[\left| \frac{\tau^{(\alpha)}}{\tau_c^{(\alpha)}} \right| \right]^{(1/m)-1} \tag{2.38}$$

where m is the rate sensitivity parameter, $\tau_c^{(\alpha)}$ is the critical resolved shear stress for the slip system α, $\dot{a}^{(\alpha)}$ is a reference strain rate on each slip system. The resolved shear stress on the slip system is $\tau^{(\alpha)} = s^{(\alpha)*} \cdot \sigma \cdot m^{(\alpha)*}$. The shear rate in each slip system is uniquely determined by power law equation (2.38), and is nonvanishing as long as the resolved shear stress on that system is not identically zero. The critical resolved shear stress $\tau_c^{(\alpha)}$ for each slip system of the material increases with plastic deformation due to work

hardening. The hardening curve needs to be determined for each possible slip system so that $\tau_c^{(\alpha)}$ can be expressed as a function of the plastic shear in that slip system $\tau_c^{(\alpha)} = g(\gamma^{(\alpha)})$. However, when more than one slip system is active, hardening in each slip system is a cumulative effect of slip in all the active slip systems. For a rate dependent model, the rate of increase of the function $\tau_c^{(\alpha)}$ has therefore been specified as (Peirce et al., 1982)

$$\dot{\tau}_c^{(\alpha)} = \sum_{\beta=1}^{n} h_{\alpha\beta} \left| \dot{\gamma}^{(\beta)} \right| \tag{2.39}$$

The form of hardening moduli $h_{\alpha\beta}$ matrix commonly used is (Hutchinson, 1970)

$$h_{\alpha\beta} = qh + (1-q)h\delta_{\alpha\beta} \tag{2.40}$$

Hardening that occurs in a slip system due to shear in another slip system is referred to as latent hardening as opposed to self-hardening which occurs due to self-activation. The parameter q is the ratio of latent hardening to self-hardening. The hardening rate, h is the rate of change of critical resolved shear stress with shear strain. Three types of hardening curve were used in our implementation to model hardening in single crystals. For materials that exhibit very small strain hardening, the hardening rate decreases rapidly to zero, and the critical resolved shear stress reaches a saturation value τ_s. The hardening curve $\tau_c(\gamma)$ and hardening rate $h(\gamma)$ for single slip in such materials are often represented using the following equations

$$\tau_c(\gamma) = \tau_0 + (\tau_s - \tau_0)\tanh\left(\frac{h_0\gamma}{\tau_s - \tau_0}\right) \text{ and } h(\gamma) = h_0 \sec h^2\left(\frac{h_0\gamma}{\tau_s - \tau_0}\right) \tag{2.41}$$

For materials that exhibit significant hardening, a power law equation is more appropriate to represent the hardening behavior (Peirce et al., 1982). The hardening curve $\tau_c(\gamma)$ and

hardening rate h(γ) are given below, where n is the hardening exponent.

$$\tau_c(\gamma) = \tau_0\left(\frac{h_0\gamma}{n\tau_0}+1\right)^n \text{ and } h(\gamma) = h_0\left(\frac{h_0\gamma}{n\tau_0}+1\right)^{n-1} \tag{2.42}$$

The following formula is used in the case of material showing hardening at large strain; so even at the large strain, material possesses the hardening rate h_s.

$$\tau_c(\gamma) = \tau_0 + h_s\gamma + (\tau_s - \tau_0)\tanh\left(\frac{(h_0 - h_s)\gamma}{(\tau_s - \tau_0)}\right) \text{ and}$$

$$h(\gamma) = h_s + (h_0 - h_s)\sec h^2\left(\frac{(h_0 - h_s)\gamma}{(\tau_s - \tau_0)}\right) \tag{2.43}$$

Deformation in Single Crystals

If a single crystal specimen is pulled in a tension test, the deformation obtained is neither homogeneous nor isotropic. Gliding along their crystallographic planes moves some portions of the crystal with respect to each other whereas regions between consecutive glide planes remain unchanged. The extent of the glide amounts to 0.1-1 (μm) and the distance between two consecutive glide planes is several microns (Kovacs and Zsoldos, 1973).

Investigations carried out on a great variety of materials have shown that those crystallographic planes, in which the atoms are arranged in a close-packed layer, always act as glide planes and that within these planes only well defined glide directions exist. Thus, for example, in a hexagonal single crystal the glide usually takes place along the (001) basal plane in the direction of the three hexagonal diameters.

The active glide plane of FCC crystals is usually one of the {111} planes and the glide takes place in the <110> directions. Four possible glide planes and three possible

slip directions make twelve different slip systems. Every slip system has an equivalent glide possibility. The active glide plane of bcc crystals may be usually one of {110}, {112} and {123} planes and the glide takes place in the <111> directions. However, glide systems are not unique in BCC crystals.

One of the usual methods of plastic deformation in metals is slipping which occurs by the gliding of blocks of the crystal over one another along definite crystallographic planes, called slip planes. Slip along a slip plane occurs in response to shear stress on that plane. Figure 2-3 is a schematic drawing to illustrate the slipping mechanism of single crystals when the crystals are loaded in a tensile test. Slip in a single crystal is initiated when the resolved shear stress on some slip system reaches critical value τ_c. Resolved shear stress τ_R on the slip plane to the slip direction can be described as follows.

$$\tau_R = (P/A) \cos\lambda \cos\alpha \tag{2.44}$$

where P is the axial loading in single crystals, A is a cross-sectional area of single crystal, α is the angle between the slip plane normal direction and loading direction, and λ is the angle between the slip direction vector and loading direction.

Latent hardening effect is a crucial factor in the deformation process of single crystals. Under the assumption initial yield stress of all the slip systems is same, geometrical conditions will completely determine the activation of slip systems. However, experimental results do not advocate this assumption.

The tensile test is performed in single slip orientation. The tensile axis reaches the symmetric borderlines with secondary slip systems. Theoretically the tensile axis should not pass this symmetric line and stay at the symmetric point between two slip systems. However, the tensile axis actually overshoots the symmetric boundary line as observed in

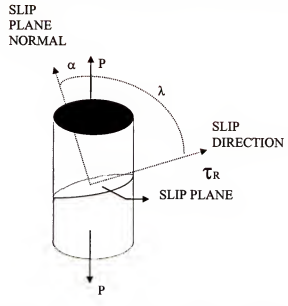

Figure 2-3 Schematic used for the illustration of slip mechanism in single crystals

the experiment. This overshoot phenomenon implies stronger hardening in the secondary slip system. This phenomenon is called latent hardening. Slip systems are hardened by slip on other systems. Because of strong latent hardening effects, the tensile axis overshoots the symmetric boundary line and secondary slip systems need a larger resolved shear stress to overcome strong latent hardening.

The Solution Procedure

An integration procedure for rate dependent constitutive formulas is explained in this section. It is a generally well known that the rate dependent constitutive equations of elastic-plastic materials are mathematically stiff (Nagtegaal et al., 1974). To overcome inherent stiff property of rate sensitivity constitutive equations and use efficient integration algorithms, numerous integration schemes have been applied in the area of finite element analysis of elastic-plastic material (Simo and Taylor, 1985, 1986; Moran et

al., 1990). An explicit integration procedure obtains the solution at time $t+\Delta t$ using the equilibrium conditions at time t whereas an implicit integration procedure obtains the solution at time $t+\Delta t$ using the equilibrium conditions at time $t+\Delta t$. The stability of explicit integration formulas is reduced so that the number of time steps required in finite element codes becomes excessive. An implicit method that solves nonlinear equations iteratively can be applied to obtain stability for stiff systems. The Newton-Raphson method is generally used for solving nonlinear equations by iteration. This category includes backward Euler, midpoint rule and higher order backward difference formulas. Many implicit methods yield unconditional stability, at the several iterations per time step.

Intermediate between explicit and implicit methods are forward gradient schemes, in which at least one of the dependent variables is expanded about the current time in a first order of Taylor series. The result is a linear equation for the increment in the appropriate variable, and this method might be categorized as semi-implicit. Since no iteration is necessary, forward gradient methods require less work per time step than implicit integrators, but, in general, they are not unconditionally stable. Hence, they require more time steps for a given problem. One advantage of forward gradient methods is that they fit in very naturally with tangent modulus finite element formulations.

A standard forward gradient procedure is explained and applied into the rate dependent constitutive equation of crystalline in this section (Peirce et al., 1983).

Suppose that all state variables are known at time t and we need to obtain them at time t+dt. Changes in all state variables during time increment Δt should be calculated.

During this time period, the strain rates are assumed to be constant variables. Hence, the strain increments from t to t+dt are

$$\Delta\varepsilon = \dot{\varepsilon}\Delta t \tag{2.45}$$

The increment in effective plastic strain $\Delta\gamma$ is taken to be

$$\Delta\gamma = \Delta t\left[(1-\alpha)\gamma_t + \alpha\gamma_{t+\Delta t}\right] = \Delta t\left[\gamma_t + \alpha\left(\gamma_{t+\Delta t} - \gamma_t\right)\right] \tag{2.46}$$

where the parameter α is used to represent the degree of implicitness of the time integration scheme. The explicit integration scheme is represented by $\alpha=0$, and $0<\alpha<1$ represents the implicit integration scheme. The function $\gamma_{t+\Delta t}$ is replaced by the first order of Taylor series about time t. For the constitutive equation (2.38), the rate of resolved shear strain is a function of resolved shear stress and critical resolved shear stress.

$$\gamma_{t+\Delta t} = \gamma_t + \frac{\partial\gamma_t}{\partial\tau_t}\frac{\partial\tau_t}{\partial t}\Delta t + \frac{\partial\gamma_t}{\partial g_t}\frac{\partial g_t}{\partial t}\Delta t \tag{2.47}$$

Application of this formula to the constitutive formula equation (2.38) will lead to the following formula.

$$\dot{\gamma}^{(\alpha)}_{t+\Delta t} = \operatorname{sign}\left(\tau^{(\alpha)}_t\right)\dot{\gamma}^{(\alpha)}_0\left|\frac{\tau^{(\alpha)}_t}{g^{(\alpha)}_t}\right|^{\frac{1}{m}}\left[1+\frac{1}{m}\left(\frac{\Delta\tau^{(\alpha)}}{\tau^{(\alpha)}_t} - \frac{\Delta g^{(\alpha)}}{g^{(\alpha)}_t}\right)\right] \tag{2.48}$$

where $\Delta\tau^{(\alpha)} = \dot{\tau}^{(\alpha)}_t\Delta t \quad \Delta g^{(\alpha)} = \dot{g}^{(\alpha)}_t\Delta t$

Next, we calculate the resolved shear stress $\tau^{(\alpha)}$ on a slip system. For slip system α, the normal to the slip plane is $\mathbf{m}^{*(\alpha)}$. Therefore, the traction vector $\mathbf{t}^{(\alpha)}$ on this slip plane is

$$\mathbf{t}^{(\alpha)} = \sigma\mathbf{m}^{*(\alpha)} \tag{2.49}$$

where σ is the Cauchy stress.

The resolved shear stress $\tau^{(\alpha)}$ is the component of $\mathbf{t}^{(\alpha)}$ in the slip direction $\mathbf{s}^{*(\alpha)}$.

$$\tau^{(\alpha)} = \mathbf{s}^{*(\alpha)} \cdot \boldsymbol{\sigma} \cdot \mathbf{m}^{*(\alpha)} = \boldsymbol{\sigma} \cdot \mathbf{P}^{(\alpha)} \tag{2.50}$$

The material time derivative of the resolved shear stress is expressed as follows.

$$\dot{\tau}^{(\alpha)} = \dot{\boldsymbol{\sigma}} \cdot \mathbf{P}^{(\alpha)} + \boldsymbol{\sigma} \cdot \dot{\mathbf{P}}^{(\alpha)} \tag{2.51}$$

Using the co-rotational rates spin with the lattice, the material time derivative of the resolved shear stress is expressed as follows.

$$\dot{\tau}^{(\alpha)} = \mathbf{P}^{\nabla *(\alpha)} \cdot \dot{\boldsymbol{\sigma}} + \mathbf{P}^{(\alpha)} \boldsymbol{\sigma}^{\nabla *} \tag{2.52}$$

where $\mathbf{P}^{\nabla *(\alpha)} \cdot \dot{\boldsymbol{\sigma}} = \mathbf{B}^{(\alpha)} \cdot \mathbf{D}^{*}$

Finally, the material time derivative of the resolved shear stress is expressed as follows.

$$\dot{\tau}^{(\alpha)} = \left(\mathbf{C}^{*} : \mathbf{P}^{(\alpha)} + \mathbf{B}^{(\alpha)}\right) \cdot \mathbf{D}^{*} = \mathbf{R}^{(\alpha)} \cdot \mathbf{D}^{*} \tag{2.53}$$

The final form of the material time derivative of the resolved shear stress is substituted to increment of resolved shear stress, i. e. $\Delta\tau = \dot{\tau}_t \Delta t$

$$\Delta\tau^{(\alpha)} = \mathbf{R}_t^{(\alpha)} \cdot \mathbf{D}\Delta t - \mathbf{R}_t^{(\alpha)} \cdot \sum_{\beta=1}^{n} \mathbf{P}_t^{(\beta)} \dot{\gamma}_t^{(\beta)} \Delta t \tag{2.54}$$

The slip resistance $g^{(\alpha)}$ is taken to evolve as $\dot{g}^{(\alpha)} = \sum h_{\alpha\beta} \left|\dot{\gamma}^{(\beta)}\right|$. Inserting of hardening evolution formula into $\Delta g = \dot{g}(t)\Delta t$ gives the following formula of increment of slip resistance.

$$\Delta g^{(\alpha)} = \sum_{\beta=1}^{n} (h_{\alpha\beta})_t \dot{\gamma}_t^{(\beta)} \operatorname{sign}\left(\dot{\gamma}_t^{(\beta)}\right) \Delta t \tag{2.55}$$

Inserting $\dot{\gamma}_{t+\Delta t}$ formula and $\dot{\gamma}_t$ formula into equation (2.46) gives an estimate for the increment of resolved shear strain as follows.

$$\Delta\gamma^{(\alpha)} = \dot{\gamma}_t^{(\alpha)} \Delta t + \frac{\alpha \Delta t \dot{\gamma}_t^{(\alpha)}}{m} \left\{ \frac{\Delta\tau^{(\alpha)}}{\tau_t^{(\alpha)}} - \frac{\Delta g^{(\alpha)}}{g_t^{(\alpha)}} \right\} \tag{2.56}$$

Rearranging equation (2.56) yields

$$\sum_{\beta=1}^{n}(N_{\alpha\beta})_t \Delta\gamma^{(\beta)} = (\dot{\gamma}_t^{(\alpha)} + \mathbf{Q}_t^{(\alpha)} : \mathbf{D})\Delta t \tag{2.57}$$

where

$$(N_{\alpha\beta})_t = \delta_{\alpha\beta} + \left(\frac{\alpha\Delta t\dot{\gamma}_t^{(\alpha)}}{m}\right)\left(\frac{\mathbf{R}_t^{(\alpha)} : \mathbf{P}_t^{(\beta)}}{\tau_t^{(\alpha)}} + \text{sign}(\tau_t^{(\beta)})\frac{(h_{\alpha\beta})_t}{g_t^{(\alpha)}}\right) \tag{2.58}$$

$$\mathbf{Q}_t^{(\alpha)} = \left(\frac{\alpha\Delta t\dot{\gamma}_t^{(\alpha)}}{m\tau_t^{(\alpha)}}\right)\mathbf{R}_t^{(\alpha)} \tag{2.59}$$

Inverting of equation (2.57) gives following formulas of increment of resolved shear strain of slip system.

$$\Delta\gamma^{(\beta)} = \sum_{\beta=1}^{n}(N_{\alpha\beta}^{-1})_t(\dot{\gamma}_t^{(\alpha)} + \mathbf{Q}_t^{(\alpha)} \cdot \mathbf{D})\Delta t = (\hat{\mathbf{f}}_t^{(\alpha)} + \mathbf{F}_t^{(\alpha)} \cdot \mathbf{D})\Delta t \tag{2.60}$$

where

$$\hat{\mathbf{f}}_t^{(\alpha)} = \sum_{\beta=1}^{n}(M_{\alpha\beta})_t \dot{\gamma}_t^{(\beta)} \tag{2.61}$$

and

$$\mathbf{F}_t^{(\alpha)} = \sum_{\beta=1}^{n}(M_{\alpha\beta})_t \mathbf{Q}_t^{(\beta)} \tag{2.62}$$

where $M_{\alpha\beta}$ is the inverse of the slip system matrix $N_{\alpha\beta}$.

In the rate dependent formulation, the slip rates on each slip system are uniquely specified. In the rate tangent-modulus formulation, the time step Δt can always be taken small enough so that the Kronecker delta in the matrix $N_{\alpha\beta}$ equation (2.58) dominates.

Next, the kinematic formulations in our finite element program are assumed to be written to provide an approximate integration of the rate of stretching and the co-rotational terms

in the Jaumann rate of Kirchoff stress, so that we are given an estimate of $\Delta\varepsilon$ corresponding to the integral of the stretching **D** over the time increment Δt. We need not concern ourselves with the co-rotational terms in calculating the increment. Then by substituting equation (2.60) into the governing equation (2.36), we have the incremental form

$$\Delta\sigma = \overline{\mathbf{C}} \cdot \Delta\varepsilon - \sum_{\alpha=1}^{n} \mathbf{R}_t^{(\alpha)} \hat{\tau}_t^{(\alpha)} \Delta t \tag{2.63}$$

where

$$\overline{\mathbf{C}} = \mathbf{C}^* - \sum_{\alpha=1}^{n} \mathbf{R}_t^{(\alpha)} \mathbf{F}_t^{(\alpha)} \tag{2.64}$$

where $\overline{\mathbf{C}}$ is the tangent stiffness matrix. Isotropic elasticity matrix is used for numerical simplicity. Note that the fourth order tensor represented by **RF** is nonsymmetric since N matrix is in general nonsymmetric. The incremental modulus $\overline{\mathbf{C}}$, which depends on the material properties, the stress and also the parameter, is reduced considerably from the elastic stiffness matrix $\mathbf{C}^*$. This permits larger strain increments while producing moderate stress increments. Therefore this leads to improved numerical stability. It should be noted that this tangent stiffness matrix reflects the structure of the underlying constitutive equations. The moduli $\overline{\mathbf{C}}$ do not possess the symmetry in general.

Once the increments of resolved shear strain in slip systems are calculated critical resolved shear stress is updated as follows.

$$g_{t+\Delta t}^{(\alpha)} = g_t^{(\alpha)} + \Delta g^{(\alpha)} \tag{2.65}$$

Next the plastic deformation gradient is also updated as follows.

$$\mathbf{F}_{t+\Delta t}^{p} = \mathbf{F}_t^{p} + \Delta\mathbf{F}^{p} \tag{2.66}$$

where

$$\Delta \mathbf{F}^{P} = \sum_{\alpha=1}^{n} \Delta\gamma^{\alpha} (\mathbf{s}^{\alpha} \cdot \mathbf{m}^{\alpha T}) \mathbf{F}_{t}^{p} \tag{2.67}$$

It is assumed that the finite element program supplies the total deformation gradient $\mathbf{F}$. Using the computed plastic part of deformation gradient $\mathbf{F}^{p}$, the elastic deformation $\mathbf{F}^{*}$ is calculated by equation (2.7). Using the elastic part of deformation gradient $\mathbf{F}^{*}$, the slip vector $\mathbf{s}^{*(\alpha)}$ and $\mathbf{m}^{*(\alpha)}$ are obtained by using equations (2.8) and (2.9). The intermediate tensors $\mathbf{P}^{(\alpha)}, \mathbf{W}^{(\alpha)}, \mathbf{B}^{(\alpha)}, \mathbf{R}^{(\alpha)}$ obtain values by equations (2.18), (2.19), (2.35) and (2.37). A new current status is thus defined and again the incremental equations are solved for the displacement increments for the next step.

All these procedures are implemented in ABAQUS through the user material subroutine UMAT. The time steps must remain small to accurately track the evolution of the state variables. Therefore many time steps are required to model the deformation, but the integration procedure is so simple that equilibrium is often achieved in the first iteration. Strain increments and state variables are determined at the beginning of increment. The user provides formulation for the tangent stiffness matrix to solve the equilibrium equations in UMAT. Newton's method is used to solve the nonlinear equilibrium equations in ABAQUS. Stress increments are calculated by equation (2.63). The deformation gradient increment is calculated and updated using deformation and stress histories. And then whole geometric components and internal state variables are updated. Updated variable including strain, stress, deformation gradient at the end of the increment will be the states of beginning of the next increment. These whole steps are repeated until it reaches the final prescribed strain. The time step between the increments

is automatically controlled by ABAQUS. The user specifies the minimum, maximum and initial suggested time increment.

CHAPTER 3
LITERATURE REVIEW

Previous Study of Localization Phenomena

Understanding of localized deformations in single crystals is of importance due to the its possible correlation with an initiation of fractures of single crystals. Localized deformation has generally been associated with shear localization. Uniform deformations are observed at the initial stages of deformation, i. e. before the plastic deformation initiates. As the deformations enter the plastic deformation regime, ductile single crystals usually display inhomogeneous status that is usually distinguished as localized modes such as necking, shear bands and kink bands. Shear band has been observed in a large number of crystalline, metals, glasses, polymers and rocks. Numerous researchers have studied localization phenomena and recognized their crucial role as precursors of upcoming fracture. There are numerous examples in which plastic flow in crystal transits from a homogeneous mode of deformation to one that is strongly concentrated in narrow localized band. Shear localization is often associated with strain softening such as microvoid initiation and growth, microcrack formation (Tvergaard, 1981). Thermal softening is usually found at high strain rates. Nonuniform plastic deformation produces nonuniform heat. This nonuniform heating promotes local thermal softening. For instance, forging processes that accompany much friction inside the material and between die and material may show localization by thermal softening effect. Zhu and Batra (1993) analyzed dynamic shear bands including thermal softening effects in an FCC single

crystal. The shear localization is often interpreted as the loss of work hardening of material due to the imperfections or material changes. However, it is well recognized that shear localization can be initiated in damage-free, strain hardening materials.

Hill and Hutchinson (1975) investigated the development of the localized deformation zones in plane strain deformation problems theoretically in rate independent frame. Bifurcation problems in tensile test have been studied for an incompressible solid. They suggested the possibility that localization is a result of a constitutive instability and is predictable from the pre-localized constitutive law relating stress increments to strain increments. The constitutive specifications are characterized by two instantaneous moduli, μ and μ^*. μ is a modulus for shearing parallel to the coordinate axes and μ^* is a modulus for shearing at 45 degrees to them. They reported the variety of possible bifurcations including necking and initiation of shear band is associated with loss of ellipticity in the governing equation.

Tvergaard et al. (1981) analyzed flow localization in the plane strain tensile test numerically. They pointed out that it is natural to see in no tendency for intense localized shearing in the previous studies (McMeeking and Rice, 1975; Burke and Nix, 1979) that used simple smooth yield surface theory of plasticity to characterize material behavior. The classical elastic-plastic solid with a smooth yield surface is quite resistant to localized deformation. They employed J_2 corner theory (Christoffersen and Hutchinson, 1979) as a yielding condition. The assumption, embodied in the classical theory of plasticity, of a smooth yield surface is at variance with models for polycrystalline aggregates based on single crystal slip. The discreteness of slip systems in each grain leads to the prediction of a yield surface vertex. A long-wave length of initial

imperfection grows into the well-known necking mode and subsequently at sufficiently large strain level bands of intense shear deformation develops in the necking region.

Asaro and Rice (1977) discussed about the possibility of localization other than due to the strain softening. Localization phenomena in metals are usually interpreted by strain softening due to the loss of hardening at a certain amount of strain. However, Price and Kelly (1964) reported observation of localization during the positive hardening. Asaro and Rice investigated the possibility of localization in positive hardening regimes for single crystals. Shear band formation was viewed as a material constitutive instability and strongly depended on material constitutive law. In order to understand the physical origin of shear band formation, bifurcation model conditions have been analyzed as a function of slip geometry, applied stress level and strain hardening behavior of the materials. The criterion for shear band formation through bifurcation analysis was reported as follows. Localized deformation occurs when the plastic strain hardening modulus h falls into critical value h_{crit}.

Inhomogeneous deformation in single crystals was studied by using a simple double symmetric slip model (Asaro, 1979). Single crystals undergoing multiple slip naturally present the prime model for yield vertex structure in the rate independent frame. He showed that loading path change from tensile to combined tensile-shear mode may lead to the elastic-plastic response at the vertex and smooth yield surface leads to elastic response. These results suggest that vertexes can lead to localized shearing. In addition to vertices there are other geometric effects, associated with the rotation of the crystal's lattice during deformation.

Chang and Asaro (1980) performed experimental work on Al-Cu single crystals to confirm their analytical predictions (Asaro, 1979) regarding the condition for localization and the effects of lattice rotation. X-ray diffraction uncovered that the lattice within the localized band has finite lattice rotations. Local lattice rotations cause softening within a band. Softening by lattice rotation is called geometrical softening.

Peirce et al. (1982) reported numerical analysis using finite element method of rate independent single crystal model as a continuation of work on their theoretical research (Asaro 1979). Shear band was observed through numerical analysis and lattice rotation was a main contributor for shear localization like they predicted through their analytical model and experiment. Shear band was formed immediately after necking occurs. The pattern of shear band was influenced by the initial imperfections. Numerical results were well matched with experiment for high strength, low hardening crystals. Patchy type of slip was reported when high value of latent hardening ratio was used.

The rate dependent formulations for single crystals were employed by Peirce et al. (1983). Such models make it possible to study the effect of properties such as strain rate sensitivity, hardening properties and crystal geometry that can not be studied using previously used rate independent models. High strain rate sensitivity delays formation of shear band. Strong latent hardening ratio for instance 1.8 prevents shear band from propagating in the specimen. When the slip system is inclined more than 45 degrees form tensile axis shear band was not formed on the active slip systems because lattice rotation leads to the decrease of resolved shear stress in the active slip system.

Most of the previous study on shear band formation in single crystals concentrated on FCC structures. Deve et al. (1988) extended their study on shear band formations in

BCC single crystal structures of internally nitrided alloys Fe-Ti-Mn. Shear band was formed in experimental studies and numerical simulation due to the geometric softening of the lattice.

Harren et al. (1988) performed experimental work and finite element analysis to study localization in plane strain compression tests. They also found that lattice rotation caused the geometric softening even during the hardening process.

Zbib et al. (1992) studied shear banding under dynamic loading in three-dimensional geometry. Shear band is observed in many manufacturing processes such as production at high strain rates and explosive forming penetration other than just quasi-static loading conditions like tensile test. They considered two constitutive models for the shear band formation analysis. Thermoviscoplasticity and elastoviscoplasiticity types of constitutive relations were used. They included thermal softening effects in their constitutive model due to the adiabatic heating for thermoviscoplasticity model. Strain softening behavior for elastoplasiticity may due to the thermal softening, damage degradation and texture softening was included. They concluded that initial imperfections and a softening terms in the constitutive equations are the main contributors for forming the shear band in their three dimensional analysis under dynamic loading.

Zhang et al (1994) studied inhomogeneous plastic deformation in ductile single crystals using so-called discrete slip model. Most of finite element analysis in the single crystals assume that the crystal is a homogeneous media but they pointed out that slip lines are distributed randomly on the whole crystal length with slip line density depending on the strain. Their discrete slip model differs from other model in that the spatial material heterogeneities as imperfections to reflect the influence of the

microscopic inhomogeneity on the plastic deformation. The crystal is divided into lots of bands in which critical resolved shear stress distributes randomly. Each band parallel to the slip planes is taken as crystal, which the crystal constitutive laws are in force.

Kink bands are another localized phenomena in single crystals. Fraser et al. (1973b) reported kink band in the compression tests of hard oriented NiAl single crystals. They reported that kink band is associated with the [010](101) or [010] $(\bar{1}01)$. Lattice rotations are caused by the constraints of the compression test. Geometric softening occurs due to the lattice rotation and causes the localized deformations.

Previous Study on Hardening of the Single Crystals

Many authors studied the interactions among the slip systems in FCC crystals (Kocks, 1964; Basinski and Basinski, 1979; Franciosi et al., 1980). From microscopic viewpoint of the deformed single crystals, they regard hardening of single crystals as the results of dislocation interactions between slip systems. Internal dislocation density and short range interacting dislocation strengths are the main parameters of the hardening analysis. Two methods are used to measure the latent hardening ratios. The first method is a measure of overshoot angles of conjugate slip system to predict amounts of latent hardening. The second method is comparing the yield stress of previously latent slip to the flow stress of primary slip.

Latent hardening test for aluminum single crystals was done by Kocks and Brown (1966). Latent hardening ratio was obtained by comparing flow stress of primary slip system and secondary slip system. Slip systems were divided into two groups. Slip systems in the primary slip plane showed similar flow stress with primary slip system. Other planes showed increase of flow stress by 10 to 30 %.

Jackson and Basinski (1967) performed latent hardening test on copper single crystals. When hardening in slip planes that are not the primary slip plane was tested, latent hardening ratio greater than one was obtained. Latent hardening ratios ranged from 2.5 in stage I to 1.4 in stage II.

Nakada and Keh (1966) studied latent hardening of iron single crystals. Latent hardening ratio was found greater than one. They concluded latent hardening was due to either the elastic interaction between glide and forest dislocations or the lack of mobile dislocations in the latent system.

In Franciosi et al. (1982), critical resolved shear stress was expressed mainly as a function of dislocation interaction coefficients [a] matrix and dislocation density ρ. They defined slip interactions using [a] matrix. Contents of [a] matrix were classified by dislocation junction such as sessile, glide, hirth lock, no junction and self-hardening according to the slip interactions between the corresponding two slip systems. For the rate dependent approach, Franciosi (1985) showed that hardening matrix [h] could be explained by [a] matrix, which represents dislocation interactions between slip systems.

Weng (1987) proposed his modified hardening law. Latent hardening ratio was determined by considering the angles between the slip systems. He pointed out that the widely used "two-parameter rule", $h_{\alpha\beta} = qh + (1-q)h\delta_{\alpha\beta}$, by Hutchinson (1970) and Asaro (1983) can not distinguish between forward and reversed slip and between acute and obtuse cross slip. He also mentioned that "undershoot" often observed in the experiment might not be predicted using two-parameter rule, which has strong latent hardening. Isotropic hardening, kinematic hardening, strong latent hardening and

Baushinger effects could be implemented into his model. He devised the following formula to express latent hardening ratios.

$$g_{ij} = \alpha_1 + (1-\alpha_1)\cos\theta_{ij}\cos\phi_{ij} + (\alpha_2 \sin\theta_{ij} + \alpha_3 \sin\phi_{ij}) \tag{3.1}$$

where θ_{ij} is the angle between the slip directions of the i-th and j-th systems. ϕ_{ij} is the angle between the slip plane normals of the i-th and j-th systems. α_1 is the degree of isotropy in work hardening and α_2 represents the anisotropic departure for the latent hardening of coplanar systems and α_3 is the additional departure for the intersection ones.

Bassani and co-workers investigated hardening criterion for multi slip condition in single crystals of FCC metals. Through careful physical observation of experiment on latent hardening measurement in the symmetrically loaded orientation of copper single crystals, they suggested following facts. Hardening in secondary slip system may lower than that in active slip system. Rapid increase of hardening rate is observed when secondary slip system is activated. Hardening behaviors change according to loading orientation.

They pointed out that widely used hardening rule, $h_{\alpha\beta} = qh + (1-q)h\delta_{\alpha\beta}$, by Hutchinson (1970) and Asaro (1983) can not predict stage II deformation of FCC crystals.

Bassani and Wu (1991) devised phenomenological hardening law based on their observations as follows.

$$h_{\alpha\alpha} = F(\gamma_\alpha)G(\gamma_\beta) \tag{3.2}$$

$$h_{\alpha\beta} = qh_{\alpha\alpha} \tag{3.3}$$

where h is the instantaneous hardening modulus. $h_{\alpha\alpha}$ represents diagonal terms of the hardening matrix and $h_{\alpha\beta}$ represents off-diagonal terms of hardening matrix.

$$F(\gamma^{\alpha}) = (h_0 - h_{\infty})\sec h^2\left[\frac{(h_0 - h_{\infty})\gamma^{\alpha}}{(\tau_1 - \tau_0)}\right] + h_{\infty} \tag{3.4}$$

$$G(\gamma^{\beta}) = 1 + \sum_{\beta=1,\beta\neq\alpha}^{n} f_{\alpha\beta}\tanh(\frac{\gamma^{\beta}}{\gamma_0}) \tag{3.5}$$

where F is the instantaneous hardening modulus under independent single slip α and G is the term represents the interactive latent hardening. G is the function of total slips except on α slip. In their hardening model, unlike the conventionally used latent hardening effects describing coupling between the two slip systems, functional form G describes interactions between slip systems has been multiplied to the self hardening modulus of hardening matrix. Whereas in Asaro's hardening model latent hardening effect has been represented by off diagonal terms through higher value of latent hardening. With this hardening formula transition from stage I to stage II in FCC crystals and orientation dependence of hardening can be explained but positive definite of hardening matrix is not guaranteed after material softening happens.

In the study of hardening characteristics of NiAl single crystals higher hardening at the large strain regime was observed in the [110] orientation (Levit et al., 1996). Asaro's hardening formula was used to represent the higher hardening in 2-DIM using two slip systems in {100} slip planes. Hardening rate formula used is as follows $h(\gamma) = h_0\sec h^2(\frac{h_0\gamma}{\tau_s - \tau_0})$. From this simple formula higher hardening and transition to higher hardening at large strain may not be expected. Even using power law type hardening law which has a higher hardening rate, the same results were obtained.

For BCC crystals Franciosi (1983) proposed hardening law as an extension of FCC crystal's hardening law. They assumed {110} and {121} slip planes are activated. Total critical resolved shear stress of the crystals is expressed as the summation of critical resolved shear stress of each different type of slip system. Between two different slip systems latent hardening curves are described by four formulas. For instance, if we have two slip systems A and B, latent hardening ratios are described by $\frac{\tau^{AS}}{\tau^{AP}}, \frac{\tau^{BS}}{\tau^{BP}}, \frac{\tau^{AS}}{\tau^{BP}}, \frac{\tau^{BS}}{\tau^{AP}}$. Here p means primary slip system s means secondary slip system.

CHAPTER 4
LOCALIZATION PHENOMENA IN NIAL SINGLE CRYSTALS

Finite Element Model for Localization Problem

An ordered intermetallic compound NiAl single crystal has a lattice structure similar to body centered cubic crystal and shows distinct slip systems at different temperatures. In general, NiAl single crystals exhibit two significantly different types of slip behavior depending on orientation. Along the <100> loading orientation, defined as hard orientation, slip systems have almost zero resolved shear stress along <100> burgers vector. Therefore, a main operative slip vector is <111> at low and intermediate temperatures and a combination of <100> and <110> at high temperatures as a result of non-<100> slip vectors activation hard orientation exhibit much higher flow stress than soft orientation. Non-<100> orientation is defined as soft orientation when loaded along soft orientations. NiAl single crystals deform mainly by shear along <100>burgers vectors.

For the localization analysis in single crystals, the following initial thickness inhomogeneity is taken (Tvergarrd et al., 1981).

$$\Delta h_0 = h_0(-\bar{\xi}_1 \cos(\frac{\pi x^2}{L_0}) + \bar{\xi}_2 \cos(\frac{m\pi x^2}{L_0})) \tag{4.1}$$

where $\bar{\xi}_1$ and $\bar{\xi}_2$ are prescribed imperfection amplitudes and m is a wave number.

We used following specimen model for the simulation, where dimension is, 22(mm) long, 5(mm) wide and 2.0 (mm) thick. This is the same dimensions used to investigate macroscopic deformation processes of NiAl single crystal. The actual specimen includes two flanges where the outer flanges are used to hold the specimen in the tensile testing machine. But for the finite element analysis only the inner flanges are included. Loading has been imposed by a prescribed constant displacement rate with the following formula, $\dot{U} = \dot{a}L_0$, at the all nodes of the top edge of specimen, where L_0 is the total length of specimen, $\dot{a}$ is the strain rate and $\dot{U}$ is the displacement rate. All nodes at the top edge of specimen were specified to have the same displacement in the loading direction. Incompatible plane stress element (CPS4I) in ABAQUS was used to capture possible localizations. This incompatible mode element has an extra deformation mode to facilitate localized deformation (ABAQUS, 1994). 1640 elements were used for this simulation.

Table 4-1 Simulation data used for NiAl single crystals for localization problem at 200°C

Elastic bulk Modulus K (MPa)	Shear Modulus G (MPa)	Poisson's ratio	Imperfection ($\bar{\xi}_1$, $\bar{\xi}_2$, m)
164916.12	68660.79	0.3172	0.0126,0.072,5

The material data used in this simulation is as in table 4-1. Shear modulus G and bulk modulus K are adopted from Miracle (1993). The initial critical resolved shear stress τ_o, saturation strength of material τ_s and initial value of hardening slope H_0 were obtained by curve fitting of hypertangent type hardening curve to the experimental τ_c vs. γ curve.

For the [110] loading directions (figure 4-1) NiAl single crystals mainly deform by activation of {100}<001> slip systems. When the specimen is loaded in <110> direction, the plane of deformation {001} contains burgers vectors, slip plane normal vectors, and tensile axis in either parallel or perpendicular to the thickness of the sample cross section. Axis of rotation is normal to the deformation plane {001}. As a consequence of geometry of slip systems in this loading direction, simulation can be performed by the assumption of planar model. For [110] loading orientation, plane of deformation is (001).

In our planar model, primary slip system is assumed to be (010)[100] and conjugate slip system is assumed to be (100)[010] for loading along [110] orientation. For this geometry, each slip system is inclined 45 degrees with respect to the tensile axis [110] and both slip planes are aligned perpendicular to the plane of deformation and are aligned symmetrically with respect to the loading axes. This symmetry of slip systems makes loading axis stable so no lattice rotations occurs during deformation. Next, boundary conditions are assigned as follows. All nodes at bottom side of specimen are fixed in the y direction, two nodes at the middle of top and bottom side are fixed in the x direction.

Next we consider different loading conditions to simulate hard-oriented specimen of NiAl single crystals in compression test. To imitate the experimental compression test, the bottom side of the specimen was fixed in the y direction and middle node of bottom side was fixed in the x direction too. However, the topside of the specimen had no constraints at all so it can move freely in x direction (figure 4-2).

Double slip ({100}<010> slip system) and single slip ({101}<100> slip system) conditions were investigated to look at the well known kink band formation in NiAl

single crystal (Fraser et al., 1973a, b). Loading direction is a few degrees off from the hard orientation <001>.

For the double slip case (figure 4-2), [010](100) slip system and [100](010) slip system is active and plane of deformation is (001) plane. For the single-slip case (figure 4-3), [010] $(\bar{1}01)$ slip system is active and plane of deformation is (101) plane. When the specimen is loaded a few degrees off from hard orientation <010>, both the plane of deformation for double slip model and the plane of deformation for single slip model contain burgers vector, slip plane normal vector, and tensile axis in either parallel or perpendicular to the thickness of the sample cross section. Therefore, the simulation can be performed using a two-dimensional planar model.

Study of Shear Band Formation in NiAl Single Crystals

We have looked through the previous studies on the localization phenomena in the previous section. Here, localized deformation, especially shear band formation in NiAl, of single crystals have been studied to investigate the characteristics and mechanism of shear band.

NiAl exhibits low ductility and low fracture toughness near room temperature. Significant ductility is obtained only above 200°C. Load versus elongation curve at various temperatures indicates that fracture stress at RT is lower than at 200°C. This seems to suggest that fracture at low temperatures may be initiated by localized deformation such as shear bands (Ebrahimi and Shrivastava, 1997a, b). While macroscopic shear band formation has not been observed experimentally in NiAl, it is possible that fracture may be initiated by a tendency towards localization. In order for a

single crystals to obtain arbitrary plastic strain, it must have at least five independent slip systems (Reid, 1973). The <100> slip directions constitutes only 3 independent slip systems. Insufficient slip systems do not afford the strain compatibility between the grains. As a result, intergranular microcracks are formed and very high internal hydrostatic stress components that provide the driving force for intergranuler crack propagation are developed (Ebrahimi and Hoyle, 1997). To understand the conditions that lead to shear localization as well as the constitutive parameters that play a significant role, numerical simulations performed with varying values of parameters, specimen geometry, orientation and boundary conditions. Previous studies on shear band formation (Peirce et al., 1982, 1983; Deve et al., 1988) indicate that both rate sensitivity and latent hardening significantly influence the formation of shear localization. In this study, these properties as well as the effect of hardening were studied. Results of the numerical simulation indicated that low rate sensitivity and low hardening facilitate shear band formation. The underlying cause for the formation of shear bands is orientation softening that creates a band where lattice rotation has made possible deformation at a lower load. As a result, further deformation localizes in the band causing highly localized shear. Shear bands were simulated numerically for elongation along the neighborhood of [110] direction. As mentioned earlier, no lattice rotation occurs for elongation along the [110] direction. However, at orientations a few degrees to either side of the [110] direction, lattice rotation occurs that tries to rotate the lattice back to the [110] symmetric orientation. Due to the specimen geometry and imposed geometric imperfections, non-uniform deformation occurs. Regions where more lattice rotation occurs become softer thus promoting shear band formation.

Simulations were performed using the hardening law described in chapter 2. Three values of strain rate sensitivity, m=0.006, m=0.01 and m=0.02 were used to show its effects on the shear band formation. $\dot{a}$ =0.0005 s^{-1} was used as a reference shear rate in equation (2.38) for localization problems. Numerical simulation of elongation 3° off from the [110] direction using low work hardening was simulated to show the formation of shear band.

Figure 4-4 shows deformed mesh plots at 12 %, 13.5 %, 15 % nominal strain using strain rate sensitivity m=0.006. Upto 12 % nominal strain deformed mesh shows homogeneous deformation (figure 4-4-a). However after this stage localized shears are accumulated on the deformed mesh (figure 4-4-b). Clear shear bands are observed at 15 % nominal strain (figure 4-4-c). Figure 4-5 shows deformed mesh plots at 12 %, 13.5 %, 15 % nominal strain using strain rate sensitivity m=0.01. Shear bands are observed at 15 % nominal strain (figure 4-5-c). In this case, shear bands are not clear as in case of m=0.006. Figure 4-6 shows homogeneous deformed meshes even at 15 % nominal strain. With higher value of rate sensitivity (figure 4-5 and figure 4-6) no clear shear bands are shown. As can be seen, sharp bands are formed only for low values of rate sensitivity (figure 4-4, m=0.006). However, as mentioned in the early section, the {100}<001> slip system has a high work hardening rate even at large deformation. Both primary slip system and conjugate slip system have a same resolved shear strain regardless of lattice rotation. So, double shear bands can be formed. However, all shear bands occur along the primary slip system due to the initial imperfection of the specimen.

Contour plots of Cauchy strain in figures 4-7, 4-8 and 4-9 indicate that intense localized strains within the shear band. In figure 4-7-c, the most strained regions in the shear bands have 0.45 Cauchy strain when the nominal strain was 15 %. Figure 4-8-c also shows intense localized strain at the middle of specimen. However, in figure 4-9-c, less intense amount of Cauchy strains are observed.

Load vs. elongation plots is shown in figure 4-24. With the lower strain rate sensitivity load drops rapidly and this load drop facilitates the slight necking. Necking begins at the point of plastic instability where the increase of strength due to strain hardening fails to compensate for the decrease in cross-sectional area of specimen. The slight necking facilitate formation of localized band. The lowest strain rate sensitivity in the simulation, m=0.006, shows abrupt load dropping compared to other cases and forms a clear shear band.

Figures 4-10, 4-11 and 4-12 show the contour plots of Cauchy stress in the loading direction. High stress region is first developed from the flange at the first stage of deformation. In the region of shear band formed intense stress is observed with lower strain rate sensitivity at the last stage of deformation (figure 4-10-c).

Figures 4-13, 4-14 and 4-15 show the contour plots of crystal lattice rotations as strain rate sensitivity varies. Lattice rotation causes geometric softening and facilitates the formation of shear band. In figure 4-13-c with low strain rate sensitivity, more lattice rotations occur than other cases at the region of shear band. So, these contour plots explain the role of lattice rotations on the formation of shear band.

Figures 4-16, 4-17 and 4-18 show the contour plots of resolved shear strain of primary slip system. In figure 4-16-c, resolved shear strain in primary slip system is 0.463

when m=0.006 was used for the simulation. Due to the lattice rotation, high resolved shear strain is accumulated at the region where large lattice rotations occurs and therefore softening occurs at this region.

The effect of parameters such as strain-rate sensitivity parameter and the geometry of slip systems have been presented to investigate effects of these parameters on the formation of shear band. As a next step, the effect of hardening characteristics on localization phenomena is presented.

Figure 4-19 shows the effect of work hardening with the moderate value of strain rate sensitivity m=0.02. These plots show that localization can occur even using high value of strain rate sensitivity if the hardening of material shows soft behavior. In figure 4-19-a, severe localization occur at the center of specimen whereas homogeneous deformation is shown along the whole specimen in figure 4-19-b and figure 4-19-c.

Contour plots of Cauchy strain, Cauchy stress, resolved shear strain and lattice rotations are shown in figure 4-20, figure 4-21, figure 4-22 and figure 4-23 respectively. With high value of saturation hardening τ_s, no localized lattice rotations are observed. Therefore, localization does not occur.

Lower strain rate sensitivity facilitates localization. However, even with the lower strain rate sensitivity m=0.006, localization is prevented when higher work hardening is used in the simulation as in figure 4-25. The deformed mesh shows homogeneous deformation and other contour plots indicate no sign of localization.

Study of Kink Band Formation in NiAl Single Crystals

Kinking is a highly localized form of deformation that has been observed in NiAl

during compression test near the hard orientation (<100> direction). When compressed along the hard orientation the resolved shear stress along <001> directions is zero, as a result glide occurs along other directions such as <111> or <110> (Miracle, 1993). However, if the direction of compression is misaligned slightly from the <001> direction, either {110}<001> or {100}<001> systems can get activated depending on the direction of misalignment. Such misorientation has been observed to favor kinking. Experimental studies by Fraser et al. (1973b) shows that deformation in the kink band occurs on {110} planes due to slip along the one of <100> direction parallel to the compression axes. However, all three <100> have been observed experimentally (Miracle 1993)

Kinking has been explained in terms of orientation softening that occurs due to large lattice rotation (Fraser et al., 1973a, b; Winton, 1995). Once a slip system is activated the lattice rotation increases the resolved shear stress in that system making it softer so that activation of the other possible systems are unlikely. When non-uniform deformation is induced due to specimen geometry or imperfections, the region where more lattice rotation occurs due to higher strains becomes softer than the rest of the specimen causing further deformation to localize in this region.

When {110}<001> slip system is activated single slip occurs, while double slip occurs when {100}<001> system is activated. Significant lattice rotation occurs in both cases. Numerical simulations were performed for both these situations with compressive load applied along directions misaligned by 5-10^{o} from the [001] direction. Initiation of the localized deformation is affected by the initial imperfection curve. Without the initial imperfection curve on the specimen localized deformation forms only at the middle of specimen.

Figure 4-26 shows the deformed mesh for double slip system when slip system is misaligned ten degrees into the {100} slip plane from the loading orientation. Kink bands are formed when τ_s is 73 (MPa) (figure 4-26-a). Lower work hardening facilitate kink bands formation. Large lattice rotations are found at the kinked region in figure 4-30-a, whereas less lattice rotations occur in figure 4-30-b and 4-30-c. Intense resolved shear strain regions are also found at the kinked region. So, this result explains that lattice rotation causes geometric softening and facilitates kink band.

Figure 4-31 shows stages of kink bands formation for single slip along (110)<001> when the loading axis is ten degrees off with respect to the hard orientation. Kink bands are observed at the early stage of deformation (figure 4-31-b). Contour plots of resolved shear strain shows two intense narrow regions in figure 4-34-a even at 2.3 % nominal strain. These narrow regions propagate as the specimen deforms further (figure 4-34-b, figure 4-34-c and figure 4-34-d). More than 60 degrees of lattice rotation has occurred along the band during single slip (figure 4-35-d). This agrees well with the experimental observation of Fraser et al. (1973a) where they have reported slip along {110}<001> slip system and ~60 degrees lattice rotation in the kink band.

Figure 4-36 shows the deformed mesh when single slip occurs during compression along an axis five degrees off with respect to the hard orientation. With less misalgnment from the hard orientation than previous case of ten degrees off from compression axis, kink bands can be seen at 2.3 % nominal strain (figure 4-36-a).

Figure 4-41 shows load vs. elongation curve for five degrees misalignment from the hard orientation. Multiple load drops indicate that kink bands propagate into the

homogeneous regions of the specimen as the specimen deforms further. As a result, inhomogeneous deformation prevails along the specimen (figure 4-38-d and 4-39-d).

Figure 4-40-d shows more than 80 degrees of lattice rotations at the kinked regions. Both single slip case and double slip case show kink bands. Lattice rotation causes orientation softening. Single slip case shows more lattice rotation in general than in double slip case.

Summary of this study

Deformation of NiAl single crystals was studied using finite element simulations. Simulation of deformation along directions slightly off from the [110] direction shows that geometrical softening associated with lattice rotation can produce shear localization if the rate sensitivity is low and the material undergoes very little work hardening. However, since NiAl has much higher values of rate sensitivity and hardening than were used in the simulation, it is unlikely that such macroscopic bands would be observed experimentally. In the localized region, strain rate sensitivity might be lower than non-localized region. This fact may suggest that micro-scale shear band can form in the region that has more lattice rotation and lead to the fracture of NiAl single crystal (Ebrahimi and Shrivastava, 1997b).

Another localization phenomenon, kink bands, is observed during compression near the hard orientation. Kink bands formed near the region which have more lattice rotations than other regions. Lower hardening facilitates kink bands formation.

From the study of localized band in NiAl single crystal, we have gathered a valuable information. All localization phenomena compete with uniform deformation. Hardening,

strain rate sensitivity, geometry and orientation etc. are crucial parameters that determine deformation status either localized deformation or uniform deformation. Localized deformations is revealed after abrupt load drops and sharp localization follows after the load drop. Micro scale localization is observed in the experiment that are similar to shear localization (Ebrahimi and Shrivastava, 1997a, b). This may trigger fracture in NiAl crystals. Therefore localization phenomena may be a crucial factor in explaining brittle fracture in NiAl single crystal at low temperatures.

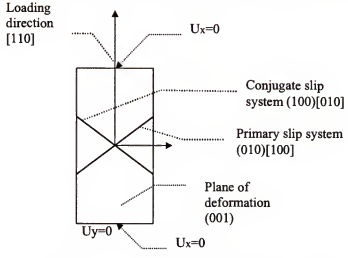

Figure 4-1 Schematic representation of double planar slip model

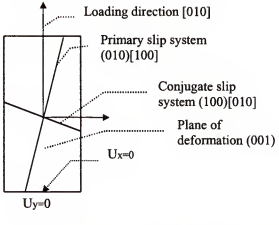

Figure 4-2 Schematic representation of hard oriented double slip specimen in compression test

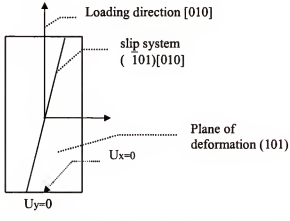

Figure 4-3 Schematic representation of hard oriented single slip specimen in compression test

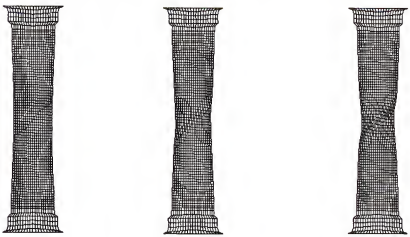

(a) (b) (c)

Figure 4-4 Plots of deformed mesh (τ_s=83 MPa, τ_0=35.9 MPa, H_0=360 MPa, m=0.006) (a) 12 % nominal strain (b) 13.5% nominal strain (c) 15% nominal strain

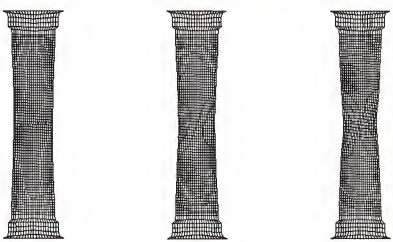

(a) (b) (c)

Figure 4-5 Plots of deformed mesh (τ_s=83 MPa, τ_0=35.9 MPa, H_0=360 MPa, m=0.01) (a) 12 % nominal strain (b) 13.5% nominal strain (c) 15% nominal strain

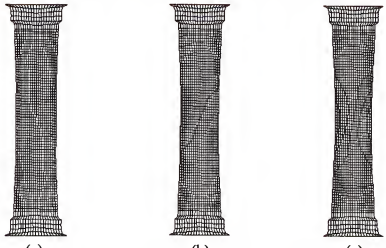

(a) (b) (c)

Figure 4-6 Plots of deformed mesh (τ_s=83 MPa, τ_0=35.9 MPa, H_0=360 MPa, m=0.02) (a) 12% nominal strain (b) 13.5% nominal strain (c) 15% nominal strain

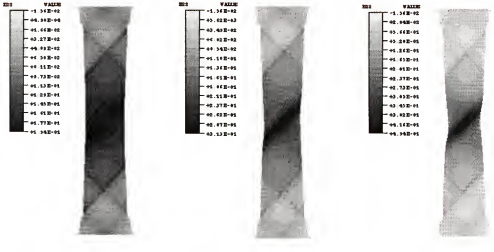

(a) (b) (c)

Figure 4-7 Contour plots of Cauchy strain in Y-dir. (τ_s=83 MPa, τ_0=35.9 MPa, H_0=360 MPa, m=0.006) (a) 12% nominal strain (b) 13.5% nominal strain (c) 15% nominal strain

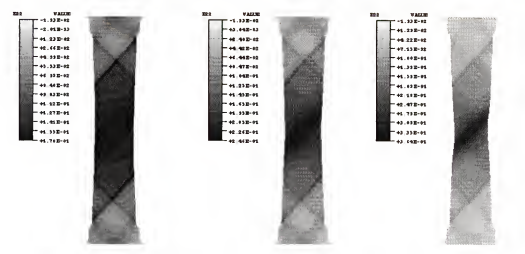

(a) (b) (c)

Figure 4-8 Contour plots of Cauchy strain in Y-dir. (τ_s=83 MPa, τ_0=35.9 MPa, H_0=360 MPa, m=0.01) (a) 12% nominal strain (b) 13.5% nominal strain (c) 15% nominal strain

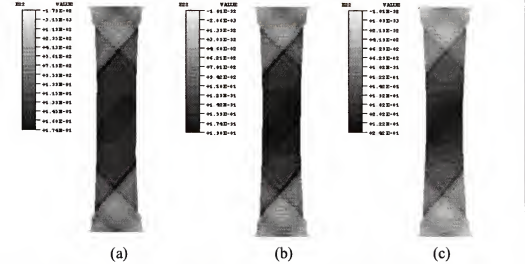

(a) (b) (c)

Figure 4-9 Contour plots of Cauchy strain in Y-dir. (τ_s=83 MPa, τ_0=35.9 MPa, H_0=360 MPa, m=0.02) (a) 12% nominal strain (b) 13.5% nominal strain (c) 15% nominal strain

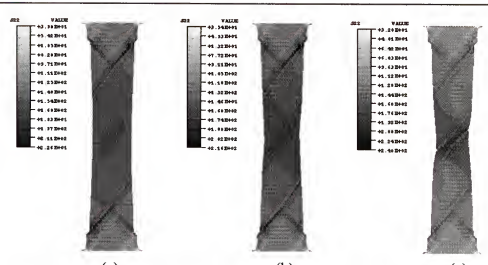

(a) (b) (c)

Figure 4-10 Contour plots of Cauchy stress in Y-dir. (τ_s=83 MPa, τ_0=35.9 MPa, H_0=360 MPa, m=0.006) (a) 12% nominal strain (b) 13.5% nominal strain (c) 15% nominal strain

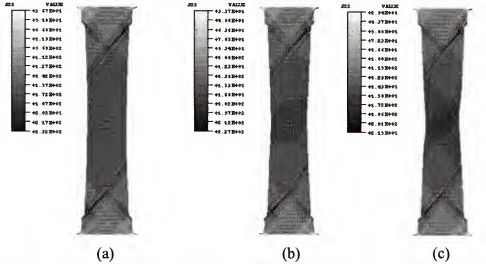

(a) (b) (c)

Figure 4-11 Contour plots of Cauchy stress in Y-dir. (τ_s=83 MPa, τ_0=35.9 MPa, H_0=360 MPa, m=0.01) (a) 12% nominal strain (b) 13.5% nominal strain (c) 15% nominal strain

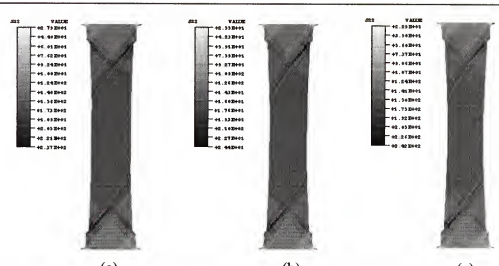

(a) (b) (c)

Figure 4-12 Contour plots of Cauchy stress in Y-dir. (τ_s=83 MPa, τ_0=35.9 MPa, H_0=360 MPa, m=0.02) (a) 12% nominal strain (b) 13.5% nominal strain (c) 15% nominal strain

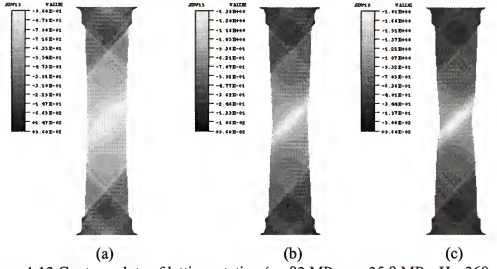

(a) (b) (c)

Figure 4-13 Contour plots of lattice rotation (τ_s=83 MPa, τ_0=35.9 MPa, H_0=360 MPa, m=0.006) (a) 12% nominal strain (b) 13.5% nominal strain (c) 15% nominal strain

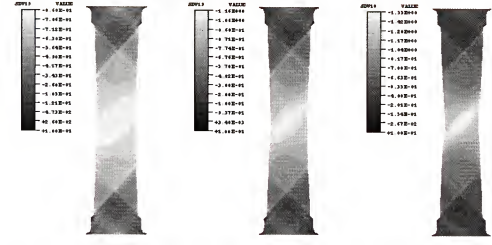

(a) (b) (c)

Figure 4-14 Contour plots of lattice rotation (τ_s=83 MPa, τ_0=35.9 MPa, H_0=360 MPa, m=0.01) (a) 12% nominal strain (b) 13.5% nominal strain (c) 15% nominal strain

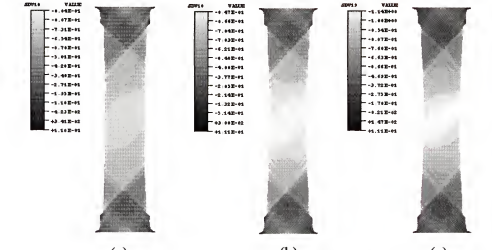

(a) (b) (c)

Figure 4-15 Contour plots of lattice rotation (τ_s=83 MPa, τ_0=35.9 MPa, H_0=360 MPa, m=0.02) (a) 12% nominal strain (b) 13.5% nominal strain (c) 15% nominal strain

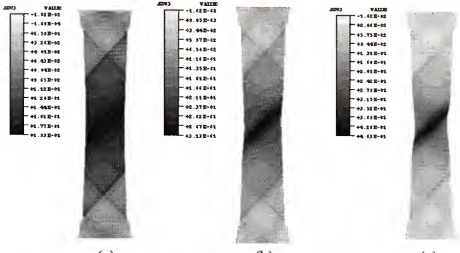

(a) (b) (c)

Figure 4-16 Contour plots of resolved shear strain (τ_s=83 MPa, τ_0=35.9 MPa, H_0=360 MPa, m=0.006) (a) 12% nominal strain (b) 13.5% nominal strain (c) 15% nominal strain

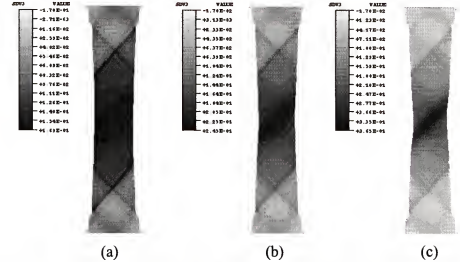

(a) (b) (c)

Figure 4-17 Contour plots of resolved shear strain (τ_s=83 MPa, τ_0=35.9 MPa, H_0=360 MPa, m=0.01) (a) 12% nominal strain (b) 13.5% nominal strain (c) 15% nominal strain

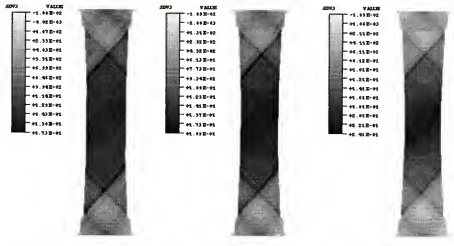

(a) (b) (c)

Figure 4-18 Contour plots of resolved shear strain (τ_s=83 MPa, τ_0=35.9 MPa, H_0=360 MPa, m=0.02) (a) 12% nominal strain (b) 13.5% nominal strain (c) 15% nominal strain

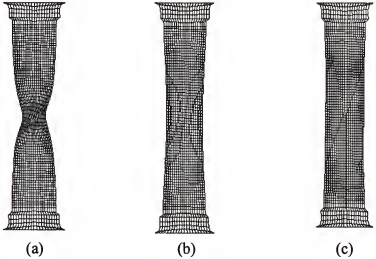

(a) (b) (c)

Figure 4-19 Plots of deformed mesh with different τ_s (strain rate sensitivity m=0.02, at 15 % nominal strain) (a) τ_s=50 (MPa) (b) τ_s = 83 (MPa) (c) τ_s =120 (MPa)

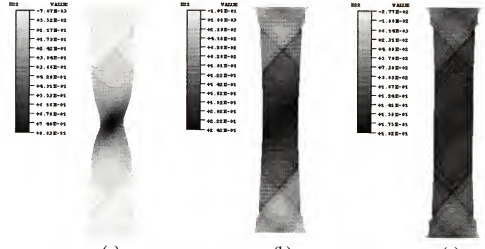

(a) (b) (c)

Figure 4-20 Contour plots of Cauchy strain in Y-dir. with different τ_s (strain rate sensitivity m=0.02, at 15 % nominal strain) (a) τ_s=50 (MPa) (b) τ_s = 83 (MPa) (c) τ_s =120 (MPa)

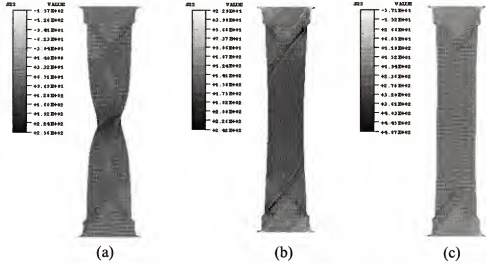

(a) (b) (c)

Figure 4-21 Contour plots of Cauchy stress in Y-dir. with different τ_s (strain rate sensitivity m=0.02, at 15 % nominal strain) (a) τ_s=50 (MPa) (b) τ_s = 83 (MPa) (c) τ_s =120 (MPa)

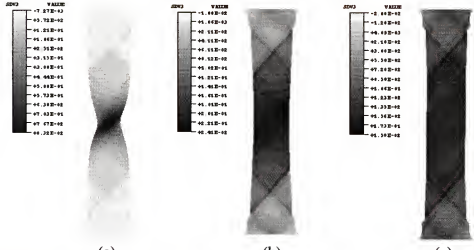

(a) (b) (c)

Figure 4-22 Contour plots of resolved shear strain with different τ_s (strain rate sensitivity m=0.02, at 15 % nominal strain) (a) τ_s=50 (MPa) (b) τ_s = 83 (MPa) (c) τ_s =120 (MPa)

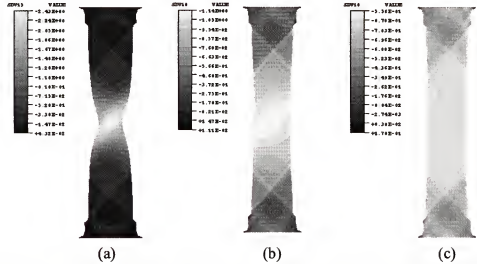

(a) (b) (c)

Figure 4-23 Contour plots of lattice rotation with different τ_s (strain rate sensitivity m=0.02, at 15 % nominal strain) (a) τ_s=50 (MPa) (b) τ_s= 83 (MPa) (c) τ_s=120 (MPa)

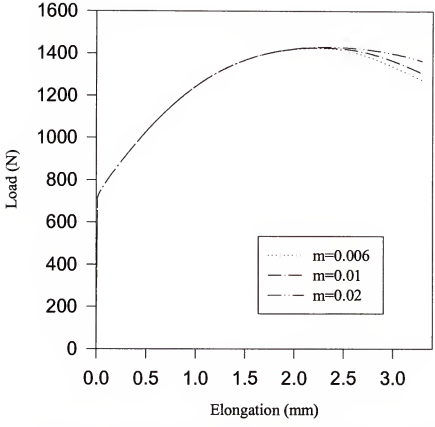

Figure 4-24 Load vs. elongation for 3 degrees off from [110] orientation with different strain rate sensitivity m

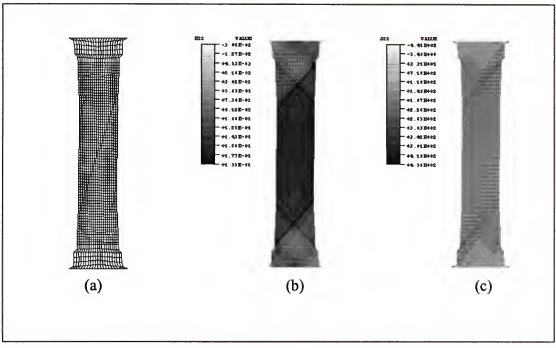

(a) (b) (c)

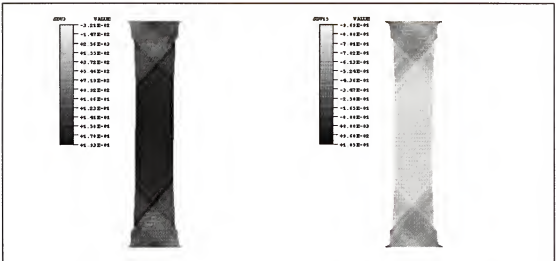

(d) (e)

Figure 4-25 Plots using high saturated critical resolved shear stress with small strain rate sensitivity (τ_s=120 MPa, τ_0=35.9 MPa, H_0=360 MPa, m=0.006), at 15 % nominal strain (a) Deformed mesh (b) Contour plot of Cauchy strain in Y-dir. (c) Contour plot of Cauchy stress in Y-dir. (d) Contour plot of resolved shear strain (e) Contour plot of lattice rotation

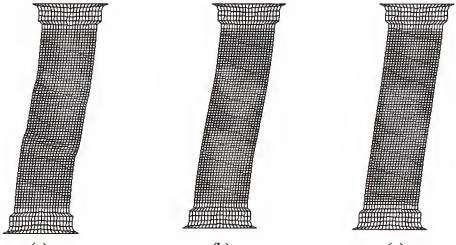

(a) (b) (c)

Figure 4-26 Plots of deformed mesh of double slip system with different τ_s, 10 degrees off from the hard orientation in compression test, at 2.8 % nominal strain (a) τ_s=73 (MPa) (b) τ_s=83 (MPa) (c) τ_s=120 (MPa)

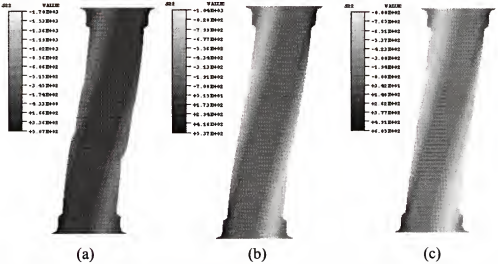

(a) (b) (c)

Figure 4-27 Contour plots of Cauchy stress in Y-dir. of double slip system with different τ_s, 10 degrees off from the hard orientation in compression test, at 2.8 % nominal strain (a) τ_s=73 (MPa) (b) τ_s=83 (MPa) (c) τ_s=120 (MPa)

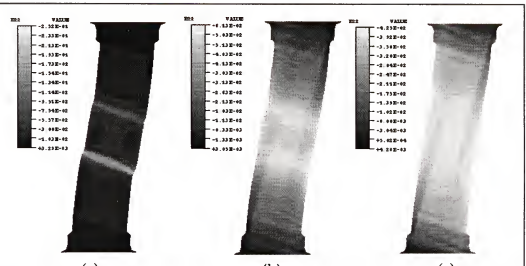

(a) (b) (c)

Figure 4-28 Contour plots of Cauchy strain in Y-dir. of double slip system with different τ_s, 10 degrees off from the hard orientation in compression test, at 2.8 % nominal strain (a) τ_s=73 (MPa) (b) τ_s=83 (MPa) (c) τ_s=120 (MPa)

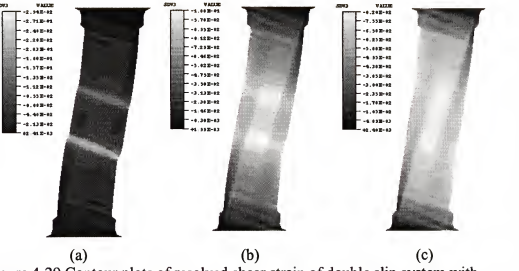

(a) (b) (c)

Figure 4-29 Contour plots of resolved shear strain of double slip system with different τ_s, 10 degrees off from the hard orientation in compression test, at 2.8 % nominal strain (a) τ_s=73 (MPa) (b) τ_s=83 (MPa) (c) τ_s=120 (MPa)

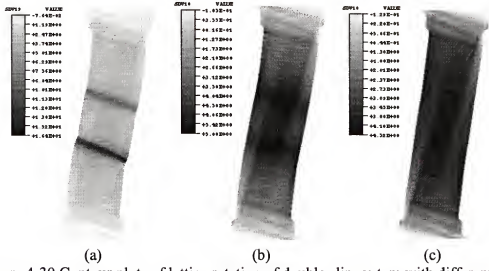

(a) (b) (c)

Figure 4-30 Contour plots of lattice rotation of double slip system with different τ_s, 10 degrees off from the hard orientation in compression test, at 2.8 % nominal strain (a) τ_s=73 (MPa) (b) τ_s=83 (MPa) (c) τ_s=120 (MPa)

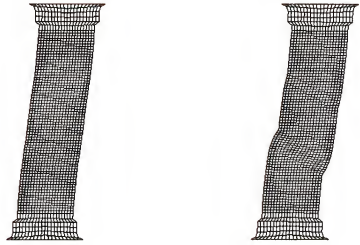

(a) (b)

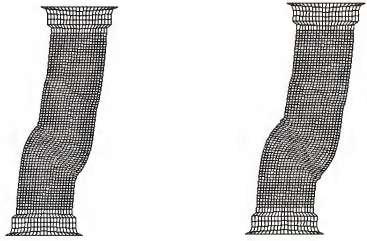

(c) (d)

Figure 4-31 Plots of deformed mesh with single slip system, 10 degrees off from hard orientation in compression test (τ_s=83 MPa, τ_0=35.9 MPa, H_0=360 MPa, m=0.02) (a) 2.3 % nominal strain (b) 3.9 % nominal strain (c) 5.5 % nominal strain (d) 7.1 % nominal strain

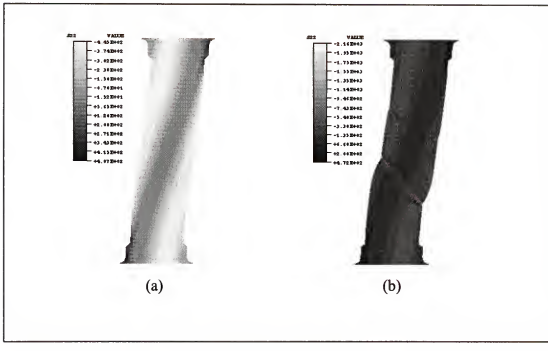

(a) (b)

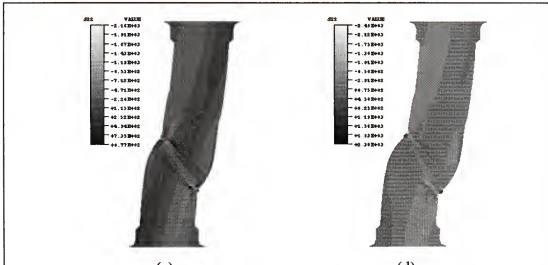

(c) (d)

Figure 4-32 Contour plots of Cauchy stress in Y-dir. with single slip system, 10 degrees off from hard orientation in compression test (τ_s=83 MPa, τ_0=35.9 MPa, H_0=360 MPa, m=0.02) (a) 2.3 % nominal strain (b) 3.9 % nominal strain (c) 5.5 % nominal strain (d) 7.1 % nominal strain

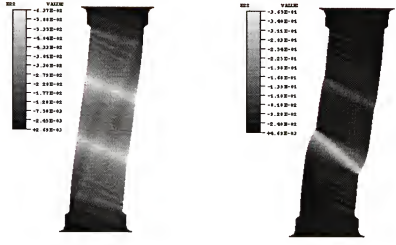

(a) (b)

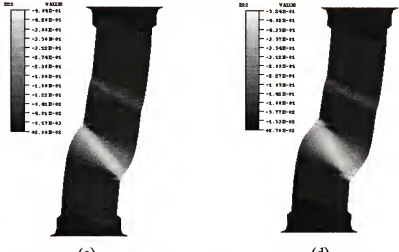

(c) (d)

Figure 4-33 Contour plots of Cauchy strain in Y-dir. with single slip system, 10 degrees off from hard orientation in compression test (τ_s=83 MPa, τ_0=35.9 MPa, H_0=360 MPa, m=0.02) (a) 2.3 % nominal strain (b) 3.9 % nominal strain (c) 5.5 % nominal strain (d) 7.1 % nominal strain

(a)

(b)

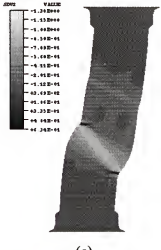

(c)

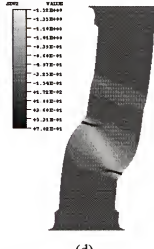

(d)

Figure 4-34 Contour plots of resolved shear strain with single slip system, 10 degrees off from hard orientation in compression test (τ_s=83 MPa, τ_0=35.9 MPa, H_0=360 MPa, m=0.02) (a) 2.3 % nominal strain (b) 3.9 % nominal strain (c) 5.5 % nominal strain (d) 7.1 % nominal strain

(a)

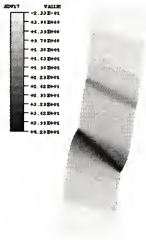

(b)

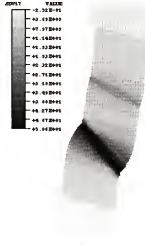

(c)

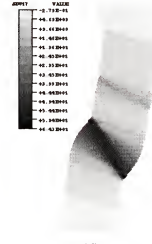

(d)

Figure 4-35 Contour plots of lattice rotation with single slip system, 10 degrees off from hard orientation in compression test (τ_s=83 MPa, τ_0=35.9 MPa, H_0=360 MPa, m=0.02) (a) 2.3 % nominal strain (b) 3.9 % nominal strain (c) 5.5 % nominal strain (d) 7.1 % nominal strain

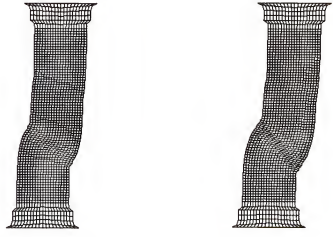

(a) (b)

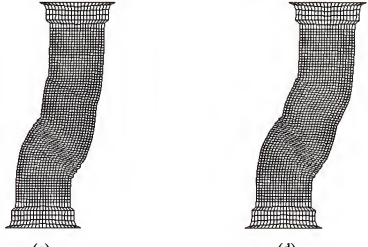

(c) (d)

Figure 4-36 Plots of deformed mesh with single slip system, 5 degrees off from the hard orientation in compression test (τ_s=83 MPa, τ_0 =35.9 MPa, H_0=360 MPa, m=0.02) (a) 2.3 % nominal strain (b)3.9 % nominal strain (c)5.5 % nominal strain (d) 7.1 % nominal strain

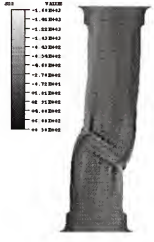

(a)

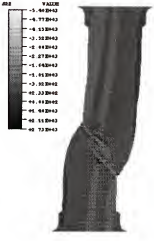

(b)

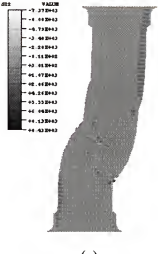

(c)

(d)

Figure 4-37 Contour plots of Cauchy stress in Y-dir. with single slip system, 5 degrees off from the hard orientation in compression test (τ_s=83 MPa, τ_0 =35.9 MPa, H_0=360 MPa, m=0.02) (a) 2.3 % nominal strain (b)3.9 % nominal strain (c)5.5 % nominal strain (d) 7.1 % nominal strain

(a)

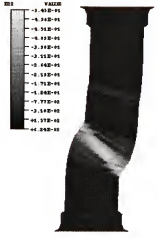

(b)

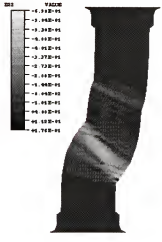

(c)

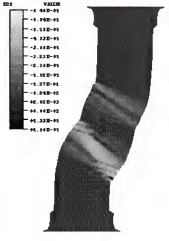

(d)

Figure 4-38 Contour plots of Cauchy strain in Y-dir. with single slip system, 5 degrees off from the hard orientation in compression test (τ_s=83 MPa, τ_0 =35.9 MPa, H_0=360 MPa, m=0.02) (a) 2.3 % nominal strain (b)3.9 % nominal strain (c)5.5 % nominal strain (d) 7.1 % nominal strain

(a)

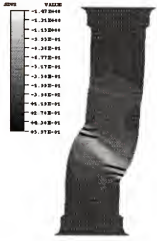

(b)

(c)

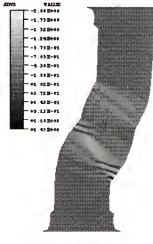

(d)

Figure 4-39 Contour plots of resolved shear strain with single slip system, 5 degrees off from the hard orientation in compression test (τ_s=83 MPa, τ_0 =35.9 MPa, H_0=360 MPa, m=0.02) (a) 2.3 % nominal strain (b)3.9 % nominal strain (c)5.5 % nominal strain (d) 7.1 % nominal strain

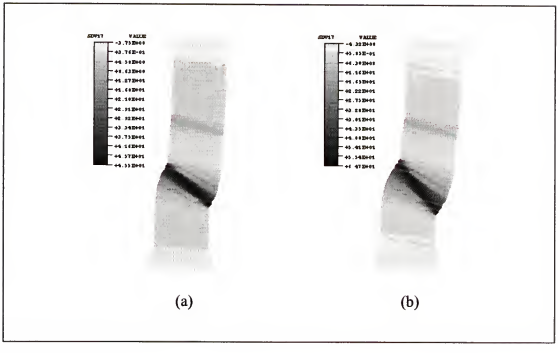

(a) (b)

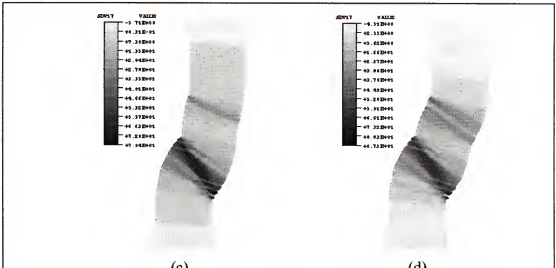

(c) (d)

Figure 4-40 Contour plots of lattice rotation with single slip system, 5 degrees off from the hard orientation in compression test (τ_s=83 MPa, τ_0 =35.9 MPa, H_0=360 MPa, m=0.02) (a) 2.3 % nominal strain (b)3.9 % nominal strain (c)5.5 % nominal strain (d) 7.1 % nominal strain

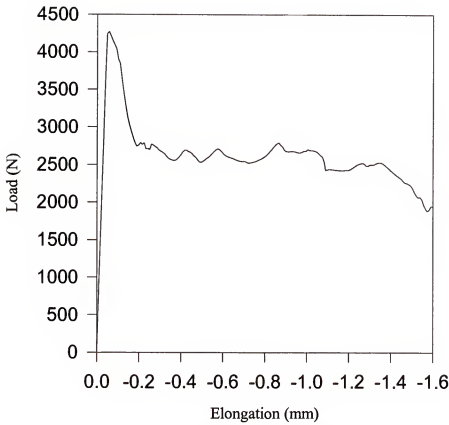

Figure 4-41 Load vs. elongation curve for 5 degrees off from the compression axis

CHAPTER 5
HARDENING CHARACTERISTICS OF NIAL SINGLE CRYSTALS

Finite Element Model for Hardening Problem

We used following specimen model for the simulation, where dimension is, 15(mm) long, 1.4(mm) wide and 2.1(mm) thick. This is the same dimension used in experiment to test mechanical properties of NiAl single crystal. The actual specimen includes two flanges where the outer flanges are used to hold the specimen in the tensile testing machine. But for the finite element analysis only the inner flanges are included. Loading has been imposed by a prescribed constant displacement rate. Strain rate $\dot{a}$ =0.001 s^{-1} was used for the simulation. All nodes at the top face of specimen were specified to have the same displacement in the loading direction. To include secondary slip systems {110}<001> in NiAl, three-dimensional model was adopted. Incompatible element for three-dimensional geometry (C3D8I) was used for the analysis. 1152 elements were used for the simulation.

Table 5-1 Simulation data used for NiAl single crystals for hardening characteristics problem at 400°C

Elastic bulk Modulus K (MPa)	Shear Modulus G (MPa)	Poisson's ratio	Imperfection	Strain rate sensitivity
161419.2	65159.79	0.3215	No imperfection	0.04

The material data used in this simulation is as in table 5-1. Shear modulus G and bulk modulus K are adopted from Miracle (1993).

Loading along [$\bar{5}57$] direction was tested to obtain hardening parameters such as saturated critical resolved shear stress, initial hardening rate for the simulation. This orientation is selected because only single slip occurs along this loading direction. The plane of deformation (110) contains burgers vector, slip plane normal vector, and tensile axis in either parallel or perpendicular to the thickness of the sample cross section. Axis of rotation is normal to the deformation plane (110). As a consequence of the geometry of the slip systems in this loading direction, simulation can be performed by the assumption of planar model. Slip occurs along {110}<001> slip system. Figure 5-1 shows the location of slip system. Boundary conditions are same as in the [110] orientation case. The same element type and loading as in [110] orientation were used. For [$\bar{5}57$] loading direction, slip system is [001] ($\bar{1}10$) and plane of deformation is (110) plane.

When the specimen is pulled along [110] orientation in NiAl single crystals, we might consider {110}<001> slip systems as a secondary slip systems. However, {110} slip planes are not perpendicular to the plane of deformation (001). As a result, these slip systems can not be modeled as a planar model. Three-dimensional geometry should be used to include all the slip systems. Figure 5-2 shows schematic representation of three-dimensional model.

Determination of Constitutive Parameters

The kinematics of single crystal deformation and the constitutive models based on Schmid's law are now well established and have been used to simulate deformation of

FCC and BCC single crystals (Peirce et al., 1983, Deve et al., 1988). Such models are capable of simulating experimentally observed modes of deformation in single crystals. However, the accuracy of the simulated results is limited by the accuracy with which the constitutive parameters can be determined. The deformation patterns observed experimentally in single crystals of different materials vary due to the differences in constitutive parameters and due to differences in the operative slips systems. The parameters that most significantly affect the deformation mode include the rate sensitivity parameter (m), the latent hardening (q) and the parameters that describe the hardening curve (τ_c vs. γ) of the material such as τ_0, τ_s and h_0. Rate sensitivity parameter m can be determined experimentally. The value of m varies with temperature and impurities/ additives.

Experimental evidence (Winton, 1995) suggests that the initial critical resolved shear stress τ_o is the same for both the {110}<001> and the {100}<001> slip systems. Loading directions that activate {110}<001> slip system such as [$\bar{5}$57] results in single slip. This provides an opportunity to experimentally determine the hardening curve for this slip system. At intermediate temperatures (400-700K) extremely high tensile elongation (100-350%) has been obtained for this orientation (Levit et al. 1996). The load versus elongation curve obtained for [$\bar{5}$57] orientation increases to a peak and then decreases gradually to a minimum before increasing again (figure 5-3). The drop in load after the peak load is due to localized deformation that results in a neck. However, the neck spreads after the initial localization. This behavior has been experimentally observed (Levit et al. 1996) and explained in terms of the orientation hardening which results from

the large amount of lattice rotation that occurs during single slip. Numerical simulation based on our finite element model confirms this phenomenon. The load versus deformation curve obtained numerically has identical shape.

Figure 5-5 shows the contour plots of strain in y direction at different stages that indicate nearly uniform deformation along the gauge length.

Figure 5-6 shows the deformed specimen at different stages of deformation with contour plots of lattice rotation. The direction of the lattice rotation is such that the Schmid factor decreases. As a result, a higher tensile load is required to produce the resolved shear stress necessary for slip on the active slip plane. The resulting increase in yield stress along the tensile direction referred to as orientation hardening prevents further deformation at the neck causing the neck to spread. Determination of the hardening curve (τ_c vs. γ) from the load versus elongation curve is difficult due to the large amount of lattice rotation accompanying the deformation that changes the Schmid factor continuously during deformation. Furthermore, one has to account for strain localization to accurately determine the true stress and true strain developed in the specimen during the deformation. Levit et al. (1996) have experimentally measured strain localization and determined the lattice rotation using electron back scattering methods during tensile elongation along the $[\bar{5}57]$. Based on these results they have calculated the hardening curve for the {110}<001> slip system. The curve thus obtained exhibits monotonic hardening followed by a saturation critical resolved shear stress at high strains and has a shape that confirms well with the shape of the hardening curve in equation (2.41).

Numerical simulation of the experiment using this hardening curve yielded a load versus elongation curve whose shape matches very well with the experimental results.

Tensile elongation along the [110] direction activates the {100}<001> slip system. However, unlike in the previous case, elongation in this direction produces double slip. Both the (100) and (010) planes become active simultaneously since the Schmid factor for both these planes are identical. In addition, no lattice rotation occurs because these planes are located symmetrically about the tensile axes and identical amount of slip occurs in both slip planes. The load versus elongation curve obtained experimentally (Levit et al., 1996) seems to suggest considerable work hardening. Determining the hardening curve however is not straightforward due to uncertainty about the contribution of latent hardening to the total hardening observed. Simulation of the elongation along [110] using the hardening curve obtained earlier for {110}<001> slip system yields poor results at large strains as seen in figure 5-7. The numerically obtained load-elongation curve is close to experimental curve initially and correctly predicts the initial peak followed by a load drop. However, the load increases at higher strains for the experimental specimen, while it drops due to a sharp neck for the numerical simulation. This suggests that there are considerable work hardening at large strains for the {100}<001> slip system and that the hardening curve for this slip system does not have a plateau as assumed in equation (2.41).

Latent hardening is normally determined by measuring overshoot. Double slip happens only when loading direction is such that (001) and (010) are active slip systems. However, the angle between them is 90^{o} therefore (001) and (010) systems become active

simultaneously. Two slip systems have a same resolved shear stress regardless of lattice rotation. So, Latent hardening is difficult to determine experimentally in this orientation.

Modified Hardening Law for NiAl Single Crystal Type

To explain the high hardening, we assumed two separate hardening moduli on each slip system such as $h(\gamma_{(100)})$ and $h(\gamma_{(110)})$ which is similar to Nakada and Keh's model (1966) and Franciosi's model (1983).

We assumed secondary slip may activate at large plastic deformations and this activation of secondary slip systems helps to raise the hardening at large strains and prevents necking. Based on this physical observation and our assumptions we draw a hardening rule which is appropriate for multislip condition in NiAl single crystals.

NiAl single crystals mainly deform by two {100}<001> slip systems for tensile load along [110] orientation at the beginning of deformations. However, slip trace analysis showed that the cross slip of <100> dislocations to {0kl} slip planes in addition to slips in {100} slip planes (Ebrahimi, F. et al., 1996; Ebrahimi, F. and Shrivastava, S., 1997a). Therefore we may assume the activation of cross slip of <100> dislocations in {110} slip planes at large strains. We have used a notation of secondary slip system in our hardening representation instead of a notation of cross slip of <100> dislocations in {110} slip planes.

Ebrahimi and Shrivastava (1997a, b) suggested that the cross slip of screw dislocations in {011} slip planes is responsible for strain hardening in <110> orientation of NiAl single crystals. The rate of hardening increases due to secondary slip activation. Potentially active slip systems in [110] orientation are shown in figure 5-8. Instantaneous

hardening modulus [h] is regarded as an accumulation of each slip system's resolved shear strains. So, hardening modulus of {100} slip planes is a function of resolved shear strains of {100} slip planes and hardening modulus of {110} slip planes is a function of resolved shear strains of {110} slip planes.

There are four latent hardening ratios in our assumed hardening model. Latent hardening ratio in {100} planes was called q_{aa}, latent hardening ratio in {110} planes was called q_{bb}, latent hardening in {100} planes due to {110} planes was called q_{ab} and latent hardening in {110} planes due to {100} planes was called q_{ba}. Hardening modulus h_1 is a function of resolved shear strains in {100} slip plane, $h_1 = h(\gamma_{(100)})$. h_2 is a function of resolved shear strains in {110} slip plane, $h_2 = h(\gamma_{(110)})$. Incremental hardening of slip systems is represented as follows.

$$\begin{Bmatrix} d\tau_c^{(1)} \\ d\tau_c^{(2)} \\ d\tau_c^{(3)} \\ d\tau_c^{(4)} \\ d\tau_c^{(5)} \\ d\tau_c^{(6)} \end{Bmatrix} = \begin{bmatrix} h_1 & q_{aa}h_1 & q_{ab}h_2 & q_{ab}h_2 & q_{ab}h_2 & q_{ab}h_2 \\ q_{aa}h_1 & h_1 & q_{ab}h_2 & q_{ab}h_2 & q_{ab}h_2 & q_{ab}h_2 \\ q_{ba}h_1 & q_{ba}h_1 & h_2 & q_{bb}h_2 & q_{bb}h_2 & q_{bb}h_2 \\ q_{ba}h_1 & q_{ba}h_1 & q_{bb}h_2 & h_2 & q_{bb}h_2 & q_{bb}h_2 \\ q_{ba}h_1 & q_{ba}h_1 & q_{bb}h_2 & q_{bb}h_2 & h_2 & q_{bb}h_2 \\ q_{ba}h_1 & q_{ba}h_1 & q_{bb}h_2 & q_{bb}h_2 & q_{bb}h_2 & h_2 \end{bmatrix} \begin{Bmatrix} d\gamma_1 \\ d\gamma_2 \\ d\gamma_3 \\ d\gamma_4 \\ d\gamma_5 \\ d\gamma_6 \end{Bmatrix} \quad (5.1)$$

Unusually high hardening at large strain means that multiple slips may be occurring at large strain. {100}<010> slip systems have a higher Schmid's factor than {110}<010> slip systems in [110] orientation. So, we assigned {100}<010> slip systems as primary slip systems in [110] orientation and {110}<010> slip systems were regarded as secondary slip systems. To activate secondary slip systems ({110}<010>), these secondary slip systems should harden less than the primary slip systems ({100}<010>).

At the next section, we will look at the hardening characteristics especially latent hardening ratios based on the experimental load vs. elongation curve.

Determination of Condition for Slip System's Activity

Ratio of resolved shear stress in primary slip system to resolved shear stress in secondary slip system is always constant number because of no lattice rotation in [110] orientation.

$$\left|\frac{\tau^{(p)}}{\tau^{(s)}}\right| = K > 1, \quad K=\text{constant} \tag{5.2}$$

If the ratio of critical resolved shear stress in primary slip system to critical resolved shear stress in secondary slip system is equal to K, secondary slip systems are also active.

$$\frac{\tau_c^{(p)}}{\tau_c^{(s)}} = K \tag{5.3}$$

For all slip systems to stay active together, constant ratio between $\tau_c^{(p)}$ and $\tau_c^{(s)}$ is required at all deformation stages. Here we define stage I as before the secondary slip system activation and stage II as after secondary slip system activation. For our model, K can be obtained by calculating resolved shear stress for each slip system. Schmid factor SF is defined as SF=cosα cosΦ. Here α is the angle between loading direction and slip plane normal direction and Φ is the angle between loading direction and slip direction.

$$SF_p = \frac{1}{\sqrt{2}}\frac{1}{\sqrt{2}} = \frac{1}{2} \qquad SF_s = \frac{1}{\sqrt{2}\sqrt{2}}\frac{1}{\sqrt{2}} = \frac{1}{2\sqrt{2}} \tag{5.4}$$

Here SF_p is the Schmid factor for primary slip system {100}<001> and SF_s is the Schmid factor for secondary slip system {110}<010>. The ratio of SF_p to SF_s is as follows.

$$\frac{SF_p}{SF_s} = K = \sqrt{2} \tag{5.5}$$

Stage I (Case I)

At this stage, only the primary slip systems are active so resolved shear strain in the secondary slip systems are almost zero. Total shear is almost equal to the slip in the primary slip systems ({100}<010>).

$$\tau(\gamma_1, \gamma_2, \gamma_3, \gamma_4, \gamma_5, \gamma_6) \cong \tau(\gamma_1, \gamma_2) \tag{5.6}$$

γ_1, γ_2 are the resolved shear strains for the {100} slip planes and γ_3,γ_4,γ_5, γ_6 are the resolved shear strains for {110} slip planes.

Changes in critical resolved shear stresses in both primary and secondary slip systems are expressed as follows.

$$d\tau_c^{\{100\}} = h_1 d\gamma_1 + q_{aa} h_1 d\gamma_2 = q_{aa} h_1 d\gamma_1 + h_1 d\gamma_2 = d\tau_c^{(1)} = d\tau_c^{(2)} \tag{5.7}$$

$$d\tau_c^{\{110\}} = (q_{ba} h_1 d\gamma_1 + q_{ba} h_1 d\gamma_2) = d\tau_c^{(3)} = d\tau_c^{(4)} = d\tau_c^{(5)} = d\tau_c^{(6)} \tag{5.8}$$

Integration of the incremental critical resolved shear stress in primary slip system gives following formulas.

$$\tau_c^{(p)} = \int_0^{\gamma_1} h_1 d\gamma + \int_0^{\gamma_2} (q_{aa} h_1) d\gamma + \tau_0^{(p)} \tag{5.9}$$

where $\gamma_1 = \gamma_2 = \gamma^{\{100\}}, d\gamma_1 = d\gamma_2 = d\gamma^{\{100\}}$

We can assume the total resolved shear strains in {100} slip planes as $\gamma_1 + \gamma_2 = 2\gamma^{\{100\}}$

$$\tau_c^{(p)} = \int_0^{\gamma^{\{100\}}} (1 + q_{aa}) h_1 (2\gamma^{\{100\}}) d\gamma + \tau_0^{(p)} \tag{5.10}$$

where $h_1 = h_0 \sec h^2 \left(\frac{h_0 \gamma^{\{100\}}}{\tau_s - \tau_0}\right)$

$$\tau_c^{(p)} = (1 + q_{aa}) \int_0^{\gamma^{(100)}} h_0 \sec h^2 \left(\frac{2h_0\gamma^{(100)}}{\tau_s - \tau_0}\right) d\gamma + \tau_0^{(p)} \tag{5.11}$$

$$\tau_c^{(p)} = (1 + q_{aa})\left(\frac{\tau_s - \tau_0}{2}\right) \tanh\left(\frac{2h_0\gamma^{(100)}}{\tau_s - \tau_0}\right) + \tau_0^{(p)} \tag{5.12}$$

Integration of incremental critical resolved shear stress in secondary slip system with the same assumptions gives following formulas for secondary slip system.

$$\tau_c^{(s)} = \tau_0^{(s)} + \int_0^{\gamma_1} q_{ba} h_1 d\gamma + \int_0^{\gamma_2} q_{ba} h_1 d\gamma = \tau_0^{(s)} + 2q_{ba} \int_0^{\gamma^{(100)}} h_1 (2\gamma^{(100)}) d\gamma \tag{5.13}$$

$$\tau_c^{(s)} = (2q_{ba}) \int_0^{\gamma^{(100)}} h_0 \sec h^2 \left(\frac{2h_0\gamma^{(100)}}{\tau_s - \tau_0}\right) d\gamma + \tau_0^{(s)} \tag{5.14}$$

$$\tau_c^{(s)} = (q_{ba})(\tau_s - \tau_0) \tanh\left(\frac{2h_0\gamma^{(100)}}{\tau_s - \tau_0}\right) + \tau_0^{(s)} \tag{5.15}$$

In this stage deformation occurs by slips in {100} slip planes. Secondary slips are assumed to be activated only at the end of stage I. During stage I hardening of primary slip systems should maintain following relations.

$$\frac{\tau_c^{(100)}}{\tau_c^{(110)}} < K \tag{5.16}$$

At the end of Stage I

We assumed that the secondary slip systems, which are {110}<001>, would activate at the end point of stage I.

Ignoring small resolved shear strain in {110} slip planes the following formulas need be satisfied to activate secondary slip systems. From these formulas we can predict possibility of secondary slip system's activation.

$$\frac{\tau_c^{(100)}}{\tau_c^{(110)}} = \frac{(1+q_{aa})(\frac{\tau_s-\tau_0}{2})\tanh(\frac{2h_0\gamma^{(100)}}{\tau_s-\tau_0})+\tau_0^{(p)}}{(q_{ba})(\tau_s-\tau_0)\tanh(\frac{2h_0\gamma^{(100)}}{\tau_s-\tau_0})+\tau_0^{(s)}} = K \tag{5.17}$$

The latent hardening ratio q_{aa}, q_{ba} are the variables that determine the activation of secondary slip systems. As soon as the ratio between two slip systems reach the value K the secondary slip systems will activate.

Stage II (Case II, Case III, Case IV)

Both {100}<001> and {110}<001> slip systems are assumed to be active at the beginning of this stage. Hardening of each slip system depends on deformation in every slip system in the crystals. According to the latent hardening parameters in the hardening matrix, deformation may be classified as 3 cases at large deformation.

Case II) {110}<001> slip systems harden much less than {100}<001> slip systems, so {110}<001> slip systems are active and {100}<001> slip systems are no longer active

$$\Longrightarrow \frac{\tau_c^{(100)}(\gamma)}{\tau_c^{(110)}(\gamma)} = \frac{d\tau_c^{(100)}(\gamma)}{d\tau_c^{(110)}(\gamma)} > K \tag{5.18}$$

Case III) {110}<001> slip systems harden exactly the same as {100}<001> slip systems

$$\Longrightarrow \frac{\tau_c^{(100)}(\gamma)}{\tau_c^{(110)}(\gamma)} = \frac{d\tau_c^{(100)}(\gamma)}{d\tau_c^{(110)}(\gamma)} = K \tag{5.19}$$

Case IV) {110}<001> slip systems harden more than {100}<001> slip systems

$$\Longrightarrow \frac{\tau_c^{(100)}(\gamma)}{\tau_c^{(110)}(\gamma)} = \frac{d\tau_c^{(100)}(\gamma)}{d\tau_c^{(110)}(\gamma)} < K \tag{5.20}$$

From the assumed hardening modulus, hardening rate and hardening of each slip system may be expressed as follows.

$$d\tau_c^{(100)} = [h(\gamma_{100}) + q_{aa}h(\gamma_{100})]d\gamma_{100} + q_{ab}[h(\gamma_{110}) + h(\gamma_{110}) + h(\gamma_{110}) + h(\gamma_{110})]d\gamma_{110}$$

$$= (1 + q_{aa})h(\gamma_{100})d\gamma_{100} + 4q_{ab}h(\gamma_{110})d\gamma_{110} \tag{5.21}$$

$$d\tau_c^{(110)} = q_{ba}[h(\gamma_{100}) + h(\gamma_{100})]d\gamma_{100} + [q_{bb}[h(\gamma_{110}) + h(\gamma_{110}) + h(\gamma_{110})] + h(\gamma_{110})]d\gamma_{110}$$

$$= 2q_{ba}h(\gamma_{100})d\gamma_{100} + (1 + 3q_{bb})h(\gamma_{110})d\gamma_{110} \tag{5.22}$$

$$\tau_c^{(100)} = q_{ab}[\int_0^{\gamma_{110}} h(\gamma)d\gamma_{110} + \int_0^{\gamma_{110}} h(\gamma)d\gamma_{110} + \int_0^{\gamma_{110}} h(\gamma)d\gamma_{110} + \int_0^{\gamma_{110}} h(\gamma)d\gamma_{110}] + \int_0^{\gamma_{100}} h(\gamma)d\gamma_{100} +$$

$$q_{aa}\int_0^{\gamma_{100}} h(\gamma)d\gamma_{100} + \tau_0^{100}$$

$$= (1 + q_{aa})\int_0^{\gamma_{100}} h(\gamma)d\gamma_{100} + 4q_{ab}\int_0^{\gamma_{110}} h(\gamma)d\gamma_{110} + \tau_0^{100} \tag{5.23}$$

$$\tau_c^{(110)} = \int_0^{\gamma_{110}} h(\gamma)d\gamma_{110} + q_{bb}[\int_0^{\gamma_{110}} h(\gamma)d\gamma_{110} + \int_0^{\gamma_{110}} h(\gamma)d\gamma_{110} + \int_0^{\gamma_{110}} h(\gamma)d\gamma_{110}] + q_{ba}[\int_0^{\gamma_{100}} h(\gamma)d\gamma_{100} +$$

$$\int_0^{\gamma_{100}} h(\gamma)d\gamma_{100}] + \tau_0^{110}$$

$$= 2q_{ba}\int_0^{\gamma_{100}} h(\gamma)d\gamma_{100} + (1 + 3q_{bb})\int_0^{\gamma_{110}} h(\gamma)d\gamma_{110} + \tau_0^{110} \tag{5.24}$$

If we define T_1 and T_2 as follows $T_1 = \int_0^{\gamma_{100}} h(\gamma)d\gamma_{100}$ and $T_2 = \int_0^{\gamma_{110}} h(\gamma)d\gamma_{110}$

critical resolved shear stress of each slip system might be expressed as follows.

$$\tau_c^{(p)} = (1 + q_{aa})T_1 + 4q_{ab}T_2 + \tau_0^{(p)} \tag{5.25}$$

$$\tau_c^{(s)} = 2q_{ba}T_1 + (1 + 3q_{bb})T_2 + \tau_0^{(s)} \tag{5.26}$$

Simulation

From our discussion in previous section on the hardening formulas, we can identify deformation process as 4 cases. We called stage I as case I and 3 cases in stage II are

called as case II, case III and case IV respectively. Each case is simulated and compared to show the different deformation process. Activation of slip system in {110} slip planes has a great effect on the hardening at large strains. Also, activation point of secondary slip system has an effect on whether specimen shows necking or neck propagation in our simulation results.

Case I (Stage I)

Like we discussed previously only {100}<001> slip systems are active in this case in our analytical prediction. However due to the effect of rate sensitivity we can expect small amount of shear in the secondary slip systems. The condition for this situation may be predicted by using ratio of hardening in {110} slip system and {100} slip system as in equation (5.17). The latent hardening ratios $q_{aa,}$ q_{ba} used in this case satisfy condition in equation (5.16). Even though there are 6 potential slip systems, deformed specimen shows different shapes due to the effect of latent hardening ratios $q_{bb,}$ q_{ab}. These latent hardening ratios have an effect on the hardening after activation of secondary slip system. As a results different combinations of latent hardening ratios can show the different deformation status.

As a first example, in figure 5-10, q_{bb}= q_{ab}= q_{ba}=1.0, q_{aa}=1.4 case shows almost zero resolved shear strain in the secondary slip systems so it looks same as that of 2-dimensional model with two slip systems. Figure 5-9 shows critical resolved shear stress on each slip system. Amounts of critical resolved shear stress in (110} slip plane are close to those of in {100} slip plane. So, secondary slip systems are difficult to activate in this circumstance. Necking happens at the top and bottom of gauge length and resolved shear strain in primary slip system shows concentrated regions in figure 5-21.

The following latent hardening ratios, q_{aa}=1.4, q_{bb}=1.0, q_{ab}=1.9 q_{ba}=0.7, show different deformation status. Activation of secondary slip can not happen according to the analytical prediction in equation (5.16). However, due to the rate sensitivity effect resolved shear strain has a small value at large strain in figure 5-12. These small resolved shear strain in the secondary slip systems cause the high hardening rate at large strain due to the combination of latent hardening ratios q_{bb}=1.0, q_{ab}=1.9 and prevents necking in the specimen.

Figure 5-11 shows critical resolved shear stress for each slip systems. High hardening rate owing to the activation of secondary slip systems at large strain cause the critical resolved shear stress to increase in the simulation.

Deformations in this case show homogeneous pattern. Figure 5-23-a shows the deformed specimen at 40 % nominal strain. Local regions show tendency of slight localization in the early stage of deformation. However, as the secondary slip system is activated neck propagation occurs rather than localized necking. Resolved shear strains are accumulated along the specimen homogeneously (figure 5-24).

As a last example in case I, latent hardening ratios, q_{bb}=q_{ab}=1.0,q_{aa}=1.4,q_{ba}=0.6, are selected to show the different deformation processes compared to the previous two cases. Same as in the second example, resolved shear strain in figure 5-14 shows some values due to the rate sensitivity effect. However combination of q_{bb}=q_{ab}=1.0 does not provide the high hardening rate. The latent hardening q_{ab} should have large value to show higher hardening rate at large strain. As a result, severely necked mesh is observed at 30 % nominal strain in figure 5-26-a.

Case II (Stage II)

This case is represented by such assumption. After the activation of {110}<100> secondary slip systems we assumed that {110}<001> slip systems harden much less than {100}<001> slip systems so at large strain regime secondary slip system {110}<001> is activated and primary slip system {100}<001> is gradually inactivated after all.

The following formula assumes no resolved shear strain in {100} slip plane makes it possible to have a condition for this case using ratio of rate of hardening in {110} slip system and {100} slip system.

$$\frac{d\tau_c^{(100)}(\gamma)}{d\tau_c^{(110)}(\gamma)} = \frac{4q_{ab}h(\gamma^{(110)})d\gamma^{(110)}}{(1+3q_{bb})h(\gamma^{(110)})d\gamma^{(110)}} > K \qquad (5.27)$$

The combination of latent hardening ratios is selected for the simulation. Two latent hardening ratio q_{aa}=1.4, q_{ba}=0.2 make possible its secondary slip systems to activate from analytical prediction in equation (5.17) and after activation of secondary slip systems the other latent hardening ratio combinations of q_{ab}=1.6 q_{bb}=1.0 satisfy the above relations. Based on assumptions resolved shear strain in {100}<011> primary slip systems would not increase at large deformations however due to the rate sensitivity effect primary slip systems still show the activation of systems. Figure 5-16 shows this trend. Resolved shear strain in secondary slip systems show a steeper trend than one in primary slip systems at large strain like we predicted in analytical formula.

Due to the early activation of secondary slip systems, High hardening rate can not be expected at large strain so we can observe the concentrated strain regions at the upper and lower of gauge length (Figure 5-29).

Case III (Stage II)

Both primary slip systems and secondary slip systems will have same hardening rate after activation of secondary slip systems. The ratio of critical resolved shear stress in primary slip system to critical resolved shear stress in secondary slip system is equal to K. K is ratio of resolved shear stress in primary slip system to resolved shear stress in secondary slip system.

Case IV (Stage II)

In this case {110}<001> slip systems harden more than {100}<001> slip systems after activation of secondary slip systems due to the latent hardening combinations of q_{ab}=1.2, q_{bb}=1.0. Secondary slip systems are difficult to activate.

The following formula make it possible to have a condition for this case using ratio of rate of hardening in {110} slip system and {100} slip system.

$$\frac{d\tau_c^{(100)}}{d\tau_c^{(110)}} = \frac{(1+q_{aa})h(\gamma^{(100)})d\gamma^{(100)} + 4q_{ab}h(\gamma^{(110)})d\gamma^{(110)}}{2q_{ba}h(\gamma^{(100)})d\gamma^{(100)} + (1+3q_{bb})h(\gamma^{(110)})d\gamma^{(110)}} < K \qquad (5.28)$$

The first terms of numerator and denominator of equation (5.28) satisfies equation (5.17) which is a condition for activation of secondary slip systems with q_{aa}=1.4, q_{ba}=0.2. The latent hardening combinations of q_{ab}=1.2, q_{aa}=1.4, q_{bb}=1.0, q_{ba}=0.2 may show this case. Even though we expect a small amount of resolved shear strain of {110}<001> slip systems large amounts of strain are observed in secondary slip systems due to the effect of rate sensitivity (Figure 5-18). As a results we expect lower hardening rate at large strains. Resolved shear strain in primary slip systems show a steeper trend than one in secondary slip systems at large strain like we predicted in our analytical formula.

Dislocation Interactions

We performed simulations under the assumptions that activation of secondary slip systems adds more hardening to the whole system. This hardening mechanism may be explained as follows.

Double glides of {100}<001> slip systems occur simultaneously due to the same Schmid factor for both slip systems and interact each other. As a result deformation shows high hardening at the beginning of deformation. However, as we have shown in our simulations, hardening between primary slip systems is not enough to show propagation in the simulation.

Glides in secondary slip systems {110}<001> may not contribute to the plastic deformations at the beginning of deformation due to the low Schmid factor.

Crimp et al. (1993) and Ebrahimi and Shrivastava (1997a) reported <100> or <110> dislocations slipping in {110} slip planes in [101] orientation through the slip trace analysis. So we may include secondary slip systems into our hardening model.

From the previous study (Kocks and Brown, 1966; Franciosi et al., 1980), we understand dislocation interactions between non-planar slip systems are stronger than that of between coplanar slip systems. Dislocation interactions in (100)[010] and (010)[100] should show strong interactions and pile-ups at barrier however these are not enough dislocation interactions as we pointed out in our simulations. So we may consider another hardening mechanism in addition to the dislocation pile-ups. The dislocation piercing the active slip planes is often called a dislocation forest.

The primary slip systems are already main active slip systems from the beginning due to the 0.5 Schmid factor and {110}<010> slip systems will activate later. So, we may

assume the primary slip systems are {001}<100> and forest slip systems are {110}<010> slip systems. The latent hardening ratio q_{ab} defined as hardening in primary system {a} due to the secondary slip system {b} may have higher value than q_{ba} defined as hardening in secondary system {b} due to the primary slip system {a}. The secondary slip system {b} may experience difficulty in piercing active primary slip system {a} so q_{ab} may have larger number whereas q_{ba} may have smaller number.

The forest dislocation may be explained as follows using <100> burgers vectors. If we assume [100] burgers vector in primary slip plane {100} interact with the [010] burgers vector in secondary slip system (forest slip system) two dislocations may undergo the following reactions.

$$[100]+[010]=[110] \tag{5.29}$$

They react to form a product segment lying in primary slip plane {100} and may glide in the primary slip planes. However, reactions are energetically stable, they may not glide in the primary slip systems and encountering point between two dislocations may act as a pinning point of the two dislocations. So, they impede the glide of primary slip systems and forest slip systems.

From this forest hardening mechanisms, we may conclude that a strong latent hardening occurs when the secondary slip systems meet the primary slip systems.

Summary of this Study

We have used our proposed hardening law to understand the hardening characteristics of NiAl single crystals. We divided deformation status into 4 categories according to which slip system is active. Latent hardening ratio q_{ba}, q_{aa} determine the

activation point of secondary slip systems and $q_{bb,}$ q_{ab} have an effect on the hardening characteristics after activation of secondary slip systems. Due to the rate sensitivity effect lower value of q_{ba} satisfy equation (5.17) causes early start of secondary slip system and does not contribute to the expected high hardening rate at large strain. In figure 5-19, different load shapes observed according to the different combinations of latent hardening ratios. Case I-b shows a quite similar result with experimental results (Levit et al., 1996). According to our formula equation (5.17) for the activation of secondary system Case I-b does not satisfy this condition. However, owing to the rate sensitivity effect, moderate value of q_{ba} causes small resolved shear strain of secondary slip system after necking occurs and does contribute to the expecting high hardening rate at large strain due to high q_{ab} value.

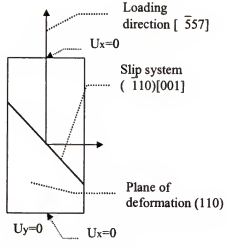

Figure 5-1 Schematic representation of [$\bar{5}57$] oriented specimen

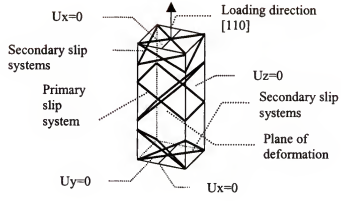

Figure 5-2 Schematic representation of 3-dimensional specimen in [110] loading

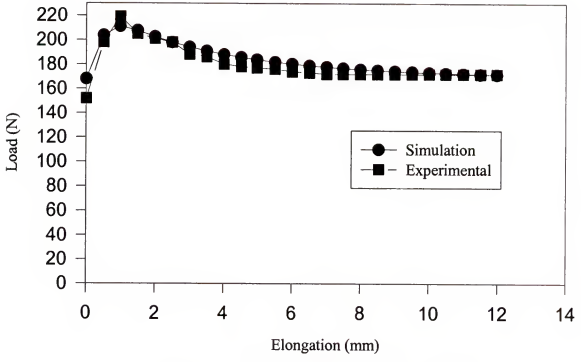

Figure 5-3 Load vs. elongation for [557] orientation

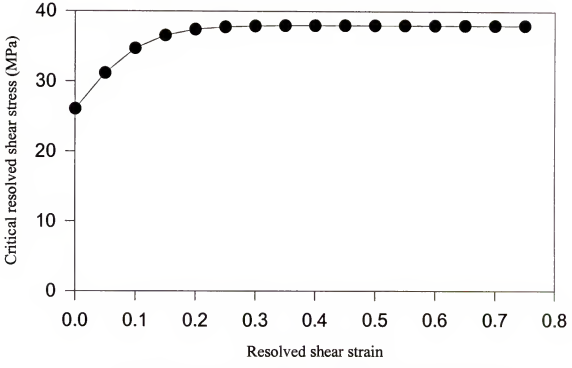

Figure 5-4 Critical resolved shear stress vs. resolved shear strain for the simulation (τ_s =38 MPa, τ_o =26 MPa, H_o =110 MPa)

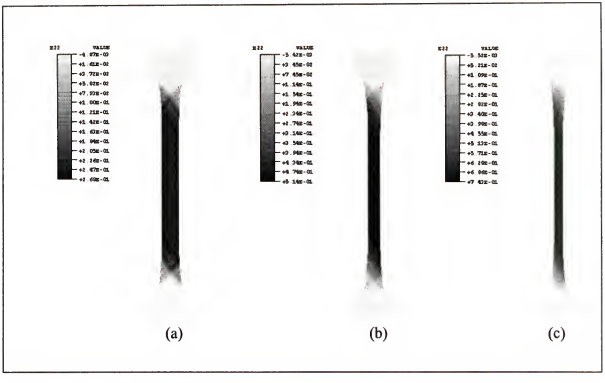

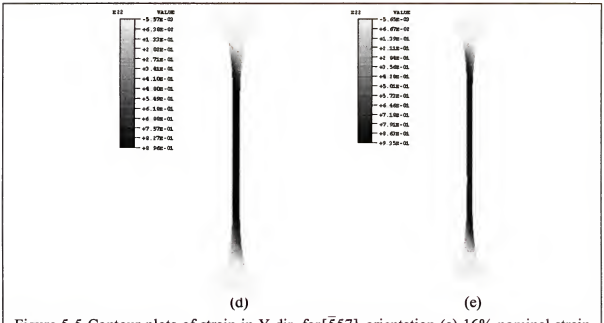

Figure 5-5 Contour plots of strain in Y-dir. for[$\bar{5}$57] orientation (a) 16% nominal strain (b) 32 % nominal strain (c) 48 % nominal strain (d) 64 % nominal strain (e) 80 % nominal strain

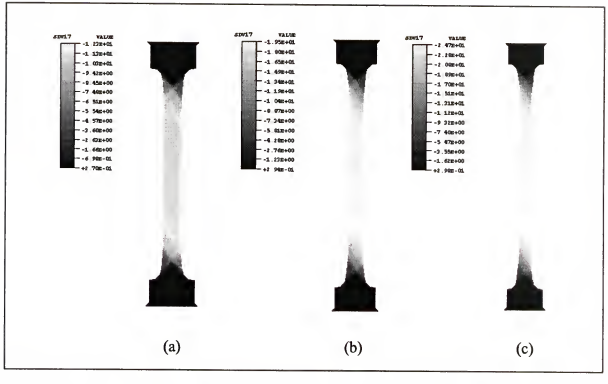

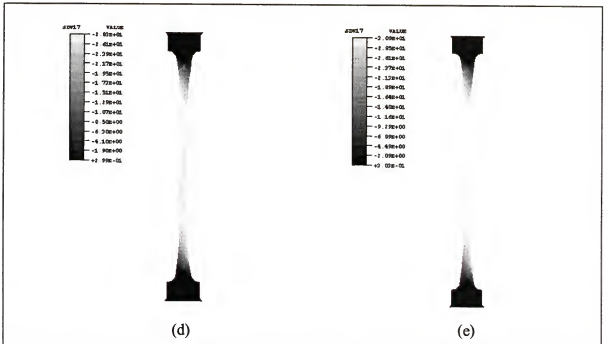

Figure 5-6 Contour plots of lattice rotation for[$\bar{5}57$] orientation (a) 16% nominal strain (b) 32 % nominal strain (c) 48 % nominal strain (d) 64 % nominal strain (e) 80 % nominal strain

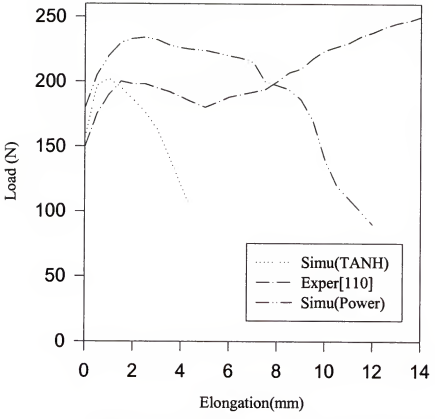

Figure 5-7 Load vs. elongation for [110]orientation using different hardening curve

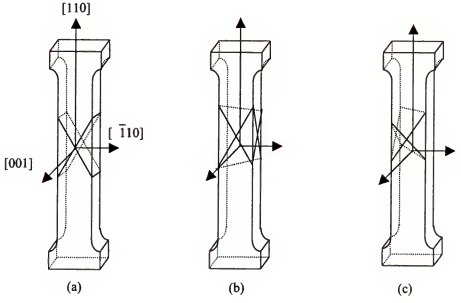

Figure 5-8 Slip systems in [110] orientation (a) (100)(010) slip plane (b) (101)($\bar{1}$01) slip plane (c) (011) (01 $\bar{1}$) slip plane

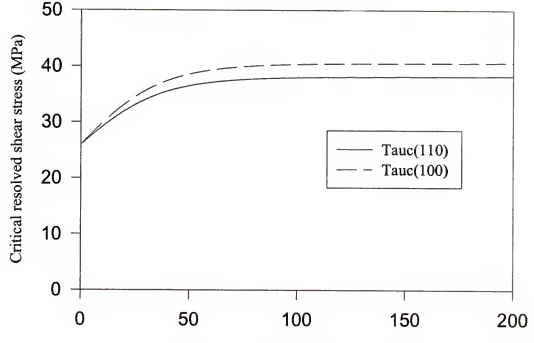

Figure 5-9 Critical resolved shear stress vs. time (case I-a)

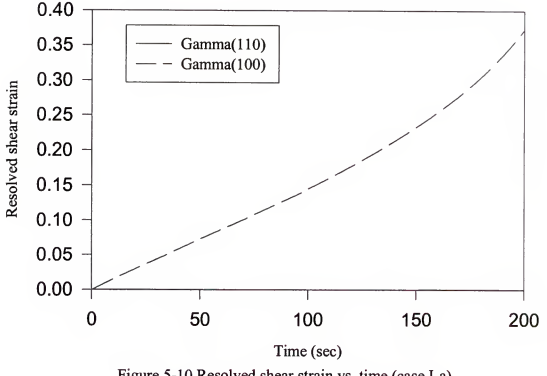

Figure 5-10 Resolved shear strain vs. time (case I-a)

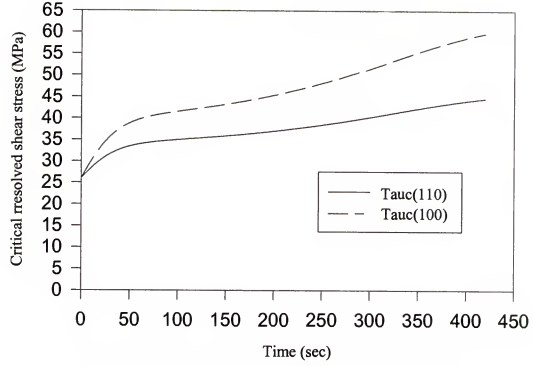

Figure 5-11 Critical resolved shear stress vs. time (case I-b)

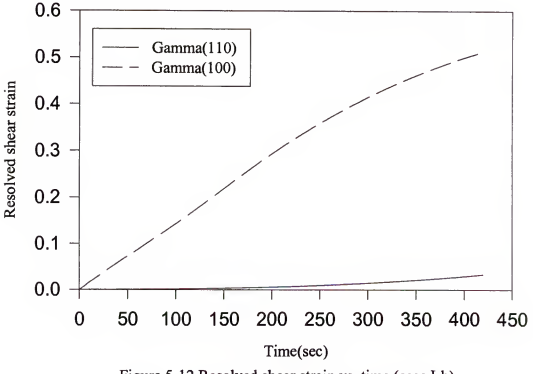

Figure 5-12 Resolved shear strain vs. time (case I-b)

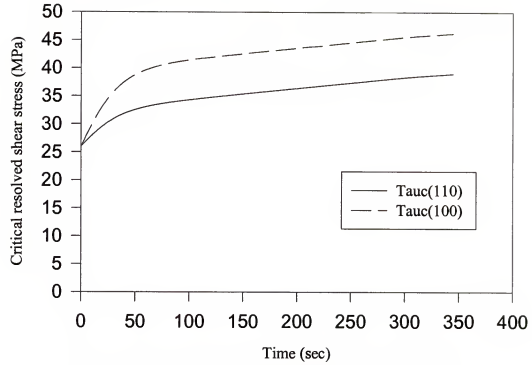

Figure 5-13 Critical resolved shear stress vs. time (case I-c)

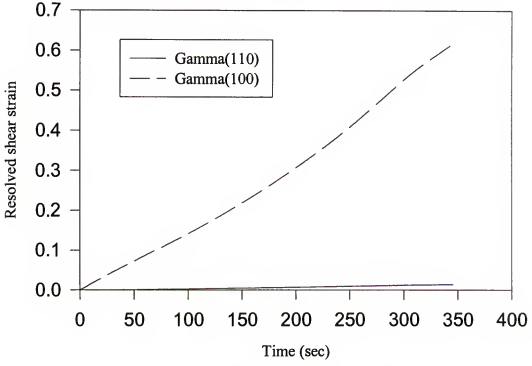

Figure 5-14 Resolved shear strain vs. time (case I-c)

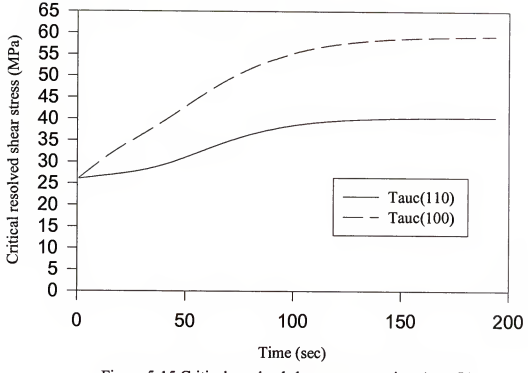

Figure 5-15 Critical resolved shear stress vs. time (case II)

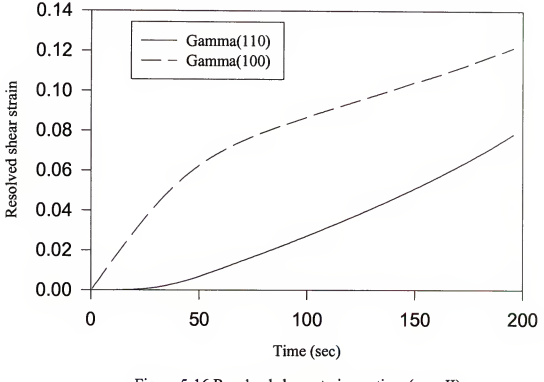

Figure 5-16 Resolved shear strain vs. time (case II)

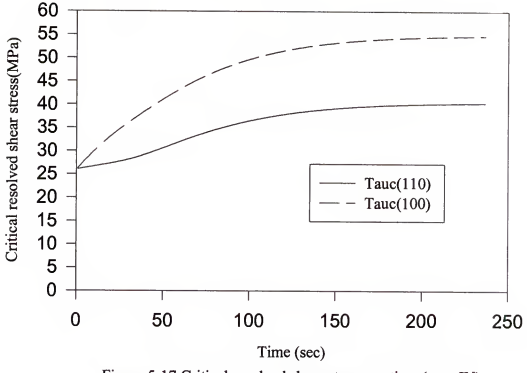

Figure 5-17 Critical resolved shear stress vs. time (case IV)

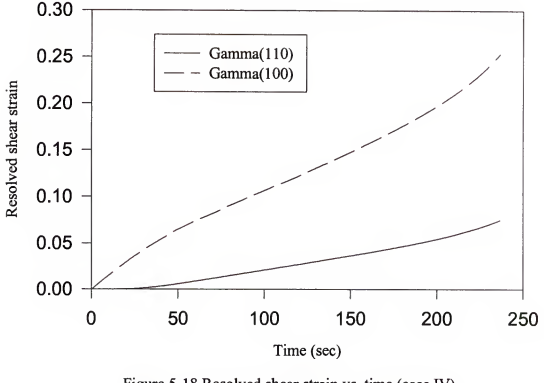

Figure 5-18 Resolved shear strain vs. time (case IV)

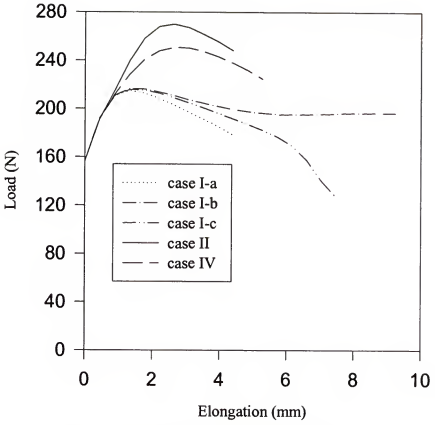

Figure 5-19 Simulated load vs.elongation for [110] orientation

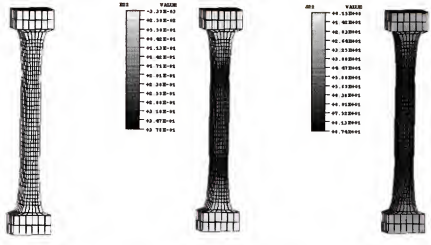

(a) (b) (c)

Figure 5-20 Case I-a, q_{aa}=1.4, q_{bb}=1.0, q_{ab}=1.0, q_{ba}=1.0, 20 % nominal strain
(a) Plot of deformed mesh (b) Contour plot of Cauchy strain in Y-dir.
(c) Contour plot of Cauchy stress in Y-dir.

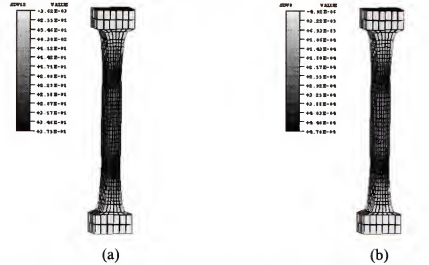

(a) (b)

Figure 5-21 Case I-a, q_{aa}=1.4, q_{bb}=1.0, q_{ab}=1.0, q_{ba}=1.0, 20 % nominal strain
(a) Contour plot of resolved shear strain in primary slip system
(b) Contour plot of resolved shear strain in secondary slip system

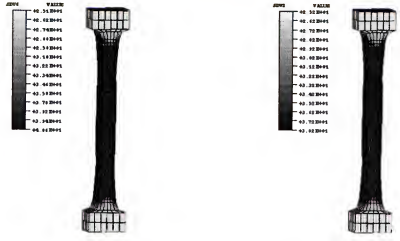

(a) (b)

Figure 5-22 Case I-a, q_{aa}=1.4, q_{bb}=1.0, q_{ab}=1.0, q_{ba}=1.0, 20 % nominal strain
(a) Contour plot of critical resolved shear stress in primary slip system
(b) Contour plot of critical resolved shear stress in secondary slip system

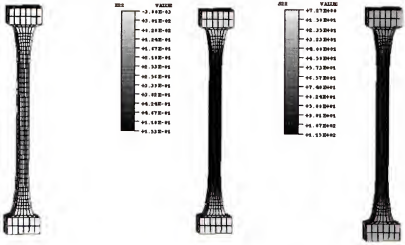

(a) (b) (c)

Figure 5-23 Case I-b, q_{aa}=1.4, q_{bb}=1.0, q_{ab}=1.9, q_{ba}=0.7, 40 % nominal strain
(a) Plot of deformed mesh (b) Contour plot of Cauchy strain in Y-dir.
(c) Contour plot of Cauchy stress in Y-dir.

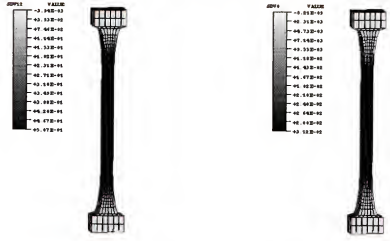

(a) (b)

Figure 5-24 Case I-b, q_{aa}=1.4, q_{bb}=1.0, q_{ab}=1.9, q_{ba}=0.7, 40 % nominal strain
(a) Contour plot of resolved shear strain in primary slip system
(b) Contour plot of resolved shear strain in secondary slip system

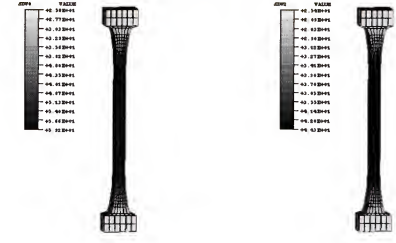

(a) (b)

Figure 5-25 Case I-b, q_{aa}=1.4, q_{bb}=1.0, q_{ab}=1.9, q_{ba}=0.7, 40 % nominal strain
(a) Contour plot of critical resolved shear stress in primary slip system
(b) Contour plot of critical resolved shear stress in secondary slip system

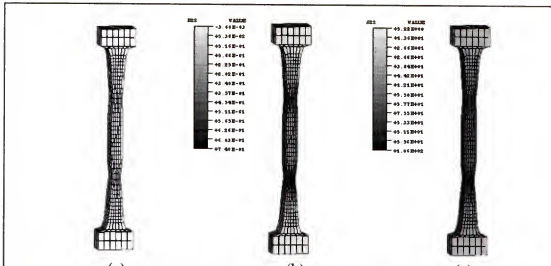

(a) (b) (c)

Figure 5-26 Case I-c, q_{aa}=1.4, q_{bb}=1.0, q_{ab}=1.0, q_{ba}=0.6, 30 % nominal strain
(a) Plot of deformed mesh (b) Contour plot of Cauchy strain in Y-dir.
(c) Contour plot of Cauchy stress in Y-dir.

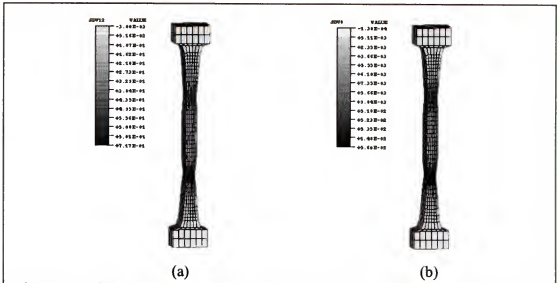

(a) (b)

Figure 5-27 Case I-c, q_{aa}=1.4, q_{bb}=1.0, q_{ab}=1.0, q_{ba}=0.6, 30 % nominal strain
(a) Contour plot of resolved shear strain in primary slip system
(b) Contour plot of resolved shear strain in secondary slip system

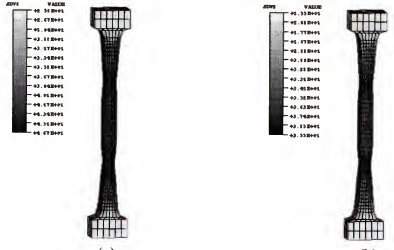

(a) (b)

Figure 5-28 Case I-c, q_{aa}=1.4, q_{bb}=1.0, q_{ab}=1.0, q_{ba}=0.6, 30 % nominal strain
(a) Contour plot of critical resolved shear stress in primary slip system
(b) Contour plot of critical resolved shear stress in secondary slip system

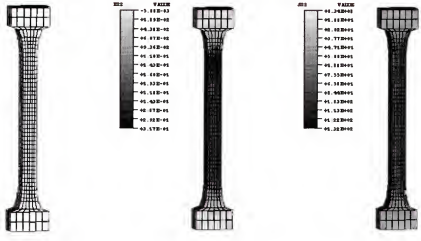

(a) (b) (c)

Figure 5-29 Case II, q_{aa}=1.4, q_{bb}=1.0, q_{ab}=1.6, q_{ba}=0.2, 19.5 % nominal strain
(a) Plot of deformed mesh (b) Contour plot of Cauchy strain in Y-dir.
(c) Contour plot of Cauchy stress in Y-dir.

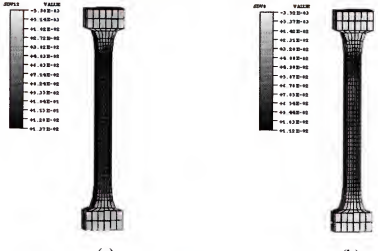

(a) (b)

Figure 5-30 Case II, q_{aa}=1.4, q_{bb}=1.0, q_{ab}=1.6, q_{ba}=0.2, 19.5 % nominal strain
(a) Contour plot of resolved shear strain in primary slip system
(b) Contour plot of resolved shear strain in secondary slip system

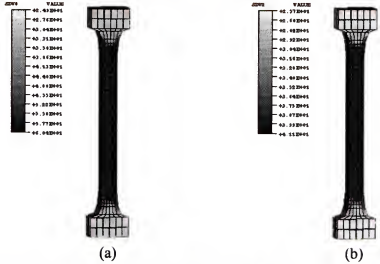

(a) (b)

Figure 5-31 Case II, q_{aa}=1.4, q_{bb}=1.0, q_{ab}=1.6, q_{ba}=0.2, 19.5 % nominal strain
(a) Contour plot of critical resolved shear stress in primary slip system
(b) Contour plot of critical resolved shear stress in secondary slip system

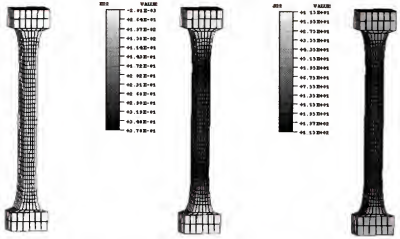

(a) (b) (c)

Figure 5-32 Case IV, q_{aa}=1.4, q_{bb}=1.0, q_{ab}=1.2, q_{ba}=0.2, 23.5 % nominal strain
(a) Plot of deformed mesh (b) Contour plot of Cauchy strain in Y-dir.
(c) Contour plot of Cauchy stress in Y-dir.

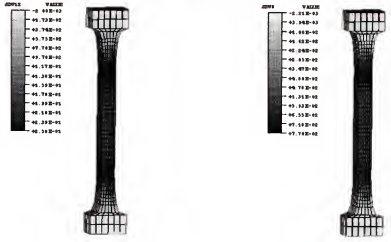

(a) (b)

Figure 5-33 Case IV, q_{aa}=1.4, q_{bb}=1.0, q_{ab}=1.2, q_{ba}=0.2, 23.5 % nominal strain
(a) Contour plot of resolved shear strain in primary slip system
(b) Contour plot of resolved shear strain in secondary slip system

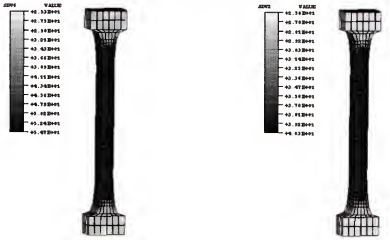

(a) (b)

Figure 5-34 Case IV, q_{aa}=1.4, q_{bb}=1.0, q_{ab}=1.2, q_{ba}=0.2, 23.5 % nominal strain
(a) Contour plot of critical resolved shear stress in primary slip system
(b) Contour plot of critical resolved shear stress in secondary slip system

CHAPTER 6
HARDENING IN FCC SINGLE CRYSTALS

Hardening characteristics of FCC single crystals are studied in this chapter. Modified hardening law for NiAl single crystals is presented in the previous chapter. This law is believed to apply to the BCC type single crystals due to the similar crystal structure and distinct slip systems. However, FCC single crystals have only one slip family, unlike BCC crystals and NiAl single crystals. So, representation of hardening law in FCC single crystals may be easier than BCC type or NiAl single crystals in some sense. Most of hardening laws were proposed for FCC single crystals (Peirce et al., 1983; Bassani and Wu, 1991). These hardening models were explained in previous chapter.

In this chapter, we will investigate these hardening models using three-dimensional finite element analysis. Various deformation behaviors revealed in FCC single crystals are investigated such as existences of stage I, stage II, stage III. There are 12 slip systems in FCC structures if reverse slip directions are not considered. Slip systems are divided into 4 groups and each group has 3 slip directions (see table 6-1). Primary slip system will be B4 and conjugate slip system will be C1 in [100] projection when the loading axis is inside of triangle of [100], [110], [111] vertices (figure 6-1). Activation of slip systems depends on the loading orientation. If the loading direction is parallel to [100] orientation, A2, C1, B4, A3, D1, B2, C3, D4 slip systems have same resolved shear stress so all can activate simultaneously in this loading direction. Due to the simultaneous activation of 8

Table 6-1 Notation for FCC crystals used in simulation

Notation	Slip system	Notation	Slip system
A2	$(111)[1\bar{1}0]$	C1	$(1\bar{1}1)[110]$
A3	$(111)[10\bar{1}]$	C3	$(1\bar{1}1)[10\bar{1}]$
A6	$(111)[0\bar{1}1]$	C5	$(1\bar{1}1)[110]$
B2	$(11\bar{1})[1\bar{1}0]$	D1	$(1\bar{1}\bar{1})[110]$
B4	$(11\bar{1})[101]$	D4	$(1\bar{1}\bar{1})[101]$
B5	$(11\bar{1})[011]$	D6	$(1\bar{1}\bar{1})[01\bar{1}]$

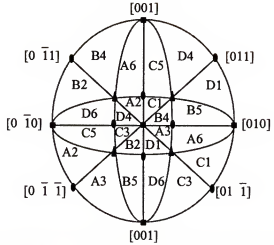

Figure 6-1 Standard stereographic projection from [100] orientation of FCC crystals

slip systems high hardening is expected. If the loading axis is parallel to [111] orientation, C1, B4, B5, D1, D4, C5 slip systems have same resolved shear stress. Slip in 6 planes can occur in this loading direction. If the loading directions are inside of triangle of stereographic projection only the single slip system B4 occurs and crystal lattice rotates toward slip direction [101]. When loading axis reaches [100]-[111] border-line secondary slip system C1 will activate.

Simulation in Single Slip Orientation

[632] orientation which is inside of triangle of stereographic projection is simulated. To compare the possible deformation processes in FCC single crystals in various hardening models three-dimensional finite element analysis is introduced so all possible 12 slip systems can be included in the simulation. Rate-dependent frame was used. All simulations used strain rate sensitivity m=0.01.

Asaro's hardening model

Two-parameter law used by Peirce et al. (1983) was tested. Identical material properties taken by Peirce et al. (1983) were used in our simulation (τ_o=60.84 (MPa), τ_s=1.8 τ_o, Ho=8.9 τ_o). All slip systems shows same amount of critical resolved shear stress due to the isotropic hardening of this law (figure 6-2). Due to the higher hardening for all slip systems only the primary slip system B4 is activated up to 12.5 % nominal strain (figure 6-3). Even the resolved shear strain in primary slip system stops increasing about 10 % nominal strain due to the strain softening (figure 6-3). This hardening model can predict stage I as seen in figure 6-2 however due to the absence of activation of conjugate slip system it never shows rapid hardening rates at large strain. Even if this

model shows activation of conjugate slip system rapid hardening will not be observed due to the lower or almost zero hardening rate at large strain in this hardening law. Material shows softening after stage I and this model does not predict stage II and stage III usually observed in FCC single crystals (figure 6-4).

The first modified version Asaro's hardening model

In two-parameter law each modulus of hardening matrix [h] is a function of total resolved shear strain. Two-parameter law is slightly modified by separating resolved shear strain as follows.

$$h_{\alpha\beta} = qh(\gamma_\beta) + (1-q)h(\gamma_\beta)\delta_{\alpha\beta} \qquad (6.1)$$

where q is the latent hardening ratio. Critical resolved shear stresses are same for all slip systems with latent hardening ratio q =1.0. Hardening modulus is not a function of total resolved shear strain but a function of each resolved shear strain. When conjugate slip system is activated (figure 6-6) rapid increase of hardening is observed (figure 6-5). Load vs. elongation plot shows increased hardening at large strain (figure 6-7). τ_c vs. γ plot show the tendency of stage II. Stage III could be observed if the specimen is pulled further.

Bassani's hardening model

Hardening model proposed by Bassani and Wu (1991) was tested in rate-dependent frame. Hardening formula for this model was introduced in chapter 3. They used rate-independent frame and neglected latent hardening effects by assigning latent hardening ratio q=0 in the simulation. We used the same hardening parameters for the simulation (τ_i=1.3 τ_o, h_s=1.5 τ_o, ho=90 τ_o, γ_o=0.001, q=0) as Bassani and Wu (1991). Due to the

strain rate sensitivity effect span of stage I is narrow but their model predicts stage II and stage III (figure 6-8). Lower critical resolved shear stresses in secondary slip systems than those of in primary slip system facilitate activation of secondary slip systems. Activation of conjugate slip system increased hardening rate and stage II was observed. Stage III was observed in their model because hardening rate of slip systems was saturated at large strain.

The second modified version of Asaro's hardening model

Finding a hardening law can describe deformation process observed in FCC single crystals is investigated. Latent hardening ratios are responsible to describe interaction between slip systems. Primary slip system B4 activates first due to the highest resolved shear stress and loading axis rotates to the boundary line and moves to the stable axis [211]. There are no rotations after reaching stable axis.

Ratio of resolved shear stress in primary slip to that in secondary slip system about stable axis [211] maintains constant value after reaching stable axis [211].

$$\left|\frac{\tau^{(p)}}{\tau^{(s)}}\right| = K \tag{6.2}$$

$$\left|\frac{\tau^{(p)}}{\tau^{(s)}}\right| = \frac{m_p}{m_s} = \frac{1/\sqrt{6}}{2/(3\sqrt{6})} = K \cong 1.5 \tag{6.3}$$

We have primary slip system B4, conjugate slip system C1 and two secondary slip systems A3, B5. Incremental critical resolved shear stresses of each slip system are coupled with other slip systems as follows.

$$\begin{Bmatrix} d\tau_c^{(B4)} \\ d\tau_c^{(C1)} \\ d\tau_c^{(A3)} \\ d\tau_c^{(B5)} \end{Bmatrix} = \begin{bmatrix} h(\gamma_{B4}) & q_{B4C1}h(\gamma_{C1}) & q_{B4A3}h(\gamma_{A3}) & q_{B4B5}h(\gamma_{B5}) \\ q_{C1B4}h(\gamma_{B4}) & h(\gamma_{C1}) & q_{C1A3}h(\gamma_{A3}) & q_{C1B5}h(\gamma_{B5}) \\ q_{A3B4}h(\gamma_{B4}) & q_{A3C1}h(\gamma_{C1}) & h(\gamma_{A3}) & q_{A3B5}h(\gamma_{B5}) \\ q_{B5B4}h(\gamma_{B4}) & q_{B5C1}h(\gamma_{C1}) & q_{B5A3}h(\gamma_{A3}) & h(\gamma_{B5}) \end{bmatrix} \begin{Bmatrix} d\gamma_{B4} \\ d\gamma_{C1} \\ d\gamma_{A3} \\ d\gamma_{B5} \end{Bmatrix} \quad (6.4)$$

Latent hardening ratio q_{ij} is symmetric so six latent hardening ratios are to be determined. From the analysis of dislocation interaction junction in FCC single crystals (Franciosi, 1982), we know that dislocation between B4 and C1, between A3 and B5 have a same kind dislocation junction (sessile junction). Dislocation interaction junctions of C1 with A3 and B5 show the same kind of interaction (glissile junction). These two dislocation interaction types show strong dislocation interactions. Dislocation junction type of B4 with A3 and B5 has similar weak dislocation interactions. Based on the knowledge on dislocation interaction junction the amounts of latent hardening ratios activate the secondary slip systems are determined.

To determine the latent hardening ratios for the simulation, we have used following assumptions. Dislocation interactions show strong trend may be explained with one latent hardening ratio. Therefore, q_{B4C1} and q_{A3B5} may be assumed to have same values. q_{C1A3} and q_{C1B5} may be assumed to have same values. Initial critical resolved shear stresses for all slip systems have same values.

Ratio of critical resolved shear stress in primary slip to that in secondary slip system is expressed as follows.

$$\frac{\tau_c^{B4}}{\tau_c^{A3}} = \frac{\int h(\gamma_{B4})d\gamma_{B4} + q_{B4C1}\int h(\gamma_{C1})d\gamma_{C1} + q_{B4A3}\int h(\gamma_{A3})d\gamma_{A3} + q_{B4B5}\int h(\gamma_{B5})d\gamma_{B5}}{q_{A3B4}\int h(\gamma_{B4})d\gamma_{B4} + q_{A3C1}\int h(\gamma_{C1})d\gamma_{C1} + \int h(\gamma_{A3})d\gamma_{A3} + q_{A3B5}\int h(\gamma_{B5})d\gamma_{B5}} \quad (6.5)$$

$$\frac{\tau_c^{B4}}{\tau_c^{B5}} = \frac{\int h(\gamma_{B4})d\gamma_{B4} + q_{B4C1}\int h(\gamma_{C1})d\gamma_{C1} + q_{B4A3}\int h(\gamma_{A3})d\gamma_{A3} + q_{B4B5}\int h(\gamma_{B5})d\gamma_{B5}}{q_{B5B4}\int h(\gamma_{B4})d\gamma_{B4} + q_{B5C1}\int h(\gamma_{C1})d\gamma_{C1} + q_{B5A3}\int h(\gamma_{A3})d\gamma_{A3} + \int h(\gamma_{B5})d\gamma_{B5}} \quad (6.6)$$

We expect the activation of secondary slip systems when the equation (6.5) and equation (6.6) equal to ratio K. Following hardening types were used in our analytical prediction for latent hardening ratio.

$$\tau_c(\gamma) = \tau_0 + (\tau_s - \tau_0)\tanh\left(\frac{h_0\gamma}{\tau_s - \tau_0}\right) \text{ and } h(\gamma) = h_0 \sec h^2\left(\frac{h_0\gamma}{\tau_s - \tau_0}\right) \quad (6.7)$$

Integration of rate of hardening gives following formulas.

$$\begin{aligned}\tau_c^{B4} &= (\tau_s - \tau_0)\tanh\left(\frac{h_0\gamma_{B4}}{\tau_s - \tau_0}\right) + q_{B4C1}\left\{(\tau_s - \tau_0)\tanh\left(\frac{h_0\gamma_{C1}}{\tau_s - \tau_0}\right)\right\} \\ &+ q_{B4A3}\left\{(\tau_s - \tau_0)\tanh\left(\frac{h_0\gamma_{A3}}{\tau_s - \tau_0}\right)\right\} + q_{B4B5}\left\{(\tau_s - \tau_0)\tanh\left(\frac{h_0\gamma_{B5}}{\tau_s - \tau_0}\right)\right\} + \tau_0\end{aligned} \quad (6.8)$$

$$\begin{aligned}\tau_c^{A3} &= q_{A3B4}\left\{(\tau_s - \tau_0)\tanh\left(\frac{h_0\gamma_{B4}}{\tau_s - \tau_0}\right)\right\} + q_{A3C1}\left\{(\tau_s - \tau_0)\tanh\left(\frac{h_0\gamma_{C1}}{\tau_s - \tau_0}\right)\right\} \\ &+ \left\{(\tau_s - \tau_0)\tanh\left(\frac{h_0\gamma_{A3}}{\tau_s - \tau_0}\right)\right\} + q_{A3B5}\left\{(\tau_s - \tau_0)\tanh\left(\frac{h_0\gamma_{B5}}{\tau_s - \tau_0}\right)\right\} + \tau_0\end{aligned} \quad (6.9)$$

$$\begin{aligned}\tau_c^{B5} &= q_{B5B4}\left\{(\tau_s - \tau_0)\tanh\left(\frac{h_0\gamma_{B4}}{\tau_s - \tau_0}\right)\right\} + q_{B5C1}\left\{(\tau_s - \tau_0)\tanh\left(\frac{h_0\gamma_{C1}}{\tau_s - \tau_0}\right)\right\} \\ &+ q_{B5A3}\left\{(\tau_s - \tau_0)\tanh\left(\frac{h_0\gamma_{A3}}{\tau_s - \tau_0}\right)\right\} + \left\{(\tau_s - \tau_0)\tanh\left(\frac{h_0\gamma_{B5}}{\tau_s - \tau_0}\right)\right\} + \tau_0\end{aligned} \quad (6.10)$$

If we assume stage III occurs at 0.3 resolved shear strain in primary slip system B4 and at 0.05 resolved shear strain in conjugate slip system C1, hypertangent curve approaches 0.997 for B4 0.505 for C1 with $h_0=8.9\tau_0$, $\tau_s=1.8\tau_0$. Resolved shear strain in A3 and B5 is zero. Latent hardening ratios of q_{A3B5} and q_{C1B4} are assumed to be 1.1. Using these

assumptions amounts of critical resolved shear stress of each slip systems are calculated as follows.

$$\tau_c^{B4} = \tau_0 + (0.8\times 0.997) + q_{B4C1}(0.8\times 0.505)$$
$$= 0.7976\tau_0 + q_{B4C1}\times 0.404\tau_0 + \tau_0 = 2.242\tau_0 \quad (6.11)$$

$$\tau_c^{B5} = q_{B5B4}(0.8\times 0.997)\tau_0 + q_{B5C1}(0.8\times 0.505)\tau_0 + \tau_0$$
$$= 0.7976q_{B5B4}\tau_0 + 0.404q_{B5C1}\tau_0 + \tau_0 \quad (6.12)$$

$$\tau_c^{A3} = q_{A3B4}(0.8\times 0.997)\tau_0 + q_{A3C1}(0.8\times 0.505)\tau_0 + \tau_0$$
$$= 0.7976q_{A3B4}\tau_0 + 0.404q_{A3C1}\tau_0 + \tau_0 \quad (6.13)$$

Using equations (6.11), (6.12) and (6.13) ratio between primary slip system and secondary slip systems is expressed as follows.

$$\frac{\tau_c^{B4}}{\tau_c^{A3}} = K = \frac{2.242}{0.7976q_{A3B4} + 0.404q_{A3C1} + 1} \quad (6.14)$$

$$\frac{\tau_c^{B4}}{\tau_c^{B5}} = K = \frac{2.242}{0.7976q_{B5B4} + 0.404q_{B5C1} + 1} \quad (6.15)$$

If we assume latent hardening ratios of q_{C1A3} and q_{C1B5} are equal to 1.0, q_{B4A3} and q_{B4B5} can be obtained from equation (6.14) and (6.15).

$$q_{B4A3}=q_{B4B5}\cong 0.1136 \quad (6.16)$$

This analytical prediction of latent hardening ratios for the activation of secondary slip systems indicate that latent hardening ratios between B4 and B5 and between A3 and B4 should have a small value. Simulation is performed when latent hardening ratios are as follows, $q_{B4A3}=q_{B4B5}=0.5$, $q_{B4C1}=q_{A3B5}=1.1$, $q_{C1A3}=q_{C1B5}=1.0$. Stages I, II and III are observed with this selected latent hardening ratios. Stage II is observed due to the activation of

conjugate slip system (figure 6-12). Stage III is observed due to the decrease of hardening rate at large strain.

Hardening model proposed by Weng (1987) was tested. Angles between slip systems are used to obtain latent hardening ratios in his model. By manipulating three coefficients α_1, α_2, α_3 arbitrarily in the hardening formula (equation 3.1), we can assign latent hardening ratios appropriate for deformation behavior of single crystals. Therefore deformation stages in FCC single crystals can be observed using this law.

Summary of this Study

Hardening models were simulated to study the behavior of single crystals. Most of the hardening models were proposed and used in 2-dimensional geometry. 2-dimensional model could not represent a real situation because slip systems are not perpendicular to the plane of deformation in FCC single crystals. Here, we used 3-dimensional model to simulate the deformation process takes place in real situation.

Asaro's model could not represent the stage I, II and III usually observed in FCC single crystals.

The first modified version of Asaro's model showed stage I, stage II when the specimen was pulled upto 12.5 % nominal strain. Stage III could be observed if the specimen is pulled further.

Bassani's model showed a typical behavior of FCC single crystals even no latent hardening ratio was used (q=0).

The second modified version of Asaro's model was proposed to understand the effects of latent hardening ratios on the activation of secondary slip systems. Activation

of secondary slip systems can be controlled by manipulating latent hardening ratios. Stage I, II, and III was observed by suppressing the activation of secondary slip systems. Stage II was shown due to the activation of conjugate slip system C1.

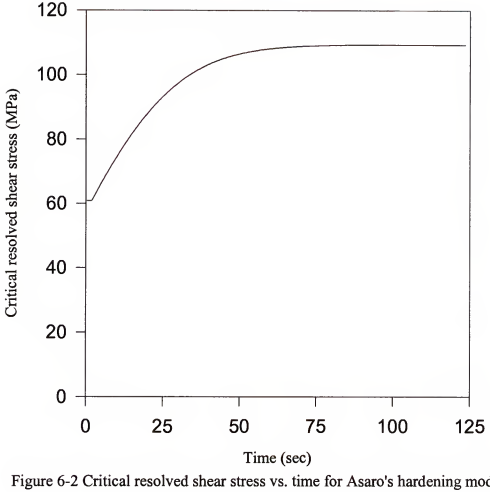

Figure 6-2 Critical resolved shear stress vs. time for Asaro's hardening model

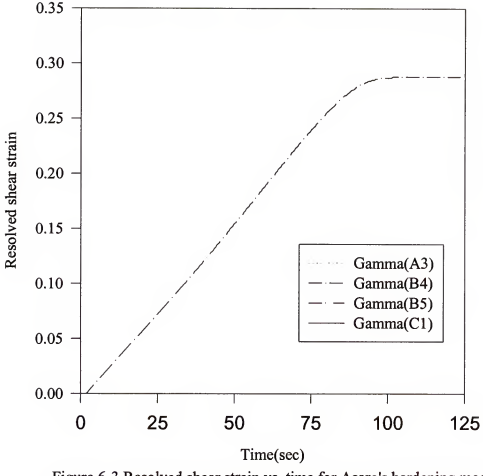

Figure 6-3 Resolved shear strain vs. time for Asaro's hardening model

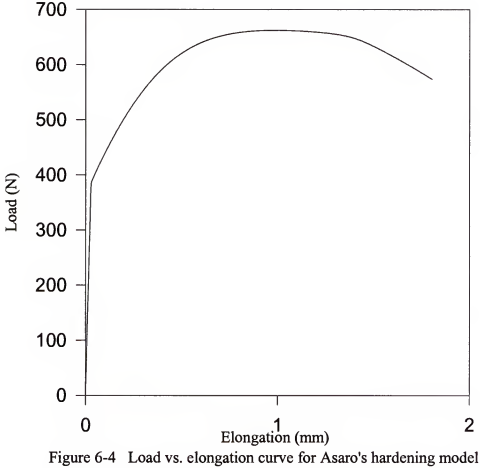

Figure 6-4 Load vs. elongation curve for Asaro's hardening model

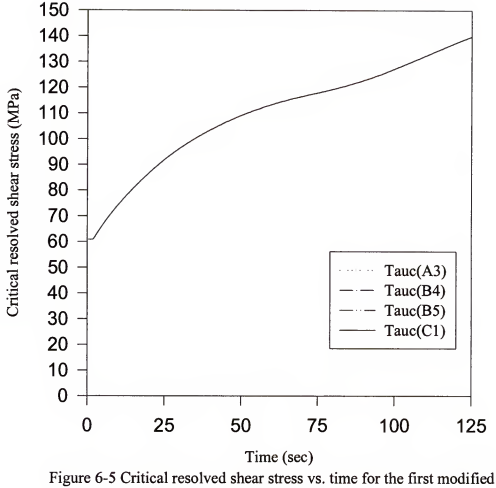

Figure 6-5 Critical resolved shear stress vs. time for the first modified version of Asaro's hardening model

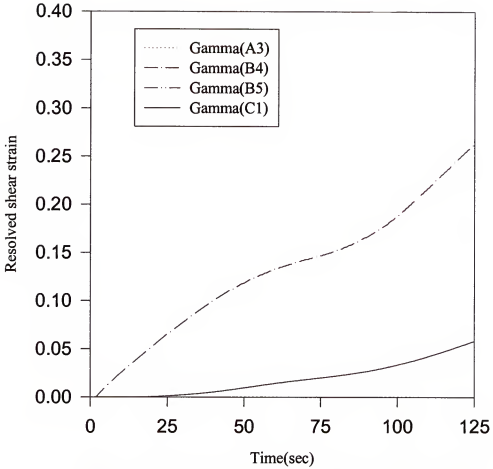

Figure 6-6 Resolved shear strain vs. time for the first modified version of Asaro's hardening model

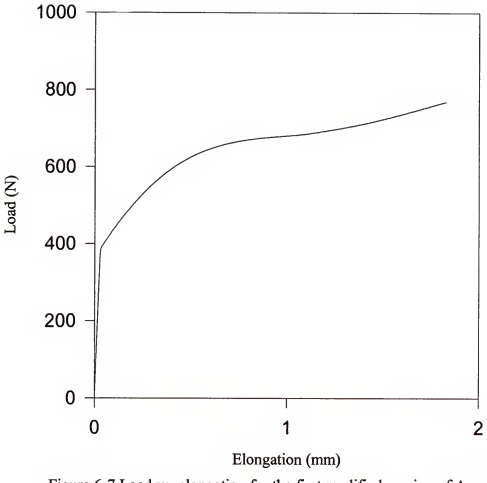

Figure 6-7 Load vs. elongation for the first modified version of Asaro's hardening model

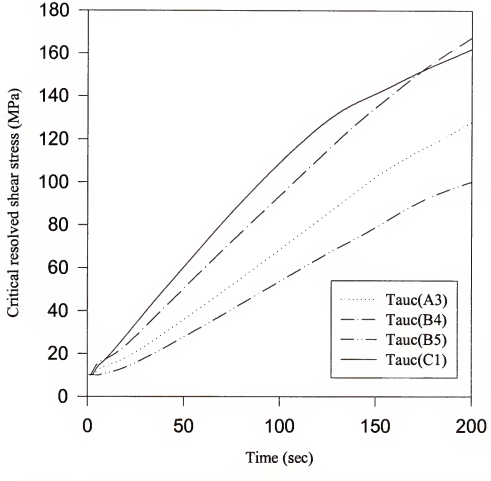

Figure 6-8 Critical resolved shear stress vs. time for Bassani's hardening model

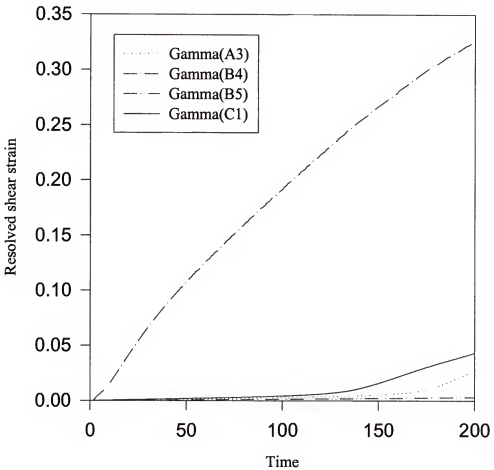

Figure 6-9 Resolved shear strain vs. time for Bassani's hardening model

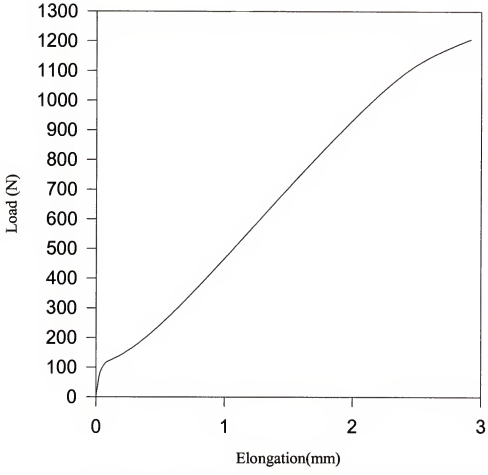

Figure 6-10 Load vs. elongation curve for Bassani's hardening model

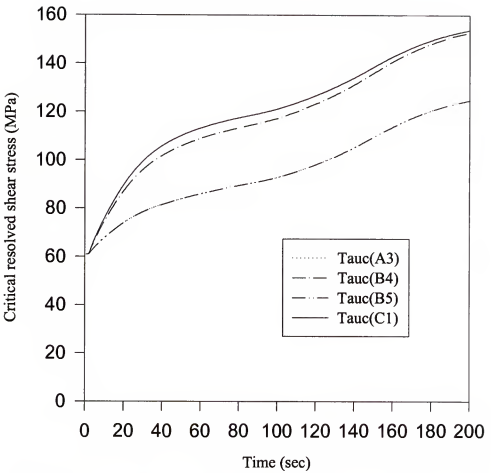

Figure 6-11 Critical resolved shear stress vs. time for the second modified version of Asaro's hardening model

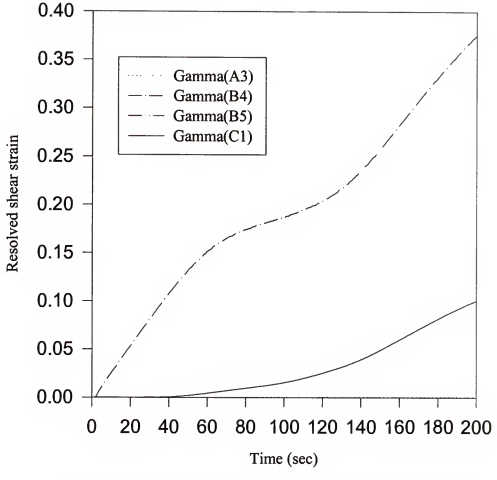

Figure 6-12 Resolved shear strain vs time for the second modified version of Asaro's hardening model

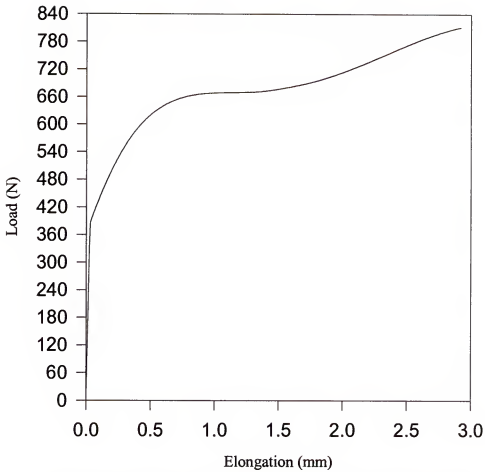

Figure 6-13 Load vs. Elongation for the second modified version of Asaro's hardening model

CHAPTER 7
CONCLUSIONS AND FUTURE WORKS

We have studied the localization phenomena and hardening characteristics of NiAl single crystals using finite element analysis. Localized deformations in NiAl single crystals were observed in experiment such as kink bands and microscopic shear bands (Fraser et al., 1973a, b; Ebrahimi, F. and Shrivastava, S., 1997a, b). To investigate the causes of low ductility of NiAl single crystals, the deformation process and mechanical property were studied throughout this thesis.

Localization phenomena such as shear bands and kink bands are formed in our simulation. Various constitutive parameters and hardening parameters are tested to show the effects on the formation of localized bands. From the simulation we obtain following results :

1. Lattice rotation of crystals causes geometric softening (orientation softening) and geometric softening causes localized bands.
2. High strain rate sensitivity delays localization whereas low strain rate sensitivity promotes localization.
3. Lower hardening facilitates localized deformation.
4. Geometry of the slip system also has a great effect on the formation of localized bands. For instance, loading along the [110] orientation does not allow lattice rotation and consequently no localized bands were observed. However, localized

deformation occurs due to the lattice rotation if the loading axes are misaligned a few degrees from the [110] symmetric orientation.

5. Kink band analysis also shows the effect of the geometry of the slip system. When the compression loading axis is along the hard orientation, no resolved shear stress is obtained and numerical difficulty occurs in the simulation.Whereas kink band is formed when loading axis is misaligned a few degrees from the hard orientation.
6. Geometric softening caused by rotation of crystal lattice is a main mechanism for the formation of kink band in NiAl single crystals.

Hardening characteristics of NiAl single crystals were studied for the purpose of understanding the effect of latent hardening and slip system interaction on the hardening behavior. The increase in load after necking for specimens loaded along [110] orientation was concluded to be due to the activation of {110} slip planes in addition to {100} slip planes. Three-dimensional finite element model is required for the simulation to include the {110} slip planes which are not perpendicular to the plane of deformation. We described four different deformation cases in chapter 5 depending on the activation of slip systems.

The following conclusions are drawn from the simulation results :

1. Activation of slip in {110} planes helps to increase in load at large strain values.
2. The latent hardening ratios q_{aa}, q_{ba} control the activation of cross slip in {110} slip families.
3. The latent hardening ratios q_{bb}, q_{ab} determine the hardening behaviors after the activation of {110} slip families.

4. Case II and Case IV satisfy the condition for activation of cross slip in {110} slip planes. However, early activation of cross slip in {110} slip planes does afford a uniform hardening along a gauge length. The early activation of cross slips in {110} slip plane families is due to the strain rate sensitivity effect.
5. Case II and Case IV can not provide enough hardening at necked region due to the early activation of cross slip in {110} slip plane families.
6. Case I does not satisfy the condition for activation of cross slip in {110} slip planes. However, Case I-b and case I-c show the activation of cross slip in {110} slip plane families due to the strain rate sensitivity.
7. Activation of cross slip in {110} slip plane families at large strain increases hardening rate at necked region and prevents necking in Case I-b.
8. We may conclude that increase in load after necking at large strain values for the <110> orientation of real specimens is due to the activation of cross slip in {110} slip plane families.

Hardening models for FCC single crystals were studied for the purpose of understanding which hardening model can predict experimentally observed deformation behavior such as stages I, II and III. The following are obtained from the simulation results :

1. The two-parameter hardening model used by Asaro (Asaro, 1983) did not show the stage II. Conjugate slip system does not activate due to the higher hardening for every slip system.

2. The first modified version of Asaro's hardening law which uses separate resolved shear strain for each slip system was tested up to 12.5 % of the nominal strain and showed the trends of stage II due to the activation of conjugate slip system.
3. The hardening law proposed by Bassani (Bassani et al., 1991) was tested and showed typical deformation behavior of FCC single crystals.
4. The second modified version of Asaro's hardening model that uses separate resolved shear strain and latent hardening ratios showed stages I, II and III by controlling latent hardening ratios. Stages I, II, and III was observed by suppressing activation of secondary slip systems.

User subroutine "UMAT" in ABAQUS (Seelam, 1995) is expanded for application to three-dimensional problem. Now UMAT subroutine has a capability to simulate real situation. Any directions of orientation of single crystals and slip systems can be included in our model. Elastic anisotropy is also implemented into the UMAT subroutine. However, isotropic elasticity was used for simulation because most of the deformation in single crystals occurs in the plastic region. Elastic anisotropy may be incorporated into the model for deformation studies at the crack tip.

We have studied the deformation processes in the form of single crystals in this study. From this study we suggest following future works :

1. Precise description of hardening based on the physical observation is needed to obtain more accurate simulation results.
2. Other integration methods to improve the speed of calculation should be considered. It took more than ten days to finish one simulation for the three-dimensional model using SGI work station with R8000 CPU.

3. The single crystal model should be extended to deal with bi-crystals or poly-crystals in order to explore their highly complex material behavior based on the observed strain hardening and material properties of single crystals.

APPENDIX
USER MATERIAL SUBROUTINE

```
C##########################################################################
C##########################################################################
C####      ABAQUS Version 5.4 user material subroutine UMAT For an explicit,  ####
C####      one-step, forward-gradient time integration procedure to integrate  ####
C####      a set of constitutive equations for non-uniform plastic deformation  ####
C####      of rate dependent single crystal                                    ####
C####                                                                          ####
C####            For: AFOSR-URI Project                                        ####
C####            Department of Materials Science and Engineering               ####
C####            University of Florida                                         ####
C####            Gainesville, FL 32611                                         ####
C##########################################################################
C##########################################################################
C####    Features:                                                             ####
C####    (1) Rate-dependent, Finite deformation, isotropic and anisotropic crystal  ####
C####        plasticity for modeling FCC and BCC crystals                      ####
C####    (2) This UMAT version is for plane strain problem, plane stress,      ####
C####        axisymmetric and 3-DIM problem                                    ####
C####    (3) For use with *STATIC analysis procedure                           ####
C##########################################################################
C##########################################################################
C NOTATIONS:
C   Tn  = time at the beginning of current increment
C   Tnp  = time at the end of current increment
C   Dt  = current time increment.
C##########################################################################
C Standard UMAT variables that are used (see the UMAT documentation)
C   STRESS  = components of the stress tensor
C   STATEV  = array of solution dependent state variables
C   DDSDDE = derivative of stress increment wrt strain increment
C   STRAN  = components of the strain tensor at Tn
C   DSTRAN = components of the  strain increment tensor in Dt
C   TIME(2)  = total solution time at the beginning of current inc
C   DTIME  = time increment Dt
C   NDI  = number of direct components (Hardwired for 3)
C   NSHR  = number of engineering shear components
C   NTENS  = total number of stress or strain components
C   NSTATV  = number of state variables entered in the *DEPVAR option
C   PROPS(NPROPS)= array of material constants entered in the *USER MATERIAL option
C   NPROPS  = number of material constants (value given to CONSTANTS parameter on
C             the *USER MATERIAL option)
C   DFGRD0(3,3)  = array containing the deformation gradient at the beginning of
```

```
C                    current increment. stored as a 3x3 matrix, DFGRD0(I,J)<=>F(I,J)
C  DFGRD1(3,3) = array containing the deformation gradient at the end of current
C                    increment. Stored as a 3x3 matrix, DFGRD1(I,J)<=>F(I,J)
C  KSTEP      = current step number
C  KINC       = current increment number
C#########################################################################
C Storage of the components of STRESS and STRAN in the UMAT:
C       STRESS(1) = XX (11)(normal or direct) component
C       STRESS(2) = YY (22)(normal or direct) component
C       STRESS(3) = ZZ (33)(normal or direct) component
C       STRESS(4) = XY (12)(engineering shear) component
C       STRESS(5) = XZ (13)(engineering shear) component
C       STRESS(6) = YZ (23)(engineering shear) component
C#########################################################################
C       3-DIM  problem                  NDI=3,NSHR=3 --> NTENS=6
C       Generalized plane strain problems  NDI=3,NSHR=1 --> NTENS=4
C       Plane stress problem            NDI=2,NSHR=1 --> NTENS=3
C       Axisymmetric problem            NDI=3,NSHR=1 --> NTENS=4
C#########################################################################
C Variables stored in the STATEV array:
C Array of critical resolved shear stresses (CRSS) G(NSLIPS)
C  STATEV(1) = G(1)
C Array of shearing on slip systems GAMMA(NSLIPS)
C  STATEV(2) = GAMMA(2)
C Plastic deformation gradient FPLAST(3,3)
C  STATEV(3)  = FPLAST(1,1)
C  STATEV(4)  = FPLAST(2,1)
C  STATEV(5)  = FPLAST(3,1)
C  STATEV(6)  = FPLAST(1,2)
C  STATEV(7)  = FPLAST(2,2)
C  STATEV(8)  = FPLAST(3,2)
C  STATEV(9)  = FPLAST(1,3)
C  STATEV(10) = FPLAST(2,3)
C  STATEV(11) = FPLAST(3,3)
C*************************************************************************
C Unrotated stress (3DIM)
C  STATEV(12) = STRESS(1)
C  STATEV(13) = STRESS(2)
C  STATEV(14) = STRESS(3)
C  STATEV(15) = STRESS(4)
C  STATEV(16) = STRESS(5)
C  STATEV(17) = STRESS(6)
C#########################################################################
C Contents of PROPS(NPROPS) array:
C  PROPS(1) PHI   - degree of implicitness (ranges from 0 to 1)
C  PROPS(2) SRS   - strain rate sensitivity parameter(m)
C  PROPS(3) EMU   - elastic shear modulus
C  PROPS(4) EKAPPA - elastic bulk modulus
C  PROPS(5) ADOT  - reference rate of shearing on system's 1 & 2
C  PROPS(6) QA    - latent hardening ratio
C  PROPS(7) QB    - latent hardening ratio
```

```
C   PROPS(8)  QAB    - latent hardening ratio
C   PROPS(9)  QBA    - latent hardening ratio
C   PROPS(10)  TAU0  - reference CRRS on all slip systems for TGAMMA=0
C   PROPS(11) TAUS   - coefficient of saturation strength for 1&2
C   PROPS(12) H0     - Hardening rate
C   PROPS(13) NTYPE  - Analysis type
C   PROPS(14) NSLIPS - number of slip system
C   PROPS(15) NSLIPS1- number of slip system in {110}
C   PROPS
C   |PROPS(16) PROPS(17) PROPS(18)|  |CMC11 CMC12 CMC13|
C   |PROPS(19) PROPS(20) PROPS(21)|= |CMC21 CMC22 CMC23|
C   |PROPS(22) PROPS(23) PROPS(24)|  |CMC31 CMC32 CMC33|
C     - CMC : material coord.
C   PROPS(25) N1:  [0 0 1] (1 1 0)  PROPS(26) N2: [0 0 1] (-1 1 0)
C   PROPS(27) N3:  [1 0 0] (0 1 -1) PROPS(28) N4: [1 0 0] (0 1 1)
C   PROPS(29) N5:  [0 1 0] (1 0 1)  PROPS(30) N6: [0 1 0] (-1 0 1)
C   PROPS(31) N7:  [1 0 0] (0 1 0)  PROPS(32) N8: [0 0 1] (0 1 0)
C   PROPS(33) N9:  [0 0 1] (1 0 0)  PROPS(34) N10:[0 1 0] (1 0 0)
C   PROPS(35) N11: [0 1 0] (0 0 1)  PROPS(36) N12:[1 0 0] (0 0 1)
C   PROPS(37)  Q     - latent hardening ratio in double slip system
C   PROPS(38) ANGLE1 - Angle between primary and  x axis
C   PROPS(39) ANGLE2 - Angle between conjugate and  x axis
C   PROPS(40) C11    - 1st component of anisotropy elasticity
C   PROPS(41) C12    - 2nd component of anisotropy elasticity
C   PROPS(42) C44    - 3rd component of anisotropy elasticity
C   PROPS(43) NF1:  [0 -1 1] (-1 1 1)  PROPS(44) NF2 : [1 0 1]  (-1 1 1)
C   PROPS(45) NF3:  [1 1 0]  (-1 1 1)  PROPS(46) NF4 : [0 -1 1]  (1 1 1)
C   PROPS(47) NF5:  [-1 0 1]  (1 1 1)  PROPS(48) NF6 : [1 1 0]  (1 1 1)
C   PROPS(49) NF7:  [0 1 1] (-1 -1 1)  PROPS(50) NF8 : [1 0 1] (-1 -1 1)
C   PROPS(51) NF9:  [-1 1 0] (-1-1 1)  PROPS(52) NF11 :[0 1 1]  (1 -1 1)
C   PROPS(53) NF11: [-1 0 1] (1 -1 1)  PROPS(54) NF12 :[1 1 0]  (1 -1 1)
C   PROPS(55) NCRTYPE : CRYSTAL TYPE
C   PROPS(56) Hs : Saturated hardening rate
C######################################################################
C  The above input for H0,TAU0,TAUS should correspond to tensile test data
C  The hardening curve used in this models i.e for FCC and BCC single crystals
C assumes isotropic yield stress for all the slip systems
C######################################################################
C  The parameter PHI controls the degree of implicitness of the integration procedure
C    PHI = 0.0  --- explicit
C    PHI = 1.0  --- fully implicit
C  Suggested value of PHI: equal to or greater than 0.50
C######################################################################
C  VARIABLES:
C######################################################################
SUBROUTINE UMAT(STRESS,STATEV,DDSDDE,SSE,SPD,SCD,
   1 RPL,DDSDDT,DRPLDE,DRPLDT,
   2 STRAN,DSTRAN,TIME,DTIME,TEMP,DTEMP,PREDEF,DPRED,CMNAME,
   3 NDI,NSHR,NTENS,NSTATV,PROPS,NPROPS,COORDS,DROT,PNEWDT,
   4 CELENT,DFGRD0,DFGRD1,NOEL,NPT,LAYER,KSPT,KSTEP,KINC)
C**********************************************************************
```

```
      INCLUDE 'ABA_PARAM.INC'
C**********************************************************************
      CHARACTER*8 CMNAME
      DIMENSION STRESS(NTENS),STATEV(NSTATV),
     1 DDSDDE(NTENS,NTENS),DDSDDT(NTENS),DRPLDE(NTENS),
     2 STRAN(NTENS),DSTRAN(NTENS),TIME(2),PREDEF(1),DPRED(1),
     3 PROPS(NPROPS),COORDS(3),DROT(3,3),DFGRD0(3,3),DFGRD1(3,3)
C######################################################################
C     Changed according to model definition
      PARAMETER (MDIM=6,MNSLIPS=12)
      DIMENSION G(MNSLIPS),GDOTT(MNSLIPS),SDV(3,MNSLIPS),
     1 SNV(3,MNSLIPS),FPLAST(3,3),SUMM(3,3),DFPLAT(3,3),FIPLAT(3,3),
     2 FELAST(3,3),PDINOT(9,MNSLIPS),PNODIT(9,MNSLIPS),
     3 PTEN(MDIM,MNSLIPS),WTEN(9,MNSLIPS),BTEN(MDIM,MNSLIPS),
     4 ELASTM(MDIM,MDIM),RTEN(MDIM,MNSLIPS),TAU(MNSLIPS),
     5 HARDM(MNSLIPS,MNSLIPS),QTEN(MDIM,MNSLIPS),FTEN(MDIM,MNSLIPS),
     6 FDOT(MNSLIPS),DGAMMA(MNSLIPS),GAMMA(MNSLIPS),FDSCAL(MNSLIPS),
     7 DG(MNSLIPS),DSTRES(MDIM),SLIPMM(MNSLIPS,MNSLIPS),
     8 SNVSTR(3,MNSLIPS),DRSTRS(MDIM),SD(3,MNSLIPS),SN(3,MNSLIPS),
     9 SLIPNM(MNSLIPS,MNSLIPS),SDVSTR(3,MNSLIPS)
C**********************************************************************
C     The following matrix is the inverse of DFGRD1 and used to calculate
C     the nominal stress for a particular node.
      DIMENSION DFGIN1(3,3)
C**********************************************************************
      PARAMETER (ZERO=0.0D0,ONE=1.0D0,TWO=2.0D0,THREE=3.0D0)
      PARAMETER (M=3)
C######################################################################
C  Step 1. NDIPL1 and PHIDT are computed for later use in the program
C######################################################################
      NDIPL1=NDI+1
      PHIDT=PROPS(1)*DTIME
C**********************************************************************
C  Step 2. The user material properties are set.
C  NOTE: some props change according to the model definition
C**********************************************************************
      PHI       = PROPS(1)
      SRS       = PROPS(2)
      EMU       = PROPS(3)
      EKAPPA    = PROPS(4)
      ADOT      = PROPS(5)
      QA        = PROPS(6)
      QB        = PROPS(7)
      QAB       = PROPS(8)
      QBA       = PROPS(9)
      TAU0      = PROPS(10)
      TAUS      = PROPS(11)
      H0        = PROPS(12)
      NTYPE     = PROPS(13)
      NSLIPS    = PROPS(14)
      NSLIPS1   = PROPS(15)
```

```
      CMC11     = PROPS(16)
      CMC12     = PROPS(17)
      CMC13     = PROPS(18)
      CMC21  = PROPS(19)
      CMC22  = PROPS(20)
      CMC23  = PROPS(21)
      CMC31  = PROPS(22)
      CMC32  = PROPS(23)
      CMC33  = PROPS(24)
      N1        = PROPS(25)
      N2        = PROPS(26)
      N3        = PROPS(27)
      N4        = PROPS(28)
      N5        = PROPS(29)
      N6        = PROPS(30)
      N7        = PROPS(31)
      N8        = PROPS(32)
      N9        = PROPS(33)
      N10       = PROPS(34)
      N11       = PROPS(35)
      N12       = PROPS(36)
      Q         = PROPS(37)
      ANGLE1 = PROPS(38)
      ANGLE2 = PROPS(39)
      C11       = PROPS(40)
      C12       = PROPS(41)
      C44       = PROPS(42)
      NF1      = PROPS(43)
      NF2      = PROPS(44)
      NF3      = PROPS(45)
      NF4      = PROPS(46)
      NF5      = PROPS(47)
      NF6      = PROPS(48)
      NF7      = PROPS(49)
      NF8      = PROPS(50)
      NF9      = PROPS(51)
      NF10     = PROPS(52)
      NF11     = PROPS(53)
      NF12     = PROPS(54)
      NCRTYPE = PROPS(55)
      Hs            = PROPS(56)
C#########################################################################
C  Step 3. The state variables from STATEV array are set.
C#########################################################################
C  The CRSS G(NSLIPS) and the shearings GAMMA(NSLIPS) are set
      K=NSLIPS
      DO 210 I=1,NSLIPS
        K=K+1
        G(I)=STATEV(I)
        GAMMA(I)=STATEV(K)
  210 CONTINUE
```

```
C*************************************************************************
C  The plastic deformation gradient, FPLAST(3,3) is set
      K=2*NSLIPS
      DO 230 J=1,3
        DO 220 I=1,3
          K=K+1
          FPLAST(I,J)=STATEV(K)
  220   CONTINUE
  230 CONTINUE
C*************************************************************************
C The unrotated STRESS of previous Inc is set. This is used to compute TAU() at time Tn
      K=2*NSLIPS+9
      DO 240 I=1,NTENS
        K=K+1
        DRSTRS(I)=STATEV(K)
  240 CONTINUE
C#########################################################################
C  Step 4. Initialize the state variables, if necessary.
C  NOTE: G(I) i.e CRSS's are changed according to model definition
C    NCRTYPE = 0 =>NIAL TYPE
C    NCRTYPE = 1 =>FCC TYPE
C*************************************************************************
C    FOR NIAL TYPE CRYSTALS
C#########################################################################
IF (NCRTYPE .EQ. 0)THEN
      TGAMMA1=ZERO
      DO 310 I=1,NSLIPS1
        TGAMMA1=TGAMMA1+DABS(GAMMA(I))
  310 CONTINUE
C*************************************************************************
      TGAMMA2=ZERO
      DO 315 I=NSLIPS1+1,NSLIPS
        TGAMMA2=TGAMMA2+DABS(GAMMA(I))
  315 CONTINUE
C*************************************************************************
     IF(TGAMMA1.EQ.ZERO) THEN
C  Initialize the CRSS's G(NSLIPS)
       DO 320 I=1,NSLIPS1
         G(I)=TAU0
  320   CONTINUE
C  Initialize the plastic deformation gradient
       DO 325 I=1,3
         FPLAST(I,I)=ONE
  325   CONTINUE
     END IF
C*************************************************************************
    IF(TGAMMA2.EQ.ZERO) THEN
C  Initialize the CRSS's G(NSLIPS)
      DO 330 I=NSLIPS1+1,NSLIPS
        G(I)=TAU0
  330   CONTINUE
```

```
C  Initialize the plastic deformation gradient
       DO 335 I=1,3
        FPLAST(I,I)=ONE
  335   CONTINUE
     END IF
C#########################################################################
C  Step 5. The possible slip vectors SD(3,NSLIPS) and SN(3,NSLIPS)
C          in the intermediate configuration are calculated.
C#########################################################################
C  Compute slip direction vector SDV(3,NSLIPS)
     IF (NTENS.EQ.6)THEN
      CALL CALSSNIAL(N1,N2,N3,N4,N5,N6,N7,N8,N9,N10,N11,N12,SD,SN)
     ELSE
      SDV(1,1)=DCOSD(ANGLE1)
      SDV(2,1)=DSIND(ANGLE1)
      SDV(3,1)=ZERO
      SDV(1,2)=DCOSD(ANGLE2)
      SDV(2,2)=DSIND(ANGLE2)
      SDV(3,2)=ZERO
C  Compute slip normal vector SNV(3,NSLIPS)
      SNV(1,1)=-DSIND(ANGLE1)
      SNV(2,1)=DCOSD(ANGLE1)
      SNV(3,1)=ZERO
      SNV(1,2)=DSIND(ANGLE2)
      SNV(2,2)=-DCOSD(ANGLE2)
      SNV(3,2)=ZERO
     END IF
C*************************************************************************
C FOR FCC CRYSTALS
C*************************************************************************
     ELSE
      TGAMMA=ZERO
      DO 336 I=1,NSLIPS
       TGAMMA=TGAMMA+DABS(GAMMA(I))
  336  CONTINUE
C
     IF(TGAMMA.EQ.ZERO) THEN
C  Initialize the CRSS's G(NSLIPS)
       DO 337 I=1,NSLIPS
        G(I)=TAU0
  337   CONTINUE
C  Initialize the plastic deformation gradient
       DO 338 I=1,3
        FPLAST(I,I)=ONE
  338   CONTINUE
     END IF
C#########################################################################
C  Step 5. The slip vectors SDV(3,NSLIPS) and SNV(3,NSLIPS) in the intermediate
C          configuration are calculated.
C  NOTE: Change according to model definition
C#########################################################################
```

```
C  Compute slip direction vector SDV(3,NSLIPS)
     IF (NTENS.EQ.6)THEN
      CALL CALSSFCC(NF1,NF2,NF3,NF4,NF5,NF6,NF7,NF8,NF9,NF10,NF11,NF12,SD,SN)
     ELSE
      SDV(1,1)=DCOSD(ANGLE1)
      SDV(2,1)=DSIND(ANGLE1)
      SDV(3,1)=ZERO
      SDV(1,2)=DCOSD(ANGLE2)
      SDV(2,2)=DSIND(ANGLE2)
      SDV(3,2)=ZERO
C  Compute slip normal vector SNV(3,NSLIPS)
      SNV(1,1)=-DSIND(ANGLE1)
      SNV(2,1)=DCOSD(ANGLE1)
      SNV(3,1)=ZERO
      SNV(1,2)=DSIND(ANGLE2)
      SNV(2,2)=-DCOSD(ANGLE2)
      SNV(3,2)=ZERO
     END IF
C*************************************************************************
    END IF
C#########################################################################
C  Step 6. The elastic deformation gradient FELAST is computed.
C#########################################################################
C  Invert FPLAST to obtain FIPLAT
    CALL FINVRST (FPLAST,FIPLAT,M)
C*************************************************************************
    DO 530 J=1,3
     DO 520 I=1,3
      FELAST(I,J)=ZERO
 520  CONTINUE
 530 CONTINUE
C*************************************************************************
    DO 560 J=1,3
     DO 550 I=1,3
      DO 540 K=1,3
       FELAST(I,J)=FELAST(I,J)+DFGRD0(I,K)*FIPLAT(K,J)
 540   CONTINUE
 550  CONTINUE
 560 CONTINUE
C#########################################################################
C  Step 7. The subroutine CONSLIPSYS computes slip systems w.r.t. global coord.
C#########################################################################
      IF (NTENS.EQ.6)THEN
     CALL CONSLIPSYS(SD,SN,CMC11,CMC12,CMC13,CMC21,CMC22,CMC23,
    +           CMC31,CMC32,CMC33,NSLIPS,SDV,SNV)
C*************************************************************************
C  Step 8. The subroutine LATVEC computes the the lattice vectors corresponding
C          to the deformed configuration at time Tn (actually at time Tnp of previous inc)-
C NOTE: SDVSTR and SNVSTR are not normalized.
C*************************************************************************
     CALL LATVEC (FELAST,SDV,SNV,SDVSTR,SNVSTR,NSLIPS)
```

```
      ELSE
        CALL LATVEC (FELAST,SDV,SNV,SDVSTR,SNVSTR,NSLIPS)
      END IF
C#####################################################################
C  Step 9. Subroutine PROSDN computes the products of SDVSTR & SNVSTR
C    i.e PDINOT & PNODIT to compute the schmid tensors PTEN(NTENS,NSLIPS)
C    & WTEN(9,NSLIPS) at time Tn (actually at time Tnp of previous inc)
C#####################################################################
      CALL PROSDN (SDVSTR,SNVSTR,PDINOT,PNODIT,NSLIPS)
C#####################################################################
C  Step 10. Subroutine SCHMIP computes PTEN(NTENS,NSLISP) at Tn,
C        PTEN is symmetric and analogous to STRAN(NTENS)
C#####################################################################
      CALL SCHMIP (PDINOT,PNODIT,PTEN,NSLIPS,NDI)
C#####################################################################
C  Step 11. Subroutine SCHMIW Calculates the schmid factor
C        WTEN(9,NSLIPS) at Tn. WTEN(9,NSLIPS) is skew symmetric.
C#####################################################################
      CALL SCHMIW (PDINOT,PNODIT,WTEN,NSLIPS)
C#####################################################################
C  Step 12. Subroutine BETA Computes BTEN at Tn BTEN is analogous to STRESS
C#####################################################################
      CALL BETA (WTEN,STRESS,NTENS,BTEN,NSLIPS,NDI)
C#####################################################################
C  Step 13. Calculate the elastic matrix with the ground state values
C#####################################################################
C  Change analysis type according to model definition
C  Axisymmetric model : NTYPE = 1
C  Plane stress model :    NTYPE = 2
C  Plane strain model :    NTYPE = 3
C  3 - DIM model     :    NTYPE = 4
C  General anisotropy :    NTYPE = 5
C*********************************************************************
      IF     (NTYPE .EQ. 1)THEN
       CALL ELMATR1(EMU,EKAPPA,NTENS,NDI,NDIPL1,ELASTM)
      ELSE IF (NTYPE .EQ. 2)THEN
       CALL ELMATR2(EMU,NTENS,NDI,NDIPL1,ELASTM)
      ELSE IF (NTYPE .EQ. 3)THEN
       CALL ELMATR3(EMU,EKAPPA,NTENS,NDIPL1,ELASTM)
      ELSE IF (NTYPE .EQ. 4)THEN
       CALL ELMATR4(EMU,EKAPPA,NDI,NTENS,NDIPL1,ELASTM)
      ELSE
       CALL CALCOORD(FELAST,CMC11,CMC12,CMC13,CMC21,CMC22,CMC23,
     +          CMC31,CMC32,CMC33,CX,CY,CZ,NTENS)
       CALL ANIELAS(C11,C12,C44,CX,CY,CZ,ELASTM,NDI)
      END IF
C#####################################################################
C  Step 14. Calculate RTEN(6,NSLIPS) at Tn
C#####################################################################
      CALL RTENS (BTEN,PTEN,ELASTM,RTEN,NSLIPS,NTENS,NDI)
C*********************************************************************
```

```
C  Step 15. Calculate the resolved shear stress TAU at Tn
C  NOTE 1: The stress used here is KIRCHOFF stress
C  NOTE 2: Here the unrotated stress tensor of previous Inc i.e DRSTRS
C            is used to compute TAU(NSLIPS)
C*************************************************************************
C  Initialize TAU
     DO 1310 K=1,NSLIPS
      TAU(K)=ZERO
 1310 CONTINUE
C*************************************************************************
C  Calculate TAU
       DO 1330 K=1,NSLIPS
        DO 1320 I=1,NTENS
C--------   TAU(K)=TAU(K)+PTEN(I,K)*STRESS(I)  ------------------------
          TAU(K)=TAU(K)+PTEN(I,K)*DRSTRS(I)
 1320     CONTINUE
 1330   CONTINUE
C*************************************************************************
C To avoid division by ZERO set the value of TAU(NSLIPS) to a small number if they become 0
       DO 1360 I=1,NSLIPS
       IF (TAU(I).EQ.ZERO) THEN
        TAU(I)=1.D-6
       END IF
 1360 CONTINUE
C#########################################################################
C  Step 16. Calculate GDOTT at time Tn. subroutine GAMDOT returns GDOTT(NSLIPS)
C#########################################################################
          CALL GAMDOT (TAU,G,GDOTT,SRS,ADOT,NSLIPS)
C#########################################################################
C  Step 17. Call subroutine QTENSO, which returns the tensor QTEN
C        based on the value of RTEN at time Tn
C#########################################################################
         CALL QTENSO (GDOTT,TAU,PHIDT,SRS,RTEN,QTEN,NSLIPS,NTENS)
C#########################################################################
C  Step 18. Calculate the hardening matrix at time Tn based on the value of TGAMMA at the
C             end of last inc. The computed value of HARDM is used in calculating SLIPMM
C   NOTE: If TGAMMA=0 then h(TGAMMA)=h0
C               NCRTYPE = 0 =>NIAL TYPE
C               NCRTYPE = 1 =>FCC TYPE
C#########################################################################
     IF (NCRTYPE .EQ. 0)THEN
     CALL HCURVM(TGAMMA1,TGAMMA2,HARDM,H0,TAUS,TAU0,QA,QB,
    +          QAB,QBA,NSLIPS,NSLIPS1,NTENS,Q)
     ELSE
      CALL HCURVMF(TGAMMA,HARDM,H0,TAUS,TAU0,NSLIPS,Q,Hs)
     END IF
C#########################################################################
C  Step 19. Call subroutine SMATRX, which returns the matrix SLIPMM based
C        on the values of RTEN, PTEN, TAU, GDOTT, HARDM and G at time Tn
C#########################################################################
     CALL SMATRX (GDOTT,RTEN,PTEN,TAU,G,HARDM,NSLIPS,PHIDT,SRS,
```

```
     + SLIPMM,NTENS,NDI)
C#########################################################################
C  Step 20.Call subroutine FDOTS (returns the value FDOT(NSLIPS) at time Tn)
C#########################################################################
      CALL FDOTS (SLIPMM,GDOTT,FDOT,NSLIPS)
C#########################################################################
C  Step 21.Call subroutine FTENSO (returns the tensor FTEN(6,NSLIPS) at time Tn)
C#########################################################################
      CALL FTENSO (SLIPMM,QTEN,FTEN,NSLIPS,NTENS)
C#########################################################################
C  Step 22.  Calculate the slip increments DGAMMA during current time inc Dt and then
C            update the slips on each slip system GAMMA.
C#########################################################################
     DO 2110 I=1,NSLIPS
      FDSCAL(I)=ZERO
 2110 CONTINUE
C*************************************************************************
C  Compute the scalar product of FTEN and DSTRAN.
      DO 2130 K=1,NSLIPS
        DO 2120 I=1,NTENS
         FDSCAL(K)=FDSCAL(K)+FTEN(I,K)*DSTRAN(I)
 2120    CONTINUE
 2130   CONTINUE
C*************************************************************************
C  Compute the slip increments
     DO 2160 I=1,NSLIPS
      DGAMMA(I)=FDOT(I)*DTIME+FDSCAL(I)
 2160 CONTINUE
C*************************************************************************
C  Update the slip increments.
     DO 2170 I=1,NSLIPS
      GAMMA(I)=GAMMA(I)+DGAMMA(I)
 2170 CONTINUE
C#########################################################################
C  Step 23. HCURVM computes the new hardening matrix for Dt with the updated value of
C            TGAMMA.
C#########################################################################
     IF (NCRTYPE .EQ.0) THEN
      TGAMMA1=ZERO
      DO 2210 I=1,NSLIPS1
       TGAMMA1=TGAMMA1+DABS(GAMMA(I))
 2210  CONTINUE
C*************************************************************************
      TGAMMA2=ZERO
      DO 2215 I=NSLIPS1+1,NSLIPS
       TGAMMA2=TGAMMA2+DABS(GAMMA(I))
 2215  CONTINUE
C*************************************************************************
     CALL HCURVM(TGAMMA1,TGAMMA2,HARDM,H0,TAUS,TAU0,QA,QB,
    +          QAB,QBA,NSLIPS,NSLIPS1,NTENS,Q)
     ELSE
```

```
      TGAMMA=ZERO
      DO 2217 I=1,NSLIPS
        TGAMMA=TGAMMA+DABS(GAMMA(I))
 2217  CONTINUE
      CALL HCURVMF(TGAMMA,HARDM,H0,TAUS,TAU0,NSLIPS,Q,Hs)
      END IF
C#######################################################################
C Step 24. Update the critical resolved shear stresses
C#######################################################################
C  Initialize the critical resolved shear stress increment array DG.
      DO 2310 I=1,NSLIPS
        DG(I)=ZERO
 2310 CONTINUE
C***********************************************************************
C  Compute the increments of crss DG during the current increment
      DO 2330 J=1,NSLIPS
        DO 2320 I=1,NSLIPS
          DG(J)=DG(J)+HARDM(J,I)*DABS(DGAMMA(I))
 2320   CONTINUE
 2330 CONTINUE
C***********************************************************************
C  Update the crss
      DO 2340 I=1,NSLIPS
        G(I)=G(I)+DG(I)
 2340 CONTINUE
C#######################################################################
C  Step 25. Compute the JACOBIAN matrix DDSDDE(NTENS,NTENS)
C  NOTE: DDSDDE is not neccessarly symmetric.
C#######################################################################
C  Calculate the tensor product of RTEN & FTEN under summation
      DO 2420 J=1,NTENS
        DO 2410 I=1,NTENS
          DDSDDE(I,J)=ZERO
 2410   CONTINUE
 2420 CONTINUE
C***********************************************************************
C  HERE the computation is done in ROW order, optimize it.
      DO 2450 K=1,NSLIPS
        DO 2440 I=1,NTENS
          DO 2430 J=1,NTENS
            DDSDDE(J,I)=DDSDDE(J,I)+RTEN(I,K)*FTEN(J,K)
 2430     CONTINUE
 2440   CONTINUE
 2450 CONTINUE
C***********************************************************************
      DO 2470 J=1,NTENS
        DO 2460 I=1,NTENS
          DDSDDE(I,J)=ELASTM(I,J)-DDSDDE(I,J)
 2460   CONTINUE
 2470 CONTINUE
C#######################################################################
```

```
C  Step 26. Calculate the stress increments and then update.
C  NOTE : The stress measure used is KIRCHOFF STRESS
C##########################################################################
C  Initialize the stress increment during the current step DSTRES
     DO 2510 I=1,NTENS
      DSTRES(I)=ZERO
 2510 CONTINUE
C**************************************************************************
C  Calculate DSTRES
       DO 2530 I=1,NTENS
        DO 2520 J=1,NTENS
         DSTRES(I)=DSTRES(I)+DDSDDE(I,J)*DSTRAN(J)
 2520    CONTINUE
 2530   CONTINUE
C**************************************************************************
C  CHECK for the shear components of RTEN.
     DO 2550 K=1,NSLIPS
      DO 2540 I=1,NTENS
       DSTRES(I)=DSTRES(I)-RTEN(I,K)*FDOT(K)*DTIME
 2540  CONTINUE
 2550 CONTINUE
C**************************************************************************
C  Update the KIRCHOFF STRESS at the end of the current increment.
       DO 2560 I=1,NTENS
        STRESS(I)=STRESS(I)+DSTRES(I)
 2560   CONTINUE
C##########################################################################
C  Step 27. Update the plastic deformation gradient FPLAST at time Tnp
C##########################################################################
C  Form the matrix of the terms in the summation sign
     DO 2620 J=1,3
      DO 2610 I=1,3
       SUMM(I,J)=ZERO
       DFPLAT(I,J)=ZERO
 2610  CONTINUE
 2620 CONTINUE
C**************************************************************************
     DO 2650 K=1,NSLIPS
      DO 2640 J=1,3
       DO 2630 I=1,3
        SUMM(I,J)=SUMM(I,J)+DGAMMA(K)*SDV(I,K)*SNV(J,K)
 2630    CONTINUE
 2640  CONTINUE
 2650 CONTINUE
C**************************************************************************
C  Calculate the increment of plastic deformation gradient.
C  Remove DFPLAT with FPLAST to optimize the code
C**************************************************************************
     DO 2603 J=1,3
      DO 2602 I=1,3
       DO 2601 K=1,3
```

```
      DFPLAT(I,J)=DFPLAT(I,J)+SUMM(I,K)*FPLAST(K,J)
 2601   CONTINUE
 2602  CONTINUE
 2603 CONTINUE
C*************************************************************************
C  Update the plastic deformation gradient.
    DO 2605 J=1,3
     DO 2604 I=1,3
      FPLAST(I,J)=FPLAST(I,J)+DFPLAT(I,J)
 2604  CONTINUE
 2605 CONTINUE
C#########################################################################
C  Step 28.  Update the STATEV array.
C#########################################################################
C  The CRSS G(NSLIPS) and the shearings GAMMA(NSLIPS) are set
    K=NSLIPS
    DO 2710 I=1,NSLIPS
     K=K+1
     STATEV(I)=G(I)
     STATEV(K)=GAMMA(I)
 2710 CONTINUE
C*************************************************************************
C  The  inverse of plastic deformation gradient, FIPLAT(3,3) is set
    K=2*NSLIPS
    DO 2730 J=1,3
     DO 2720 I=1,3
      K=K+1
      STATEV(K)=FPLAST(I,J)
 2720  CONTINUE
 2730 CONTINUE
C*************************************************************************
C store the unrotated stress to compute TAU in the next inc.
    K=2*NSLIPS+9
      DO 2750 I=1,NTENS
       K=K+1
       STATEV(K)=STRESS(I)
 2750   CONTINUE
C*************************************************************************
    RETURN
    END
C#########################################################################
    SUBROUTINE CALSSNIAL(N1,N2,N3,N4,N5,N6,N7,N8,N9,N10,N11,N12,SD,SN)
C#########################################################################
    INCLUDE 'ABA_PARAM.INC'
     PARAMETER (MDIM=6,MNSLIPS=12)
    DIMENSION SD(3,MNSLIPS),SN(3,MNSLIPS)
C*************************************************************************
      K=1
     IF(N1.EQ.0)THEN
     SD(1,K)=0.0D0
     SD(2,K)=0.0D0
```

```
      SD(3,K)=1.0D0
      SN(1,K)=1.0D0/DSQRT(2.0D0)
      SN(2,K)=1.0D0/DSQRT(2.0D0)
      SN(3,K)=0.0D0
      K=K+1
      ENDIF
C*************************************************************************
      IF(N2.EQ.0)THEN
      SD(1,K)=0.0D0
      SD(2,K)=0.0D0
      SD(3,K)=1.0D0
      SN(1,K)=-1.0D0/DSQRT(2.0D0)
      SN(2,K)=1.0D0/DSQRT(2.0D0)
      SN(3,K)=0.0D0
      K=K+1
      ENDIF
C*************************************************************************
      IF(N3.EQ.0)THEN
      SD(1,K)=1.0D0
      SD(2,K)=0.0D0
      SD(3,K)=0.0D0
      SN(1,K)=0.0D0
      SN(2,K)=-1.0D0/DSQRT(2.0D0)
      SN(3,K)=1.0D0/DSQRT(2.0D0)
      K=K+1
      ENDIF
C*************************************************************************
      IF(N4.EQ.0)THEN
      SD(1,K)=1.0D0
      SD(2,K)=0.0D0
      SD(3,K)=0.0D0
      SN(1,K)=0.0D0
      SN(2,K)=1.0D0/DSQRT(2.0D0)
      SN(3,K)=1.0D0/DSQRT(2.0D0)
      K=K+1
      ENDIF
C*************************************************************************
      IF(N5.EQ.0)THEN
      SD(1,K)=0.0D0
      SD(2,K)=1.0D0
      SD(3,K)=0.0D0
      SN(1,K)=1.0D0/DSQRT(2.0D0)
      SN(2,K)=0.0D0
      SN(3,K)=1.0D0/DSQRT(2.0D0)
      K=K+1
      ENDIF
C*************************************************************************
      IF(N6.EQ.0)THEN
      SD(1,K)=0.0D0
      SD(2,K)=1.0D0
      SD(3,K)=0.0D0
```

```
      SN(1,K)=-1.0D0/DSQRT(2.0D0)
      SN(2,K)=0.0D0
      SN(3,K)=1.0D0/DSQRT(2.0D0)
      K=K+1
     ENDIF
C*****************************************************************************
     IF(N7.EQ.0)THEN
      SD(1,K)=1.0D0
      SD(2,K)=0.0D0
      SD(3,K)=0.0D0
      SN(1,K)=0.0D0
      SN(2,K)=1.0D0
      SN(3,K)=0.0D0
      K=K+1
     ENDIF
C*****************************************************************************
     IF(N8.EQ.0)THEN
      SD(1,K)=0.0D0
      SD(2,K)=0.0D0
      SD(3,K)=1.0D0
      SN(1,K)=0.0D0
      SN(2,K)=1.0D0
      SN(3,K)=0.0D0
      K=K+1
     ENDIF
C*****************************************************************************
     IF(N9.EQ.0)THEN
      SD(1,K)=0.0D0
      SD(2,K)=0.0D0
      SD(3,K)=1.0D0
      SN(1,K)=1.0D0
      SN(2,K)=0.0D0
      SN(3,K)=0.0D0
      K=K+1
     ENDIF
C*****************************************************************************
     IF(N10.EQ.0)THEN
      SD(1,K)=0.0D0
      SD(2,K)=1.0D0
      SD(3,K)=0.0D0
      SN(1,K)=1.0D0
      SN(2,K)=0.0D0
      SN(3,K)=0.0D0
      K=K+1
     ENDIF
C*****************************************************************************
     IF(N11.EQ.0)THEN
      SD(1,K)=0.0D0
      SD(2,K)=1.0D0
      SD(3,K)=0.0D0
      SN(1,K)=0.0D0
```

```
      SN(2,K)=0.0D0
      SN(3,K)=1.0D0
      K=K+1
     ENDIF
C*************************************************************************
     IF(N12.EQ.0)THEN
      SD(1,K)=1.0D0
      SD(2,K)=0.0D0
      SD(3,K)=0.0D0
      SN(1,K)=0.0D0
      SN(2,K)=0.0D0
      SN(3,K)=1.0D0
      K=K+1
     ENDIF
C*************************************************************************
     RETURN
     END
C#########################################################################
     SUBROUTINE CALSSFCC(NF1,NF2,NF3,NF4,NF5,NF6,NF7,NF8,NF9,NF10,NF11,
    +                    NF12,SD,SN)
C#########################################################################
     INCLUDE 'ABA_PARAM.INC'
      PARAMETER (MDIM=6,MNSLIPS=12)
     DIMENSION SD(3,MNSLIPS),SN(3,MNSLIPS)
C*************************************************************************
      K=1
     IF(NF1.EQ.0)THEN
      SD(1,K)=1.0D0/DSQRT(2.0D0)
      SD(2,K)=-1.0D0/DSQRT(2.0D0)
      SD(3,K)=0.0D0
      SN(1,K)=1.0D0/DSQRT(3.0D0)
      SN(2,K)=1.0D0/DSQRT(3.0D0)
      SN(3,K)=1.0D0/DSQRT(3.0D0)
      K=K+1
     ENDIF
C*************************************************************************
     IF(NF2.EQ.0)THEN
      SD(1,K)=1.0D0/DSQRT(2.0D0)
      SD(2,K)=0.0D0
      SD(3,K)=-1.0D0/DSQRT(2.0D0)
      SN(1,K)=1.0D0/DSQRT(3.0D0)
      SN(2,K)=1.0D0/DSQRT(3.0D0)
      SN(3,K)=1.0D0/DSQRT(3.0D0)
      K=K+1
     ENDIF
C*************************************************************************
     IF(NF3.EQ.0)THEN
      SD(1,K)=0.0D0
      SD(2,K)=-1.0D0/DSQRT(2.0D0)
      SD(3,K)=1.0D0/DSQRT(2.0D0)
      SN(1,K)=1.0D0/DSQRT(3.0D0)
```

```
      SN(2,K)=1.0D0/DSQRT(3.0D0)
      SN(3,K)=1.0D0/DSQRT(3.0D0)
      K=K+1
      ENDIF
C*************************************************************************
      IF(NF4.EQ.0)THEN
      SD(1,K)=1.0D0/DSQRT(2.0D0)
      SD(2,K)=-1.0D0/DSQRT(2.0D0)
      SD(3,K)=0.0D0
      SN(1,K)=-1.0D0/DSQRT(3.0D0)
      SN(2,K)=-1.0D0/DSQRT(3.0D0)
      SN(3,K)=1.0D0/DSQRT(3.0D0)
      K=K+1
      ENDIF
C*************************************************************************
      IF(NF5.EQ.0)THEN
      SD(1,K)=1.0D0/DSQRT(2.0D0)
      SD(2,K)=0.0D0
      SD(3,K)=1.0D0/DSQRT(2.0D0)
      SN(1,K)=-1.0D0/DSQRT(3.0D0)
      SN(2,K)=-1.0D0/DSQRT(3.0D0)
      SN(3,K)=1.0D0/DSQRT(3.0D0)
      K=K+1
      ENDIF
C*************************************************************************
      IF(NF6.EQ.0)THEN
      SD(1,K)=0.0D0
      SD(2,K)=1.0D0/DSQRT(2.0D0)
      SD(3,K)=1.0D0/DSQRT(2.0D0)
      SN(1,K)=-1.0D0/DSQRT(3.0D0)
      SN(2,K)=-1.0D0/DSQRT(3.0D0)
      SN(3,K)=1.0D0/DSQRT(3.0D0)
      K=K+1
      ENDIF
C*************************************************************************
      IF(NF7.EQ.0)THEN
      SD(1,K)=1.0D0/DSQRT(2.0D0)
      SD(2,K)=1.0D0/DSQRT(2.0D0)
      SD(3,K)=0.0D0
      SN(1,K)=1.0D0/DSQRT(3.0D0)
      SN(2,K)=-1.0D0/DSQRT(3.0D0)
      SN(3,K)=1.0D0/DSQRT(3.0D0)
      K=K+1
      ENDIF
C*************************************************************************
      IF(NF8.EQ.0)THEN
      SD(1,K)=1.0D0/DSQRT(2.0D0)
      SD(2,K)=0.0D0
      SD(3,K)=-1.0D0/DSQRT(2.0D0)
      SN(1,K)=1.0D0/DSQRT(3.0D0)
      SN(2,K)=-1.0D0/DSQRT(3.0D0)
```

```
      SN(3,K)=1.0D0/DSQRT(3.0D0)
      K=K+1
      ENDIF
C*************************************************************************
      IF(NF9.EQ.0)THEN
      SD(1,K)=0.0D0
      SD(2,K)=1.0D0/DSQRT(2.0D0)
      SD(3,K)=1.0D0/DSQRT(2.0D0)
      SN(1,K)=1.0D0/DSQRT(3.0D0)
      SN(2,K)=-1.0D0/DSQRT(3.0D0)
      SN(3,K)=1.0D0/DSQRT(3.0D0)
      K=K+1
      ENDIF
C*************************************************************************
      IF(NF10.EQ.0)THEN
      SD(1,K)=1.0D0/DSQRT(2.0D0)
      SD(2,K)=1.0D0/DSQRT(2.0D0)
      SD(3,K)=0.0D0
      SN(1,K)=1.0D0/DSQRT(3.0D0)
      SN(2,K)=-1.0D0/DSQRT(3.0D0)
      SN(3,K)=-1.0D0/DSQRT(3.0D0)
      K=K+1
      ENDIF
C*************************************************************************
      IF(NF11.EQ.0)THEN
      SD(1,K)=1.0D0/DSQRT(2.0D0)
      SD(2,K)=0.0D0
      SD(3,K)=1.0D0/DSQRT(2.0D0)
      SN(1,K)=1.0D0/DSQRT(3.0D0)
      SN(2,K)=-1.0D0/DSQRT(3.0D0)
      SN(3,K)=-1.0D0/DSQRT(3.0D0)
      K=K+1
      ENDIF
C*************************************************************************
      IF(NF12.EQ.0)THEN
      SD(1,K)=0.0D0
      SD(2,K)=1.0D0/DSQRT(2.0D0)
      SD(3,K)=-1.0D0/DSQRT(2.0D0)
      SN(1,K)=1.0D0/DSQRT(3.0D0)
      SN(2,K)=-1.0D0/DSQRT(3.0D0)
      SN(3,K)=-1.0D0/DSQRT(3.0D0)
      K=K+1
      ENDIF
C*************************************************************************
      RETURN
      END
C#########################################################################
      SUBROUTINE CONSLIPSYS(SD,SN,CMC11,CMC12,CMC13,CMC21,CMC22,CMC23,
     + CMC31,CMC32,CMC33,NSLIPS,SDV,SNV)
C#########################################################################
C  Subroutine CONSLIPSYS will calculate slip systems w.r.t the global coord. system
```

```
C*********************************************************************
      INCLUDE 'ABA_PARAM.INC'
       PARAMETER (MDIM=6,MNSLIPS=12)
      DIMENSION SDV(3,MNSLIPS),SNV(3,MNSLIPS)
      DIMENSION SD(3,MNSLIPS),SN(3,MNSLIPS)
C*********************************************************************
      DO 11 K=1,NSLIPS
       SDV(1,K)=SD(1,K)*CMC11+SD(2,K)*CMC12+SD(3,K)*CMC13
       SDV(2,K)=SD(1,K)*CMC21+SD(2,K)*CMC22+SD(3,K)*CMC23
       SDV(3,K)=SD(1,K)*CMC31+SD(2,K)*CMC32+SD(3,K)*CMC33
       SNV(1,K)=SN(1,K)*CMC11+SN(2,K)*CMC12+SN(3,K)*CMC13
       SNV(2,K)=SN(1,K)*CMC21+SN(2,K)*CMC22+SN(3,K)*CMC23
       SNV(3,K)=SN(1,K)*CMC31+SN(2,K)*CMC32+SN(3,K)*CMC33
 11   CONTINUE
C*********************************************************************
      RETURN
      END
C#####################################################################
      SUBROUTINE GAMDOT (TAU,G,GDOTT,SRS,ADOT,NSLIPS)
C#####################################################################
C  Subroutine GAMDOT will calculate the rate of shearing on each slip system
C  at the beginning of each increment i.e tn based on the values at time tn of the
C  resolved shear stresses and the critical resolved shear stresses
C  In this subroutine GDOTT1 and GDOTT2 are the shearing rates at time tn
C*********************************************************************
      INCLUDE 'ABA_PARAM.INC'
       PARAMETER (MDIM=6,MNSLIPS=12)
      DIMENSION TAU(MNSLIPS),G(MNSLIPS),GDOTT(MNSLIPS)
      DIMENSION TAUOG(MNSLIPS)
      PARAMETER (ZERO=0.0D0,ONE=1.0D0,TWO=2.0D0,THREE=3.0D0)
C*********************************************************************
C  Compute the exponential.
      EXPONT=(ONE/SRS)-ONE
C  Compute TAU over G
      DO 10 I=1,NSLIPS
       TAUOG(I)=TAU(I)/G(I)
  10  CONTINUE
C*********************************************************************
C  Compute GDOTT
      DO 30 I=1,NSLIPS
       GDOTT(I)=(ADOT*TAUOG(I))*((DABS(TAUOG(I)))**EXPONT)
  30  CONTINUE
C*********************************************************************
      RETURN
      END
C#####################################################################
      SUBROUTINE QTENSO (GDOTT,TAU,PHIDT,SRS,RTEN,QTEN,NSLIPS,NTENS)
C#####################################################################
      INCLUDE 'ABA_PARAM.INC'
       PARAMETER (MDIM=6,MNSLIPS=12)
      DIMENSION GDOTT(MNSLIPS),TAU(MNSLIPS),RTEN(MDIM,MNSLIPS),
```

```
     + QTEN(MDIM,MNSLIPS)
      DIMENSION COEFF(MNSLIPS)
      PARAMETER (ZERO=0.0D0,ONE=1.0D0,TWO=2.0D0,THREE=3.0D0)
C*************************************************************************
C  Calculate the coefficient of RTEN
      DO 10 I=1,NSLIPS
       COEFF(I)=(PHIDT*GDOTT(I))/(SRS*TAU(I))
   10 CONTINUE
C*************************************************************************
C  Compute QTEN(6,NSLIPS)
      DO 30 K=1,NSLIPS
        DO 20 I=1,NTENS
          QTEN(I,K)=COEFF(K)*RTEN(I,K)
   20   CONTINUE
   30 CONTINUE
C*************************************************************************
      RETURN
      END
C#########################################################################
      SUBROUTINE SMATRX (GDOTT,RTEN,PTEN,TAU,G,HARDM,NSLIPS,PHIDT,SRS,
     1 SLIPMM,NTENS,NDI)
C#########################################################################
      INCLUDE 'ABA_PARAM.INC'
       PARAMETER (MDIM=6,MNSLIPS=12)
      DIMENSION GDOTT(MNSLIPS),RTEN(MDIM,MNSLIPS),PTEN(MDIM,MNSLIPS),
     1 TAU(MNSLIPS),G(MNSLIPS),HARDM(MNSLIPS,MNSLIPS)
      DIMENSION SLIPMM(MNSLIPS,MNSLIPS),FACT(MNSLIPS),
     1 SLIPNM(MNSLIPS,MNSLIPS),RPSCAL(MNSLIPS,MNSLIPS)
C*************************************************************************
       PARAMETER (ZERO=0.0D0,ONE=1.0D0,TWO=2.0D0,THREE=3.0D0)
C*************************************************************************
C  Compute the multiplicative factor before the square bracket.
      DO 10 I=1,NSLIPS
       FACT(I)=(PHIDT*GDOTT(I))/SRS
   10 CONTINUE
C*************************************************************************
C  Compute the scalar product of RTEN & PTEN.
C  Note that since PTEN is represented as STRAN with engineering shear components,
C there is no need to multiply with 2 for scalar product in shear components
       DO 30 J=1,NSLIPS
       DO 20 I=1,NSLIPS
         RPSCAL(I,J)=ZERO
   20  CONTINUE
   30 CONTINUE
      DO 60 K=1,NSLIPS
        DO 50 L=1,NSLIPS
          DO 40 I=1,NTENS
            RPSCAL(L,K)=RPSCAL(L,K)+RTEN(I,L)*PTEN(I,K)
   40     CONTINUE
   50   CONTINUE
   60  CONTINUE
```

```
C*************************************************************************
C  Compute SLIPNM
      DO 130 J=1,NSLIPS
        DO 120 I=1,NSLIPS
          IF (I.EQ.J) THEN
            SLIPNM(I,J)=ONE+FACT(I)*((RPSCAL(I,J)/TAU(I))+
     1            (TAU(J)/DABS(TAU(J)))*(HARDM(I,J)/G(I)))
          ELSE
            SLIPNM(I,J)=FACT(I)*((RPSCAL(I,J)/TAU(I))+
     1            (TAU(J)/DABS(TAU(J)))*(HARDM(I,J)/G(I)))
          END IF
  120   CONTINUE
  130 CONTINUE
C*************************************************************************
C  Invert SLIPNM using the standard elimination procedures. SLIPMM calculated
C*************************************************************************
      IF (NSLIPS .EQ. 2)THEN
       DETMNT=(SLIPNM(1,1)*SLIPNM(2,2))-(SLIPNM(2,1)*SLIPNM(1,2))
C*************************************************************************
       SLIPMM(1,1)=SLIPNM(2,2)/DETMNT
       SLIPMM(2,1)=-SLIPNM(2,1)/DETMNT
       SLIPMM(1,2)=-SLIPNM(1,2)/DETMNT
       SLIPMM(2,2)=SLIPNM(1,1)/DETMNT
      ELSE
       CALL FINVRST(SLIPNM,SLIPMM,NSLIPS)
      END IF
C*************************************************************************
      RETURN
      END
C#########################################################################
      SUBROUTINE FDOTS (SLIPMM,GDOTT,FDOT,NSLIPS)
C#########################################################################
      INCLUDE 'ABA_PARAM.INC'
       PARAMETER (MDIM=6,MNSLIPS=12)
      DIMENSION SLIPMM(MNSLIPS,MNSLIPS),GDOTT(MNSLIPS),FDOT(MNSLIPS)
      PARAMETER (ZERO=0.0D0,ONE=1.0D0,TWO=2.0D0,THREE=3.0D0)
C*************************************************************************
      DO 10 I=1,NSLIPS
       FDOT(I)=ZERO
   10 CONTINUE
C*************************************************************************
      DO 30 J=1,NSLIPS
        DO 20 I=1,NSLIPS
          FDOT(J)=FDOT(J)+SLIPMM(J,I)*GDOTT(J)
   20   CONTINUE
   30 CONTINUE
C*************************************************************************
      RETURN
      END
C#########################################################################
      SUBROUTINE FTENSO (SLIPMM,QTEN,FTEN,NSLIPS,NTENS)
```

```
C##########################################################################
      INCLUDE 'ABA_PARAM.INC'
       PARAMETER (MDIM=6,MNSLIPS=12)
      DIMENSION SLIPMM(MNSLIPS,MNSLIPS),QTEN(MDIM,MNSLIPS),
     1 FTEN(MDIM,MNSLIPS)
      PARAMETER (ZERO=0.0D0,ONE=1.0D0,TWO=2.0D0,THREE=3.0D0)
C**************************************************************************
C  Initialize FTEN
      DO 20 K=1,NSLIPS
       DO 10 I=1,NTENS
         FTEN(I,K)=ZERO
   10  CONTINUE
   20 CONTINUE
C  Calculate FTEN.
      DO 50 L=1,NSLIPS
       DO 40 I=1,NTENS
         DO 30 K=1,NSLIPS
          FTEN(I,L)=FTEN(I,L)+SLIPMM(L,K)*QTEN(I,K)
   30    CONTINUE
   40  CONTINUE
   50 CONTINUE
C**************************************************************************
      RETURN
      END
C##########################################################################
SUBROUTINE LATVEC (FELAST,SDV,SNV,SDVSTR,SNVSTR,NSLIPS)
C##########################################################################
      INCLUDE 'ABA_PARAM.INC'
       PARAMETER (MDIM=6,MNSLIPS=12)
      DIMENSION FELAST(3,3),SDV(3,MNSLIPS),SNV(3,MNSLIPS),
     1 SDVSTR(3,MNSLIPS),SNVSTR(3,MNSLIPS)
      DIMENSION FIELAT(3,3)
C**************************************************************************
      PARAMETER (ZERO=0.0D0,ONE=1.0D0,TWO=2.0D0,THREE=3.0D0)
      PARAMETER (M=3)
C**************************************************************************
C  Compute the inverse of FELAST, i.e FIELAT
      CALL FINVRST (FELAST,FIELAT,M)
C**************************************************************************
C  Initialize
      DO 20 K=1,NSLIPS
       DO 10 I=1,3
         SDVSTR(I,K)=ZERO
         SNVSTR(I,K)=ZERO
   10  CONTINUE
   20 CONTINUE
C**************************************************************************
C  Compute
      DO 50 K=1,NSLIPS
       DO 40 J=1,3
         DO 30 I=1,3
```

```
      SDVSTR(J,K)=SDVSTR(J,K)+FELAST(J,I)*SDV(I,K)
      SNVSTR(J,K)=SNVSTR(J,K)+SNV(I,K)*FIELAT(I,J)
 30   CONTINUE
 40  CONTINUE
 50 CONTINUE
C*************************************************************************
C SDVSTR & SNVSTR are being normalized.
C NOTE: by normalizing there was little change in the solution.
C*************************************************************************
    RETURN
    END
C#########################################################################
    SUBROUTINE PROSDN (SDVSTR,SNVSTR,PDINOT,PNODIT,NSLIPS)
C#########################################################################
C  Subroutine PROSDN computes the product of vectors SDVSTR & SNVSTR
C*************************************************************************
    INCLUDE 'ABA_PARAM.INC'
     PARAMETER (MDIM=6,MNSLIPS=12)
    DIMENSION SDVSTR(3,MNSLIPS),SNVSTR(3,MNSLIPS)
    DIMENSION PDINOT(9,MNSLIPS),PNODIT(9,MNSLIPS)
    PARAMETER (ZERO=0.0D0,ONE=1.0D0,TWO=2.0D0,THREE=3.0D0)
C*************************************************************************
C  Calculate the tensor product PDINOT of vectors SDVSTR & SNVSTR
    DO 30 K=1,NSLIPS
     N=0
     DO 20 J=1,3
      DO 10 I=1,3
       L=N+I
       PDINOT(L,K)=SDVSTR(I,K)*SNVSTR(J,K)
       PNODIT(L,K)=SNVSTR(I,K)*SDVSTR(J,K)
 10    CONTINUE
     N=N+3
 20  CONTINUE
 30 CONTINUE
C*************************************************************************
    RETURN
    END
C#########################################################################
    SUBROUTINE SCHMIP (PDINOT,PNODIT,PTEN,NSLIPS,NDI)
C#########################################################################
    INCLUDE 'ABA_PARAM.INC'
     PARAMETER (MDIM=6,MNSLIPS=12)
    DIMENSION PDINOT(9,MNSLIPS),PNODIT(9,MNSLIPS),PTEN(MDIM,MNSLIPS)
    PARAMETER (ZERO=0.0D0,ONE=1.0D0,TWO=2.0D0,THREE=3.0D0)
C*************************************************************************
C  Compute PTEN(6,2) like STRESS(NTENS)
     IF (NDI.EQ.3)THEN
      DO 10 K=1,NSLIPS
       PTEN(1,K)=(ONE/TWO)*(PDINOT(1,K)+PNODIT(1,K))
       PTEN(2,K)=(ONE/TWO)*(PDINOT(5,K)+PNODIT(5,K))
       PTEN(3,K)=(ONE/TWO)*(PDINOT(9,K)+PNODIT(9,K))
```

```
        PTEN(4,K)=(PDINOT(2,K)+PNODIT(2,K))
        PTEN(5,K)=(PDINOT(3,K)+PNODIT(3,K))
        PTEN(6,K)=(PDINOT(6,K)+PNODIT(6,K))
  10    CONTINUE
       ELSE
        DO 20 K=1,NSLIPS
        PTEN(1,K)=(ONE/TWO)*(PDINOT(1,K)+PNODIT(1,K))
        PTEN(2,K)=(ONE/TWO)*(PDINOT(5,K)+PNODIT(5,K))
        PTEN(3,K)=(PDINOT(2,K)+PNODIT(2,K))
  20    CONTINUE
       END IF
C*************************************************************************
      RETURN
      END
C#########################################################################
      SUBROUTINE SCHMIW (PDINOT,PNODIT,WTEN,NSLIPS)
C#########################################################################
C  Subroutine calculates WTEN(9,MNSLIPS)
C*************************************************************************
      INCLUDE 'ABA_PARAM.INC'
       PARAMETER (MDIM=6,MNSLIPS=12)
      DIMENSION PDINOT(9,MNSLIPS),PNODIT(9,MNSLIPS),WTEN(9,MNSLIPS)
      PARAMETER (ZERO=0.0D0,ONE=1.0D0,TWO=2.0D0,THREE=3.0D0)
C*************************************************************************
      DO 20 K=1,NSLIPS
       DO 10 I=1,9
        WTEN(I,K)=(ONE/TWO)*(PDINOT(I,K)-PNODIT(I,K))
  10   CONTINUE
  20  CONTINUE
C*************************************************************************
      RETURN
      END
C#########################################################################
SUBROUTINE BETA (WTEN,STRESS,NTENS,BTEN,NSLIPS,NDI)
C#########################################################################
      INCLUDE 'ABA_PARAM.INC'
       PARAMETER (MDIM=6,MNSLIPS=12)
      DIMENSION WTEN(9,MNSLIPS),STRESS(NTENS),BTEN(MDIM,MNSLIPS)
      DIMENSION TRBTEN(9,MNSLIPS),DUMMYB(9,MNSLIPS),DUMMYT(9)
      PARAMETER (ZERO=0.0D0,ONE=1.0D0,TWO=2.0D0,THREE=3.0D0)
C*************************************************************************
C  Convert the array STRESS(NTENS) to a dummy tensor DUMMYT(9)
      IF (NTENS .EQ. 6)THEN
       DUMMYT(1)=STRESS(1)
       DUMMYT(2)=STRESS(4)
       DUMMYT(3)=STRESS(5)
       DUMMYT(4)=STRESS(4)
       DUMMYT(5)=STRESS(2)
       DUMMYT(6)=STRESS(6)
       DUMMYT(7)=STRESS(5)
       DUMMYT(8)=STRESS(6)
```

```
      DUMMYT(9)=STRESS(3)
     ELSE IF (NTENS .EQ. 4)THEN
      DUMMYT(1)=STRESS(1)
      DUMMYT(2)=STRESS(4)
      DUMMYT(3)=ZERO
      DUMMYT(4)=STRESS(4)
      DUMMYT(5)=STRESS(2)
      DUMMYT(6)=ZERO
      DUMMYT(7)=ZERO
      DUMMYT(8)=ZERO
      DUMMYT(9)=STRESS(3)
     ELSE
      DUMMYT(1)=STRESS(1)
      DUMMYT(2)=STRESS(3)
      DUMMYT(3)=ZERO
      DUMMYT(4)=STRESS(3)
      DUMMYT(5)=STRESS(2)
      DUMMYT(6)=ZERO
      DUMMYT(7)=ZERO
      DUMMYT(8)=ZERO
      DUMMYT(9)=ZERO
     END IF
C*************************************************************************
C  Initialize BTEN
     DO 20 K=1,NSLIPS
      DO 10 I=1,9
       DUMMYB(I,K)=ZERO
  10  CONTINUE
  20 CONTINUE
C*************************************************************************
C  Computes the product of tensors WTEN*STRESS
     N=0
     DO 70 K=1,NSLIPS
      M=0
      DO 60 J=1,3
       DO 30 I=1,3
        L1=M+I
        L2=N+I
        DUMMYB(L2,K)=DUMMYB(L2,K)+WTEN(L1,K)*DUMMYT(J)
  30   CONTINUE
       M=M+I
  60  CONTINUE
      N=N+J
  70 CONTINUE
C*************************************************************************
C  Calculate the product STRESS*WTEN. This is simply minus times transpose of
C WTEN*STRESS i.e minus times transpose of the above calculated
C DUMMYB stored as TRBTEN(9,NSLIPS)
C*************************************************************************
     DO 180 K=1,NSLIPS
      TRBTEN(1,K)=-DUMMYB(1,K)
```

```
      TRBTEN(2,K)=-DUMMYB(4,K)
      TRBTEN(3,K)=-DUMMYB(7,K)
      TRBTEN(4,K)=-DUMMYB(2,K)
      TRBTEN(5,K)=-DUMMYB(5,K)
      TRBTEN(6,K)=-DUMMYB(8,K)
      TRBTEN(7,K)=-DUMMYB(3,K)
      TRBTEN(8,K)=-DUMMYB(6,K)
      TRBTEN(9,K)=-DUMMYB(9,K)
  180 CONTINUE
C*************************************************************************
C  Calculate the DUMMYB by subtracting TRBTEN from DUMMYB
     DO 210 K=1,NSLIPS
      DO 200 I=1,9
        DUMMYB(I,K)=DUMMYB(I,K)-TRBTEN(I,K)
  200  CONTINUE
  210 CONTINUE
C*************************************************************************
C  since the resulting DUMMYB is symmetric it is set as BTEN(6,2)
C  analogous to STRESS(NTENS)
     IF (NDI .EQ.3)THEN
     DO 220 K=1,NSLIPS
      BTEN(1,K)=DUMMYB(1,K)
      BTEN(2,K)=DUMMYB(5,K)
      BTEN(3,K)=DUMMYB(9,K)
      BTEN(4,K)=DUMMYB(4,K)
      BTEN(5,K)=DUMMYB(7,K)
      BTEN(6,K)=DUMMYB(8,K)
  220 CONTINUE
     ELSE
      DO 230 K=1,NSLIPS
      BTEN(1,K)=DUMMYB(1,K)
      BTEN(2,K)=DUMMYB(5,K)
      BTEN(3,K)=DUMMYB(4,K)
  230  CONTINUE
     END IF
C*************************************************************************
     RETURN
     END
C#########################################################################
     SUBROUTINE HCURVM(TGAMMA1,TGAMMA2,HARDM,H0,TAUS,TAU0,QA,
    + QB,QAB,QBA,NSLIPS,NSLIPS1,NTENS,Q)
C#########################################################################
C  This subroutine computes the hardening matrix HARDM(NSLIPS,NSLIPS) for NiAl
C*************************************************************************
     INCLUDE 'ABA_PARAM.INC'
     PARAMETER (MDIM=6,MNSLIPS=12)
     DIMENSION HARDM(MNSLIPS,MNSLIPS)
     PARAMETER (ZERO=0.0D0,ONE=1.0D0,TWO=2.0D0,THREE=3.0D0)
C*************************************************************************
C  H1 is hardening rate for {110} plane
C  H2 is hardening rate for {100} plane
```

```
C*************************************************************************
      NSLIPS2=NSLIPS1+1
      H1=H0*((ONE/DCOSH((H0*TGAMMA1)/(TAUS-TAU0)))**TWO)
      H2=H0*((ONE/DCOSH((H0*TGAMMA2)/(TAUS-TAU0)))**TWO)
C  Calculate the hardening matrix
       IF (NTENS.EQ.6 .AND. NSLIPS.NE.2) THEN
        DO 20 K=1,NSLIPS1
         DO 10 L=1,NSLIPS1
          IF (L.EQ.K) THEN
           HARDM(L,K)=H1
          ELSE
           HARDM(L,K)=QA*H1
          END IF
   10   CONTINUE
   20   CONTINUE
C*************************************************************************
      DO 40 K=NSLIPS2,NSLIPS
       DO 30 L=NSLIPS2,NSLIPS
        IF (L.EQ.K) THEN
         HARDM(L,K)=H2
        ELSE
         HARDM(L,K)=QB*H2
        END IF
   30   CONTINUE
   40 CONTINUE
C*************************************************************************
      DO 60 K=NSLIPS2,NSLIPS
       DO 50 L=1,NSLIPS1
         HARDM(L,K)=QAB*H2
   50   CONTINUE
   60 CONTINUE
C*************************************************************************
      DO 80 K=1,NSLIPS1
       DO 70 L=NSLIPS2,NSLIPS
         HARDM(L,K)=QBA*H1
   70   CONTINUE
   80 CONTINUE
      ELSE IF(NTENS.EQ.6 .AND. NSLIPS.EQ.2)THEN
       DO 100 K=1,NSLIPS
        DO 90 L=1,NSLIPS
         IF (L.EQ.K)THEN
          HARDM(L,K)=H2
         ELSE
          HARDM(L,K)=Q*H2
         END IF
   90    CONTINUE
  100   CONTINUE
      ELSE
       DO 120 K=1,NSLIPS
        DO 110 L=1,NSLIPS
         IF (L.EQ.K) THEN
```

```
       HARDM(L,K)=H2
      ELSE
       HARDM(L,K)=Q*H2
      END IF
  110  CONTINUE
  120 CONTINUE
    END IF
C*************************************************************************
    RETURN
    END
C#########################################################################
    SUBROUTINE HCURVMF(TGAMMA,HARDM,H0,TAUS,TAU0,NSLIPS,Q,Hs)
C#########################################################################
C  This subroutine computes the hardening matrix HARDM(NSLIPS,NSLIPS)
C*************************************************************************
    INCLUDE 'ABA_PARAM.INC'
    PARAMETER (MDIM=6,MNSLIPS=12)
    DIMENSION HARDM(MNSLIPS,MNSLIPS)
    PARAMETER (ZERO=0.0D0,ONE=1.0D0,TWO=2.0D0,THREE=3.0D0)
C*************************************************************************
C  H is hardening rate for FCC CRYSTALS
C*************************************************************************
C     H=H0*((ONE/DCOSH((H0*TGAMMA)/(TAUS-TAU0)))**TWO)+10.0
     H=Hs+(H0-Hs)*((ONE/DCOSH(((H0-Hs)*TGAMMA)/(TAUS-TAU0)))**TWO)
C  Calculate the hardening matrix
     DO 140 K=1,NSLIPS
      DO 130 L=1,NSLIPS
       IF (L.EQ.K) THEN
        HARDM(L,K)=H
       ELSE
        HARDM(L,K)=Q*H
       END IF
  130  CONTINUE
  140 CONTINUE
C*************************************************************************
    RETURN
    END
C#########################################################################
    SUBROUTINE RTENS (BTEN,PTEN,ELASTM,RTEN,NSLIPS,NTENS,NDI)
C#########################################################################
C  Subroutine computes RTEN(NTENS,MNSLIPS)
C*************************************************************************
    INCLUDE 'ABA_PARAM.INC'
    PARAMETER (MDIM=6,MNSLIPS=12)
    DIMENSION BTEN(MDIM,MNSLIPS),PTEN(MDIM,MNSLIPS),
   +ELASTM(MDIM,MDIM),RTEN(MDIM,MNSLIPS)
    PARAMETER (ZERO=0.0D0,ONE=1.0D0,TWO=2.0D0,THREE=3.0D0)
C*************************************************************************
C  Calculate  RTEN(6,NSLIPS)
    DO 40 K=1,NSLIPS
     DO 30 I=1,NTENS
```

```
      RTEN(I,K)=ZERO
  30  CONTINUE
  40 CONTINUE
C*********************************************************************
     DO 70 K=1,NSLIPS
      DO 60 J=1,NTENS
       DO 50 I=1,NTENS
       RTEN(J,K)=RTEN(J,K)+ELASTM(J,I)*PTEN(I,K)
  50    CONTINUE
  60   CONTINUE
  70  CONTINUE
C*********************************************************************
     DO 90 K=1,NSLIPS
      DO 80 I=1,NTENS
       RTEN(I,K)=RTEN(I,K)+BTEN(I,K)
  80    CONTINUE
  90  CONTINUE
C*********************************************************************
    RETURN
    END
C#####################################################################
SUBROUTINE ELMATR1(EMU,EKAPPA,NTENS,NDI,NDIPL1,ELASTM)
C#####################################################################
    INCLUDE 'ABA_PARAM.INC'
     PARAMETER (MDIM=6)
    DIMENSION ELASTM(MDIM,MDIM)
    PARAMETER (ZERO=0.0D0,ONE=1.0D0,TWO=2.0D0,THREE=3.0D0)
C*********************************************************************
    X1=EMU
    X2=TWO*EMU
    X3=EKAPPA-X2/THREE
C*********************************************************************
    DO 20 I=1,NTENS
     DO 10 J=1,NTENS
      ELASTM(J,I)=ZERO
 10   CONTINUE
 20  CONTINUE
C*********************************************************************
    DO 30 I=1,NDI
     ELASTM(I,I)=X2
 30  CONTINUE
    DO 40 I=NDIPL1,NTENS
     ELASTM(I,I)=X1
 40  CONTINUE
C*********************************************************************
    DO 60 J=1,NDI
     DO 50 I=1,NDI
      ELASTM(I,J)=ELASTM(I,J)+X3
 50   CONTINUE
 60  CONTINUE
C*********************************************************************
```

```
      RETURN
      END
C#######################################################################
      SUBROUTINE ELMATR2(EMU,NTENS,NDI,NDIPL1,ELASTM)
C#######################################################################
      INCLUDE 'ABA_PARAM.INC'
       PARAMETER (MDIM=6)
      DIMENSION ELASTM(MDIM,MDIM)
      PARAMETER (PR=.3236D0,ZERO=0.0D0,ONE=1.0D0,TWO=2.0D0,THREE=3.0D0)
C***********************************************************************
      X1=(TWO*EMU*PR)/(1-PR)
      X2=EMU
      X3=TWO*EMU
C***********************************************************************
      DO 20 I=1,NTENS
       DO 10 J=1,NTENS
        ELASTM(J,I)=ZERO
 10    CONTINUE
 20   CONTINUE
C***********************************************************************
      DO 30 J=1,NDI
       DO 40 I=1,NDI
        ELASTM(I,J)=X1
 40    CONTINUE
 30   CONTINUE
      DO 50 I=1,NDI
       ELASTM(I,I)=ELASTM(I,I)+X3
 50   CONTINUE
       DO 60 I=NDIPL1,NTENS
       ELASTM(I,I)=ELASTM(I,I)+X2
 60   CONTINUE
C***********************************************************************
      RETURN
      END
C#######################################################################
      SUBROUTINE ELMATR3(EMU,EKAPPA,NTENS,NDIPL1,ELASTM)
C#######################################################################
      INCLUDE 'ABA_PARAM.INC'
       PARAMETER (MDIM=6)
      DIMENSION ELASTM(MDIM,MDIM)
      PARAMETER (ZERO=0.0D0,ONE=1.0D0,TWO=2.0D0,THREE=3.0D0)
C***********************************************************************
      X1=TWO*EMU
      X2=EMU
      X3=EKAPPA-X1/THREE
      X4=TWO*EKAPPA+X1/THREE
C***********************************************************************
      DO 20 I=1,NTENS
       DO 10 J=1,NTENS
        ELASTM(J,I)=ZERO
 10    CONTINUE
```

```
 20   CONTINUE
C*******************************************************************************
      DO 30 I=1,2
       ELASTM(I,I)=X1
 30   CONTINUE
      DO 40 I=NDIPL1,NTENS
       ELASTM(I,I)=X2
 40   CONTINUE
C*******************************************************************************
      DO 60 J=1,2
       DO 50 I=1,2
        ELASTM(I,J)=ELASTM(I,J)+X3
 50     CONTINUE
 60   CONTINUE
      DO 80 J=1,2
       DO 70 I=3,3
        ELASTM(I,J)=ELASTM(I,J)+X4
 70     CONTINUE
 80   CONTINUE
C*******************************************************************************
      RETURN
      END
C###############################################################################
      SUBROUTINE ELMATR4(EMU,EKAPPA,NDI,NTENS,NDIPL1,ELASTM)
C###############################################################################
      INCLUDE 'ABA_PARAM.INC'
       PARAMETER (MDIM=6)
      DIMENSION ELASTM(MDIM,MDIM)
      PARAMETER (ZERO=0.0D0,ONE=1.0D0,TWO=2.0D0,THREE=3.0D0)
C*******************************************************************************
      X1=TWO*EMU
      X2=EMU
      X3=EKAPPA-X1/THREE
C*******************************************************************************
      DO 20 I=1,NTENS
       DO 10 J=1,NTENS
        ELASTM(J,I)=ZERO
 10     CONTINUE
 20   CONTINUE
C*******************************************************************************
      DO 30 I=1,NDI
       ELASTM(I,I)=X1
 30   CONTINUE
      DO 40 I=NDIPL1,NTENS
       ELASTM(I,I)=X2
 40   CONTINUE
C*******************************************************************************
      DO 60 J=1,NDI
       DO 50 I=1,NDI
        ELASTM(I,J)=ELASTM(I,J)+X3
 50     CONTINUE
```

```
 60   CONTINUE
C*********************************************************************
      RETURN
      END
C#####################################################################
      SUBROUTINE CALCOORD(FELAST,CMC11,CMC12,CMC13,CMC21,CMC22,
     + CMC23,CMC31,CMC32,CMC33,CX,CY,CZ,NTENS)
C#####################################################################
      NCLUDE 'ABA_PARAM.INC'
      DIMENSION FELAST(3,3),FIELAT(3,3),CX(3),CY(3),CZ(3)
      PARAMETER (M=3)
      PARAMETER (ZERO=0.0D0,ONE=1.0D0,TWO=2.0D0,THREE=3.0D0)
C*********************************************************************
      CALL FINVRST (FELAST,FIELAT,M)
      DO 10 I=1,3
       CX(I)=0.0
       CY(I)=0.0
       CZ(I)=0.0
 10   CONTINUE
      DO 20 I=1,3
      CX(I)=CX(I)+FELAST(I,1)*CMC11+FELAST(I,2)*CMC21+FELAST(I,3)*CMC31
      CY(I)=CY(I)+CMC12*FIELAT(I,1)+CMC22*FIELAT(I,2)+CMC32*FIELAT(I,3)
 20   CONTINUE
C*********************************************************************
C Normalize direction cosine in 3D
C*********************************************************************
      IF (NTENS.EQ.6)THEN
       CX(1)=CX(1)/(DSQRT(CX(1)*CX(1)+CX(2)*CX(2)+CX(3)*CX(3)))
       CX(2)=CX(2)/(DSQRT(CX(1)*CX(1)+CX(2)*CX(2)+CX(3)*CX(3)))
       CX(3)=CX(3)/(DSQRT(CX(1)*CX(1)+CX(2)*CX(2)+CX(3)*CX(3)))
       CY(1)=CY(1)/(DSQRT(CY(1)*CY(1)+CY(2)*CY(2)+CY(3)*CY(3)))
       CY(2)=CY(2)/(DSQRT(CY(1)*CY(1)+CY(2)*CY(2)+CY(3)*CY(3)))
       CY(3)=CY(3)/(DSQRT(CY(1)*CY(1)+CY(2)*CY(2)+CY(3)*CY(3)))
       CZ(1)=CX(2)*CY(3)-CX(3)*CY(2)
       CZ(2)=CX(3)*CY(1)-CX(1)*CY(3)
       CZ(3)=CX(1)*CY(2)-CX(2)*CY(1)
      ELSE
C*********************************************************************
C  Normalize direction cosine in 2D
C*********************************************************************
       CX(1)=CX(1)/(DSQRT(CX(1)*CX(1)+CX(2)*CX(2)))
       CX(2)=CX(2)/(DSQRT(CX(1)*CX(1)+CX(2)*CX(2)))
       CX(3)=ZERO
       CY(1)=CY(1)/(DSQRT(CY(1)*CY(1)+CY(2)*CY(2)))
       CY(2)=CY(2)/(DSQRT(CY(1)*CY(1)+CY(2)*CY(2)))
       CY(3)=ZERO
       CZ(1)=ZERO
       CZ(2)=ZERO
       CZ(3)=ONE
      END IF
C*********************************************************************
```

```
      RETURN
      END
C######################################################################
      SUBROUTINE ANIELAS(C11,C12,C44,a1,a2,a3,ELASTM,NDI)
C######################################################################
      INCLUDE 'ABA_PARAM.INC'
      DIMENSION ELASTM(6,6),a1(3),a2(3),a3(3)
C**********************************************************************
C  Anisotropy component for 3D
C**********************************************************************
      IF(NDI.EQ.3)THEN
      ELASTM(1,1)=(a1(1)**4+a1(2)**4+a1(3)**4)*C11+2*(a1(2)**2*a1(1)**2+a1(3)**2*a1(1)
     +**2+a1(2)**2*a1(3)**2)*C12+4*(a1(1)**2*a1(2)**2+a1(2)**2*a1(3)**2+a1(1)**2*
     + a1(3)**2)*C44
      ELASTM(2,2)=ELASTM(1,1)
      ELASTM(3,3)=ELASTM(1,1)
      ELASTM(4,4)=(a1(1)**2*a2(1)**2+a1(2)**2*a2(2)**2+a1(3)**2*a2(3)**2
     +)*C11+2*(a1(1)*a2(1)*a1(2)*a2(2)+a1(1)*a2(1)*a1(3)*a2(3))*C12+(
     +a1(1)**2*a2(2)**2+a1(2)**2*a2(1)**2+a1(2)*a2(1)*a1(1)*a2(2)+a1(1)*
     +a2(2)*a1(2)*a2(1)+a1(2)**2*a2(3)**2+a1(3)**2*a2(2)**2+a1(3)*a2(2)*
     +a1(2)*a2(3)+a1(2)*a2(3)*a1(3)*a2(2)+a1(1)**2*a2(3)**2+a1(3)**2*
     +a2(1)**2+a1(3)*a2(1)*a1(1)*a2(3)+a1(1)*a2(3)*a1(3)*a2(1))*C44
      ELASTM(5,5)=ELASTM(4,4)
      ELASTM(6,6)=ELASTM(4,4)
C**********************************************************************
      ELASTM(1,2)=(a1(1)**2*a2(1)**2+a1(2)**2*a2(2)**2+a1(3)**2*a2(3)**2
     +)*C11+(a1(1)**2*a2(2)**2+a1(2)**2*a2(1)**2+a1(1)**2*a2(3)**2+a1(3)
     +**2*a2(1)**2+a1(2)**2*a2(3)**2+a1(3)**2*a2(2)**2)*C12+4*(a1(1)*
     +a1(2)*a2(1)*a2(2)+a1(2)*a1(3)*a2(3)*a2(2)+a1(1)*a1(3)*a2(1)*a2(3))
     + *C44
      ELASTM(1,3)=ELASTM(1,2)
      ELASTM(2,1)=ELASTM(1,2)
      ELASTM(2,3)=ELASTM(1,2)
      ELASTM(3,1)=ELASTM(1,2)
      ELASTM(3,2)=ELASTM(1,2)
C**********************************************************************
      ELASTM(1,4)=(a1(1)**3*a2(1)+a1(2)**3*a2(2)+a1(3)**3*a2(3))*C11+
     +(a1(1)**2*(a1(2)*a2(2)+a1(3)*a2(3))+a1(2)**2*(a1(1)*a2(1)+a1(3)*
     +a2(3))+a1(3)**2*(a1(1)*a2(1)+a1(2)*a2(2)))*C12+2*(a1(1)*a1(2)*
     +(a1(1)*a2(2)+a1(2)*a2(1))+a1(2)*a1(3)*(a1(2)*a2(3)+a1(3)*a2(2))+
     + a1(1)*a1(3)*(a1(1)*a2(3)+a1(3)*a2(1)))*C44
      ELASTM(4,1)=ELASTM(1,4)
C**********************************************************************
      ELASTM(2,4)=(a2(1)**3*a1(1)+a2(2)**3*a1(2)+a2(3)**3*a1(3))*C11+
     +(a2(1)**2*(a1(2)*a2(2)+a1(3)*a2(3))+a2(2)**2*(a1(1)*a2(1)+a1(3)*
     +a2(3))+a2(3)**2*(a1(1)*a2(1)+a1(2)*a2(2)))*C12+2*(a2(2)*a2(1)*
     +(a1(1)*a2(2)+a1(2)*a2(1))+a2(2)*a2(3)*(a1(2)*a2(3)+a1(3)*a2(2))+
     +a2(3)*a2(1)*(a1(1)*a2(3)+a1(3)*a2(1)))*C44
      ELASTM(4,2)=ELASTM(2,4)
C**********************************************************************
      ELASTM(3,4)=(a3(1)**2*a1(1)*a2(1)+a3(2)**2*a1(2)*a2(2)+a3(3)**2
```

```
     +*a1(3)*a2(3))*C11+(a3(1)**2*(a1(2)*a2(2)+a1(3)*a2(3))+a3(2)**2*
     +(a1(1)*a2(1)+a1(3)*a2(3))+a3(3)**2*(a1(1)*a2(1)+a1(2)*a2(2)))*C12
     ++2*(a3(1)*a3(2)*(a1(1)*a2(2)+a1(2)*a2(1))+a3(2)*a3(3)*(a1(2)*a2(3)
     ++a1(3)*a2(2))+a3(1)*a3(3)*(a1(1)*a2(3)+a1(3)*a2(1)))*C44
      ELASTM(4,3)=ELASTM(3,4)
C*********************************************************************
      ELASTM(1,5)=(a1(1)**2*a2(1)*a3(1)+a1(2)**2*a2(2)*a3(2)+a1(3)**2*
     + a2(3)*a3(3))*C11+(a1(1)**2*(a2(2)*a3(2)+a2(3)*a3(3))+a1(2)**2*
     + (a2(1)*a3(1)+a2(3)*a3(3))+a1(3)**2*(a2(1)*a3(1)+a2(2)*a3(2)))*C12
     + +2*(a1(1)*a1(2)*(a2(1)*a3(2)+a2(2)*a3(1))+a1(2)*a1(3)*(a2(2)*
     + a3(3)+a2(3)*a3(2))+a1(1)*a1(3)*(a2(1)*a3(3)+a2(3)*a3(1)))*C44
      ELASTM(5,1)=ELASTM(1,5)
C*********************************************************************
      ELASTM(2,5)=(a2(1)**3*a3(1)+a2(2)**3*a3(2)+a2(3)**3*a3(3))*C11+
     +(a2(1)**2*(a2(2)*a3(2)+a2(3)*a3(3))+a2(2)**2*(a2(1)*a3(1)+a2(3)*
     +a3(3))+a2(3)**2*(a2(1)*a3(1)+a2(2)*a3(2)))*C12+2*(a2(1)*a2(2)*
     +(a2(1)*a3(2)+a2(2)*a3(1))+a2(2)*a2(3)*(a2(2)*a3(3)+a2(3)*a3(2))+
     +a2(1)*a2(3)*(a2(1)*a3(3)+a2(3)*a3(1)))*C44
      ELASTM(5,2)=ELASTM(2,5)
C*********************************************************************
      ELASTM(3,5)=(a3(1)**3*a2(1)+a3(2)**3*a2(2)+a3(3)**3*a2(3))*C11+
     +(a3(1)**2*(a2(2)*a3(2)+a2(3)*a3(3))+a2(2)**2*(a2(1)*a3(1)+a2(3)*
     +a3(3))+a3(3)**2*(a2(1)*a3(1)+a2(2)*a3(2)))*C12+2*(a3(1)*a3(2)*
     +(a2(1)*a3(2)+a2(2)*a3(1))+a3(2)*a3(3)*(a2(2)*a3(3)+a2(3)*a3(2))+
     +a3(1)*a3(3)*(a2(1)*a3(3)+a2(3)*a3(1)))*C44
      ELASTM(5,3)=ELASTM(3,5)
C*********************************************************************
      ELASTM(4,5)=(a2(1)**2*a1(1)*a3(1)+a2(2)**2*a1(2)*a3(2)+a2(3)**2
     + *a1(3)*a3(3))*C11+(a1(1)*a2(1)*(a2(2)*a3(2)+a2(3)*a3(3))+a1(2)*
     + a2(2)*(a2(1)*a3(1)+a2(3)*a3(3))+a1(3)*a2(3)*(a2(1)*a3(1)+a1(2)*
     + a3(2)))*C12+(a1(1)*a2(2)*(a2(1)*a3(2)+a2(2)*a3(1))+a1(2)*a2(1)*
     + (a2(2)*a3(1)+a2(1)*a3(2))+a1(2)*a2(3)*(a2(2)*a3(3)+a2(3)*a3(2))+
     + a1(3)*a2(2)*(a2(3)*a3(2)+a2(2)*a3(3))+a1(1)*a2(3)*(a2(1)*a3(3)+
     + a2(3)*a3(1))+a1(3)*a2(1)*(a2(3)*a3(1)+a2(1)*a3(3)))*C44
      ELASTM(5,4)=ELASTM(4,5)
C*********************************************************************
      ELASTM(1,6)=(a1(1)**3*a3(1)+a1(2)**3*a3(2)+a1(3)**3*a3(3))*C11+
     + (a1(1)**2*(a1(2)*a3(2)+a1(3)*a3(3))+a1(2)**2*(a1(1)*a3(1)+a1(3)*
     + a3(3))+a1(3)**2*(a1(1)*a3(1)+a1(2)*a3(2)))*C12+2*(a1(1)*a1(2)*
     + (a1(1)*a3(2)+a1(2)*a3(1))+a1(2)*a1(3)*(a1(2)*a3(3)+a1(3)*a3(2))+
     + a1(1)*a1(3)*(a1(1)*a3(3)+a1(3)*a3(1)))*C44
      ELASTM(6,1)=ELASTM(1,6)
C*********************************************************************
      ELASTM(2,6)=(a2(1)**2*a1(1)*a3(1)+a2(2)**2*a1(2)*a3(2)+a2(3)**2
     + *a1(3)*a3(3))*C11+(a2(1)**2*(a1(2)*a3(2)+a1(3)*a3(3))+a2(2)**2
     + *(a1(1)*a3(1)+a1(3)*a3(3))+a2(3)**2*(a1(1)*a3(1)+a1(2)*a3(2)))*
     + C12+2*(a2(1)*a2(2)*(a1(1)*a3(2)+a1(2)*a3(1))+a2(2)*a2(3)*
     +(a1(2)*a3(3)+a1(3)*a3(2))+a2(1)*a2(3)*(a1(1)*a3(3)+a1(3)*a3(1)))
     + *C44
      ELASTM(6,2)=ELASTM(2,6)
C*********************************************************************
```

```
      ELASTM(3,6)=(a3(1)**3*a1(1)+a3(2)**3*a1(2)+a3(3)**3*a1(3))*C11+
     + (a3(1)**2*(a1(2)*a3(2)+a1(3)*a3(3))+a3(2)**2*(a1(1)*a3(1)+a1(3)
     + *a3(3))+a3(3)**2*(a1(1)*a3(1)+a1(2)*a3(2)))*C12+2*(a3(1)*a3(2)*
     + (a1(1)*a3(2)+a1(2)*a3(1))+a3(2)*a3(3)*(a1(2)*a3(3)+a1(3)*a3(2))
     + +a3(1)*a3(3)*(a1(1)*a3(3)+a1(3)*a3(1)))*C44
      ELASTM(6,3)=ELASTM(3,6)
C*********************************************************************
      ELASTM(4,6)=(a1(1)**2*a2(1)*a3(1)+a1(2)**2*a2(2)*a3(2)+a1(3)**2*
     + a2(3)*a3(3))*C11+(a1(1)*a2(1)*(a1(2)*a3(2)+a1(3)*a3(3))+a1(2)*
     + a2(2)*(a1(1)*a3(1)+a1(3)*a3(3))+a1(3)*a2(3)*(a1(1)*a3(1)+a1(2)*
     + a3(2)))*C12+(a1(1)*a2(2)*(a1(1)*a3(2)+a1(2)*a3(1))+a1(2)*a2(1)*
     + (a1(2)*a3(3)+a1(3)*a3(2))+a1(2)*a2(3)*(a1(1)*a3(3)+a1(3)*a3(1))
     + +a1(3)*a2(2)*(a1(3)*a3(2)+a1(2)*a3(3))+a1(1)*a2(3)*(a1(1)*a3(3)
     + +a1(3)*a3(1))+a1(3)*a2(1)*(a1(3)*a3(1)+a1(1)*a3(3)))*C44
      ELASTM(6,4)=ELASTM(4,6)
C*********************************************************************
      ELASTM(5,6)=(a3(1)**2*a2(1)*a1(1)+a3(2)**2*a1(2)*a2(2)+a3(3)**2
     + *a2(3)*a1(3))*C11+(a2(1)*a3(1)*(a1(2)*a3(2)+a1(3)*a3(3))+a3(2)
     + *a2(2)*(a1(1)*a3(1)+a1(3)*a3(3))+a3(3)*a2(3)*
     +  (a1(1)*a3(1)+a1(2)*a3(2)))*C12+(a2(1)*a3(2)*(a1(1)*a3(2)+a1(2)*
     +  a3(1))+a2(2)*a3(1)*(a1(2)*a3(3)+a1(3)*a3(2))+a2(2)*a3(3)*(a1(1)
     + *a3(3)+a1(3)*a3(1))+a2(3)*a3(2)*(a1(3)*a3(2)+a1(2)*a3(3))+a2(1)*
     + a3(3)*(a1(1)*a3(3)+a1(3)*a3(1))+a2(3)*a3(1)*(a1(3)*a3(1)+
     +  a1(1)*a3(3)))*C44
      ELASTM(6,5)=ELASTM(5,6)
C*********************************************************************
      ELSE
C*********************************************************************
C  Anisotropy component for plane stress
C*********************************************************************
      ELASTM(1,1)=(a1(1)**4+a1(2)**4+a1(3)**4)*C11+2*(a1(2)**2*a1(1)**2+
     +a1(3)**2*a1(1)**2+a1(2)**2*a1(3)**2)*C12+4*(a1(1)**2*a1(2)**2+
     +a1(2)**2*a1(3)**2+a1(1)**2*a1(3)**2)*C44
C*********************************************************************
      ELASTM(2,2)=ELASTM(1,1)
C*********************************************************************
      ELASTM(3,3)=(a1(1)**2*a2(1)**2+a1(2)**2*a2(2)**2+a1(3)**2*a2(3)**2
     +)*C11+2*(a1(1)*a2(1)*a1(2)*a2(2)+a1(1)*a2(1)*a1(3)*a2(3))*C12+(
     +a1(1)**2*a2(2)**2+a1(2)**2*a2(1)**2+a1(2)*a2(1)*a1(1)*a2(2)+a1(1)*
     +a2(2)*a1(2)*a2(1)+a1(2)**2*a2(3)**2+a1(3)**2*a2(2)**2+a1(3)*a2(2)*
     +a1(2)*a2(3)+a1(2)*a2(3)*a1(3)*a2(2)+a1(1)**2*a2(3)**2+a1(3)**2*
     +a2(1)**2+a1(3)*a2(1)*a1(1)*a2(3)+a1(1)*a2(3)*a1(3)*a2(1))*C44
C*********************************************************************
      ELASTM(1,2)=(a1(1)**2*a2(1)**2+a1(2)**2*a2(2)**2+a1(3)**2*a2(3)**2
     +)*C11+(a1(1)**2*a2(2)**2+a1(2)**2*a2(1)**2+a1(1)**2*a2(3)**2+a1(3)
     +**2*a2(1)**2+a1(2)**2*a2(3)**2+a1(3)**2*a2(2)**2)*C12+4*(a1(1)*
     +a1(2)*a2(1)*a2(2)+a1(2)*a1(3)*a2(3)*a2(2)+a1(1)*a1(3)*a2(1)*a2(3))
     + *C44
C*********************************************************************
      ELASTM(2,1)=ELASTM(1,2)
C*********************************************************************
```

```
      ELASTM(1,3)=(a1(1)**3*a2(1)+a1(2)**3*a2(2)+a1(3)**3*a2(3))*C11+
     +(a1(1)**2*(a1(2)*a2(2)+a1(3)*a2(3))+a1(2)**2*(a1(1)*a2(1)+a1(3)*
     +a2(3))+a1(3)**2*(a1(1)*a2(1)+a1(2)*a2(2)))*C12+2*(a1(1)*a1(2)*
     +(a1(1)*a2(2)+a1(2)*a2(1))+a1(2)*a1(3)*(a1(2)*a2(3)+a1(3)*a2(2))+
     + a1(1)*a1(3)*(a1(1)*a2(3)+a1(3)*a2(1)))*C44
C*********************************************************************
      ELASTM(3,1)=ELASTM(1,3)
      END IF
C*********************************************************************
       RETURN
       END
C#####################################################################
      SUBROUTINE FINVRST (A,Y,N)
C#####################################################################
      INCLUDE 'ABA_PARAM.INC'
C*********************************************************************
       PARAMETER (MNSLIPS=12)
       DIMENSION A(MNSLIPS,MNSLIPS),Y(MNSLIPS,MNSLIPS)
       INTEGER INDX(MNSLIPS)
C*********************************************************************
       DO 12 I=1,N
        DO 11 J=1,N
         Y(I,J)=0.0D0
11      CONTINUE
        Y(I,I)=1.0D0
12     CONTINUE
       CALL LUDCMP(A,N,INDX,D)
       DO 13 J=1,N
        CALL LUDKSB(A,N,INDX,Y(1,J))
13     CONTINUE
C*********************************************************************
       RETURN
       END
C#####################################################################
      SUBROUTINE LUDCMP(A,N,INDX,D)
C#####################################################################
      INCLUDE 'ABA_PARAM.INC'
C*********************************************************************
      PARAMETER (MNSLIPS=12,NMAX=500,TINY=1.0D-20)
C*********************************************************************
      DIMENSION A(MNSLIPS,MNSLIPS),INDX(MNSLIPS),VV(NMAX)
C*********************************************************************
       D=1.0
       DO 12 I=1,N
        AAMAX=0.0D0
        DO 11 J=1,N
        IF(DABS(A(I,J)).GT.AAMAX)THEN
         AAMAX=DABS(A(I,J))
        END IF
11       CONTINUE
        IF(AAMAX.EQ.0.0D0)THEN
```

```
      PRINT *, 'singular matrix in LUDCMP'
      STOP
      END IF
       VV(I)=1.0D0/AAMAX
12    CONTINUE
     DO 19 J=1,N
      DO 14 I=1,J-1
       SUM=A(I,J)
       DO 13 K=1,I-1
        SUM=SUM-A(I,K)*A(K,J)
13      CONTINUE
       A(I,J)=SUM
14    CONTINUE
      AAMAX=0.0
     DO 16 I=J,N
      SUM=A(I,J)
      DO 15 K=1,J-1
       SUM=SUM-A(I,K)*A(K,J)
15     CONTINUE
      A(I,J)=SUM
      DUM=VV(I)*DABS(SUM)
      IF(DUM.GE.AAMAX)THEN
       IMAX=I
       AAMAX=DUM
      ENDIF
16     CONTINUE
      IF(J.NE.IMAX)THEN
       DO 17 K=1,N
        DUM=A(IMAX,K)
        A(IMAX,K)=A(J,K)
        A(J,K)=DUM
17      CONTINUE
       D=-D
       VV(IMAX)=VV(J)
       ENDIF
       INDX(J)=IMAX
       IF(A(J,J).EQ.0.0D0)THEN
         A(J,J)=TINY
       END IF
       IF(J.NE.N)THEN
         DUM=1.0D0/A(J,J)
         DO 18 I=J+1,N
          A(I,J)=A(I,J)*DUM
18        CONTINUE
       ENDIF
19     CONTINUE
C*********************************************************************************
     RETURN
     END
C#################################################################################
     SUBROUTINE LUDKSB(A,N,INDX,B)
```

```
C#########################################################################
      INCLUDE 'ABA_PARAM.INC'
C*************************************************************************
      PARAMETER (MNSLIPS=12)
      DIMENSION A(MNSLIPS,MNSLIPS),B(MNSLIPS),INDX(MNSLIPS)
C*************************************************************************
     II=0
     DO 12 I=1,N
      LL=INDX(I)
      SUM=B(LL)
      B(LL)=B(I)
      IF(II.NE.0)THEN
       DO 11 J=II,I-1
        SUM=SUM-A(I,J)*B(J)
11     CONTINUE
      ELSE IF(SUM.NE.0.0D0)THEN
       II=I
      ENDIF
      B(I)=SUM
12    CONTINUE
     DO 14 I=N,1,-1
      SUM=B(I)
      DO 13 J=I+1,N
       SUM=SUM-A(I,J)*B(J)
13     CONTINUE
      B(I)=SUM/A(I,I)
14    CONTINUE
C*************************************************************************
      RETURN
      END
C#########################################################################
```

REFERENCES

ABAQUS, Reference Manuals version 5.4, Hibbit, Karlsson and Sorensen Inc., Providence, Rhode Island, 1994

Asaro, R. J. and Rice, J. R., "Strain localization in ductile single crystals," J. Mech. Phys. Solids, Vol. 25, pp. 309-338, 1977

Asaro, R., J. "Geometrical effects in the inhomogeneous deformation of ductile single crystals," Acta Metall., Vol. 27, pp. 445-453, 1979

Asaro, R. J., "Micromechanics of crystals and polycrystals," Adv. Appl. Mech., Vol. 23, pp. 1-115, 1983

Asaro, R. J., "Crystal plasticity," J. Appl. Mech., Vol. 50, pp. 921-934, 1983

Barrett, C. S., Structure of Metals, McGraw-Hill, Inc., New York., 1952

Basinski S. J. and Basinski, Z. S., "Plastic deformation and work hardening," in: Dislocations in Solids (edited by Nabarro, F. R.), North Holland, Amsterdam, p. 262, 1979

Bassani, J. L. and Wu, T., "Latent hardening in single crystals II. Analytical characterization and predictions," Proc. R. Soc. London, Vol. A435, pp. 21-41, 1991

Bassani, J. L., "Plastic Flow of Crystals," Adv. Appl. Mech., Vol. 30, pp. 192-258, 1994

Bathe, K. J., Finite Element Procedures in Engineering Analysis, Prentice-Hall, Inc., Englewood Cliffs, New Jersey, 1985

Burke, M. A. and Nix, W. D., "Numerical analysis of void growth in tension creep," Int. J. Solids Struct., Vol. 15, p. 379, 1979

Chang Y. W. and Asaro, R. J, "Lattice rotations and localized shearing in single crystals," Arch. Mech., Vol. 32, No. 3, pp. 369-388, 1980

Christoffersen, J. and Hutchinson, J. W., "Class of phenomenological corner theories of plasticity," J. Mech. Phys. Solids, Vol. 27, p. 465, 1979

Cook, R. D., Malkus, D. S. and Plesha, M. E., Concepts and Applications of Finite Element Analysis, John Wiely & Sons, Inc., New York, 1989

Crimp, M. A., Tonn, S. C. and Zhang, Y., "Dislocation core structures in B2 NiAl alloys," J. Materials Science and Engineering, A170, pp. 95-102, 1993

Cuitino, A. M. and Ortiz, M., "Computational modelling of single crystals," Modelling Simul. Mater. Sci. Eng., Vol. 1, pp. 225-263, 1992

Darolia, R., "NiAl alloys for high-temperature structural applications," J. Metals, Vol. 43, No. 3, pp. 44-49, 1991

Darolia, R., Lahrman, D. F., Field, R. D., Dobbs, J. R., Chang, K. M., Goldman, E. H. and Konitzer, D. G., "Overview of NiAl alloys for high temperature applications," in: Ordered Intermetallics- Physical Metallurgy and Mechanical Behavior," (edited by Lui, C. T., Cahn, R. and Sauthoff, G.), Dordrecht, The Netherlands, Kluwer, pp. 679-698, 1992

Deve, H., Harren, S., McCullough, C. and Asaro, R. J., "Micro and macroscopic aspects of shear band formation in internally nitried single crystal of Fe-Ti-Mn alloys," Acta Metall., Vol. 36, No. 2, pp. 341-365, 1988

Dieter, G. E., Mechanical Metallurgy, McGraw-Hill, Inc., New York, 1986

Ebrahimi, F., Gomez, A. and Hicks, T. G., "Nature of slip during indentation on {100} surface of NiAl," Scripta Metall. Et Mater., Vol. 35, pp. 337-342, 1996

Ebrahimi, F. and Hoyle, G. T., "Brittle-to-ductile transition in polycrystalline NiAl," Acta Mater., Vol. 45, pp. 4193-4204, 1997

Ebrahimi, F. and Shrivastava, S., "Crack initiation and propagation in brittle-to-ductile transition regime of NiAl single crystals," J. Materials Science and Engineering, in press, 1997a

Ebrahimi, F. and Shrivastava, S., "Brittle-to-ductile transition in NiAl single crystals," J. Acta Mater., in press, 1997b

Field, R. D., Lahrman, D. F. and Darolia, R., "Slip systems in <001> oriented NiAl single crystals," Acta Metall., Vol. 39, No. 12, pp. 2951-2959, 1991

Franciosi, P., "Glide mechanisms in BCC crystals: An investigation of the case of α- iron through multislip and latent hardening tests," Acta Metall., Vol. 31, No. 9, pp. 1331-1342, 1983

Franciosi, P., "Concepts of latent hardening and strain hardening in metallic single crystals," Acta Metall., Vol. 33, No. 9, pp. 1601-1612, 1985

Franciosi, P., Berveiller, M. and Zaoui, A., "Latent hardening in copper and aluminum single crystals," Acta Metall., Vol. 28, pp. 273-283, 1980

Franciosi, P. and Zaoui, A., "Multislip in FCC crystals: A theoretical approach compared with experimental data," Acta Metall., Vol. 30, pp. 1627-1637, 1982a

Franciosi, P.and Zaoui, A., "Multislip tests on copper crystals: A junctions hardening effect," Acta Metall., Vol. 30, pp. 2141-2151, 1982b

Fraser, H. L., Loretto, M. H. and Smallman, R. E., "The plastic deformation of NiAl single crystals between 300°K and 1050°K- II. The mechanism of kinking and uniform deformation," Phil. Mag., Vol. 28, pp. 667-677, 1973a

Fraser, H. L., Smallman, R. E. and Loretto, M. H., "The plastic deformation of NiAl single crystals between 300°K and 1050°K- I. Experimental evidence on the role of kinking and uniform deformation in crystals compressed along <001>," Phil. Mag., Vol. 28, pp. 651-665, 1973b

Fung, Y. C., Foundations of Solid Mechanics, Prentice-Hall Inc., Eaglewood Cliffs, New Jersey, 1965

Havner, K. S., Finite Plastic Deformation of Crystalline Solids, Cambridge Univ. Press, New York, 1992

Hill, R., "Continuum micro-mechanics of elastoplastic polycrystals," J. Mech. Phys. Solids, Vol. 13, pp. 89-101, 1965

Hill, R. and Hutchinson, J. W., "Bifurcation phenomena in the plane tension test," J. Mech. Phys. Solids, Vol. 23, pp. 239-264, 1975

Hill, R. and Rice, J. R., "Constitutive analysis of elastic-plastic crystals at arbitrary strain," J. Mech. Phys. Solids, Vol. 20, pp. 401-413, 1972

Harren, S. V., Deve, H. E. and Asaro, R. J., "Shear band formation in plane strain compression," Acta Metall., Vol. 36, No. 9, pp. 2435-2480, 1988

Hughes, T. J. R., Finite Element Method – Linear Static and Dynamic Analysis, Prentice-Hall, Inc., Englewood Cliffs, New Jersey, 1987

Hutchinson, J. W., "Elastic-plastic behavior of polycrystalline metals and composites," Proc. R. Soc., London, Vol. A319, pp. 247-272, 1970

Jackson, P. J. and Basinski, Z. S., "Latent hardening and the flow stress in copper single crystals," Can. J. Phys., Vol. 45, pp. 707-735, 1967

Khan, A. S. and Huang, S., Continuum Theory of Plasticity, John Wiely & Sons, Inc., New York, 1995

Kocks, U. F., "Latent hardening and secondary slip in aluminum and silver," Trans. Metall. Soc. AIME, Vol. 230, p. 1160, 1964

Kocks, U. F. and Brown, T. J., "Latent Hardening in Aluminum," Acta Metall., Vol. 14, pp. 87-98, 1966

Kovacs, I. and Zsoldos, L., Dislocations and Plastic Deformation, Pergamon Press Ltd., Oxford, 1973

Lahrman, D. F., Field, R. D. and Darolia, R., "The effect of strain rate on the mechanical properties of single crystals NiAl," in: High Temperature Ordered Intermetallic Alloys IV (edited by Johnson, L. et al.), MRS Proc., Vol. 213, pp. 603-607, 1991

Lee, E. H. "Elastic-plastic deformation at finite strains," J. Appl. Mech., Vol. 36, pp. 1-6, 1969

Levit, V. I., Winton, J. S., Gornostyrev, Yu and Kaufman, M. J., "Mechanism of high tensile elongation in NiAl single crystals at intermediate temperatures," Proceedings of ReX 96, The Third International Conference on Recrystalization and Related Phenomena (edited by Terry R. McNelley), Monterrey, CA, pp. 637-644, 1996

Lubliner, J., Plasticity Theory, MacMillan Publishing Company, NewYork, 1990

Malvern, L. E., Introduction to the Mechanics of Continuous Medium, Prentice-Hall, Inc., Englewood Cliffs, New Jersey, 1969

McMeeking, R. M. and Rice, J. R., "Finite Element Formulations for Problems of Large Elastic-Plastic Deformation," Int. J. Solids Struct. Vol. 11, pp. 601-616, 1975

Miracle, D. B., "The physical and mechanical properties of NiAl," Acta Metall., Vol. 41, No.3, pp. 649-684, 1993

Moran, B., Ortiz, M. and Shih, C. F., "Formulation of implicit finite element methods for multiplicative finite deformation plasticity," Int. J. Num. Meth. Eng., Vol. 29, pp. 483-514, 1990

Nagtegaal, J. C., Parks, D. M. and Rice, J. R., "On numerically accurate finite element solutions in the fully plastic range," Comp. Meth. Appl. Mech. Eng., Vol. 4, pp. 153-177, 1974

Nakada Y.and Keh, A. S., "Latent hardening in iron single crystals," Acta Metall.,Vol. 14, pp. 961-973, 1966

Needleman, A., Asaro, R. J. and Lemonds, J., "Finite element analysis of crystalline solids," Comp. Meth. Appl. Mech. Eng., Vol. 52, pp. 689-708, 1985

Ortiz, M, Leroy, Y. and Needleman, A., "A finite element method for localized failure analysis," Comp. Meth. Appl. Mech. Eng., Vol. 61, pp. 189-214, 1987

Pan, J. and Rice, J. R., "Rate sensitivity of plastic flow and implications for yield-surface vertices," Int. J. Solid Struct, Vol. 19, pp. 973-987, 1983

Peirce, D., Asaro, R. J. and Needleman, A., "An Analysis of nonuniform and localized deformation in ductile single crystal," Acta Metall., Vol. 30, pp. 1087-1119, 1982

Peirce, D., Asaro, R. J. and Needleman, A., "Material rate dependence and localized deformation in crystalline solids," Acta Metall. Vol. 31, No.12, pp. 1951-1976, 1983

Peirce, D., Shih, C. F. and Needleman, A., "A tangent modulus method for rate dependent solids," Comp. Struct. Vol. 18, pp. 875-887, 1984

Price, R. J. and Kelly, A., "Deformation of age-hardened aluminum alloy crystals- II. Fracture," Acta Metall., Vol. 12, pp. 979-991, 1964

Rashid, M. M. and Nemat-Nasser, S., "A constitutive algorithm for rate-dependent crystal plasticity," Comp. Meth. Appl. Mech. Eng., Vol. 92, pp. 201-228, 1992

Reid, C. N., Deformation Geometry for Material Scientists, Pergamon Press Ltd., Oxford, 1973

Seelam, V. B. R., Finite Element Analysis of Deformation Processes in Metallic Single Crystals, MS thesis, Univ. of Florida, 1995

Shrivastava, S and Ebrahimi, F., "Effect of prestraining on the brittle-to-ductile transition of NiAl single crystals," in: High Temperature Ordered Intermetallic Alloys VII, MRS Proc., Vol. 460, pp. 393-398, 1997

Simo, J. C. and Armero, F., " Geometrically non-linear enhanced strain mixed methods and the method of incompatible modes," Int. J. Numer. Meth. Eng., Vol. 33, pp. 1413-1449, 1992

Simo, J. C. and Rifai, M. S., "A class of mixed assumed strain methods and the method of incompatible modes," Int. J. Numer. Meth. Eng., Vol. 29, pp. 1595-1638, 1990

Simo, J. C. and Taylor, R. L., "Consistent tangent operators for rate-independent elastoplasticity," Comp. Meth. Appl. Mech. Eng., Vol. 48, pp. 101-118, 1985

Simo, J. C. and Taylor, R. L., "A Return mapping algorithm for plane stress elastoplasticity," Int. J. Numer. Meth. Eng., Vol. 22, pp. 649-670, 1986

Takasugi, T., Kishino, J. and Hanada, S., "Anomalous elongation behavior of stoichiometric NiAl single crystals at intermediate temperatures," Acta Metall. Mater., Vol. 41, No. 4, pp. 1009-1020, 1993

Taylor, G. I., "The mechanism of plastic deformation of crystals Part I, Theoretical," Proc. R. Soc. London, Vol. A145, pp. 362-387, 1934

Taylor, G. I., "The mechanism of plastic deformation of crystals Part II, Comparison with Observations," Proc. R. Soc. London, Vol. A145, pp. 388-404, 1934

Tvergaard, V., "Influnce of voids on shear band instabilities under plane strain conditions," Int. J. Fract., Vol. 17, No. 4, pp. 389-407, 1981

Tvergaard, V., Needleman, A., and Lo, K. K., "Flow localization in the plane strain tensile test," J. Mech. Phys. Solids, Vol. 29, pp. 115-142, 1981

Wasilewski, R. J., Butler, S. R. and Hanlon, J. E., "Plastic deformation of single crystal NiAl", Trans. Metall. Soc. AIME, Vol. 239, pp. 1357-1364, 1967

Weng, G. J., "Anisotropic hardening in single crystals and the plasticity of polycrystals," Int. J. Plasticity, Vol. 3, pp. 315-339, 1987

Wenner, M. L., "A generalized forward gradient procedure for rate sensitive constitutive equations," Int. J. Numer. Meth. Eng., Vol. 36, pp. 985-995, 1993

Winton, J. S., The Effect of Orientation, Temperature, and Strain Rate on the Mechanical Properties of NiAl Single Crystals, MS thesis, Univ. of Florida, 1995

Wu, T., Bassani, J. L. and Laird, C., "Latent hardening in single crystals I. Theory and experiments," Proc. R. Soc. London, Vol. A435, pp. 1-19, 1991

Yang, C. and Kumar, A. V., "Simulation of deformation in NiAl single crystals," Int. ME Congress and Exposition, Winter Annual Meeting of ASME, Dallas, TX, Nov., 1997

Yang, C., Seelam, V. B. R. and Kumar, A. V., "Investigation of Localized Deformation in NiAl Single Crystals," submitted to the ASME J. Eng. Mater. Tech., 1997

Zbib, H. M. and Jubran, J. S., "Dynamic shear banding: A three-dimensional analysis," Int. J. Plasticity, Vol. 8, pp. 619-641, 1992

Zhang, Y. W., Wang, T. C. and Liang, N. G., "The inhomogeneity of plastic deformation in ductile single crystals," Modelling Simul. Mater. Eng., Vol. 2, pp. 1171-1193, 1994

Zhu, Z. G. and Batra, R. C., "Analysis of dynamic shear bands in an FCC single crystal," Int. J. of Plasticity, Vol. 9, No. 6, pp. 653-696, 1993

Zienkiewicz, O. C., The Finite Element Method in Engineering Science, McGraw-Hill, London, 1971

BIOGRAPHICAL SKETCH

Chulho Yang was born on January 29, 1968, in Seoul, South Korea. He earned a Bachelor of Science degree from Inha University, in 1991, and Master of Science in mechanical engineering specializing in fracture mechanics from Inha University, in 1993. He went to the University of Florida and earned another Master of Science specializing in control and vibration in mechanical engineering, in 1995. He continued his study toward a doctoral degree. He will earn the degree of Doctor of Philosophy in December of 1997.

I certify that I have read this study and that in my opinion it conforms to acceptable standards of scholarly presentation and is fully adequate, in scope and quality, as a dissertation for the degree of Doctor of Philosophy.

Ashok V. Kumar, Chairman
Assistant Professor of Mechanical Engineering

I certify that I have read this study and that in my opinion it conforms to acceptable standards of scholarly presentation and is fully adequate, in scope and quality, as a dissertation for the degree of Doctor of Philosophy.

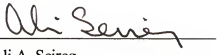

Ali A. Seireg
Ebaugh Professor of Mechanical Engineering

I certify that I have read this study and that in my opinion it conforms to acceptable standards of scholarly presentation and is fully adequate, in scope and quality, as a dissertation for the degree of Doctor of Philosophy.

John C. Ziegert
Associate Professor of Mechanical Engineering

I certify that I have read this study and that in my opinion it conforms to acceptable standards of scholarly presentation and is fully adequate, in scope and quality, as a dissertation for the degree of Doctor of Philosophy.

Michael J. Kaufman
Professor of Materials Science and Engineering

I certify that I have read this study and that in my opinion it conforms to acceptable standards of scholarly presentation and is fully adequate, in scope and quality, as a dissertation for the degree of Doctor of Philosophy.

Fereshteh Ebrahimi

Fereshteh Ebrahimi
Associate Professor of Materials
Science and Engineering

This dissertation was submitted to the Graduate Faculty of the college of Engineering and to the Graduate School and was accepted as partial fulfillment of the requirements for the degree of Doctor of Philosophy.

December, 1997

Winfred M. Phillips
Dean, College of Engineering

Karen A. Holbrook
Dean, Graduate School